

INVESTIGATIONS OF NAPHTHALIMIDE AND PYRENE DERIVATIVES BASED ORGANIC LIGHT EMITTING DIODES

Thesis

Submitted in partial fulfillment of the requirements for the degree of

DOCTOR OF PHILOSOPHY

by

HIDAYATH ULLA



DEPARTMENT OF PHYSICS

NATIONAL INSTITUTE OF TECHNOLOGY KARNATAKA

SURATHKAL, MANGALORE – 575025

MAY, 2016

DECLARATION

I hereby *declare* that the Research Thesis entitled “**Investigations of Naphthalimide and Pyrene Derivatives Based Organic Light Emitting Diodes**” which is being submitted to the National Institute of Technology Karnataka, Surathkal in partial fulfillment of the requirements for the award of the Degree of **Doctor of Philosophy in Physics** is a *bonafide report of the research work carried out by me*. The material contained in this Research Thesis has not been submitted to any University or Institution for the award of any degree.

Mr. Hidayath Ulla

(Reg. No. 092024PH09F03)

Department of Physics

Place: NITK, Surathkal

Date: May 18, 2016

CERTIFICATE

This is to *certify* that the Research Thesis entitled “**Investigations of Naphthalimide and Pyrene Derivatives Based Organic Light Emitting Diodes**” submitted by **Hidayath Ulla** (Register Number: **092024PH09F03**) as the record of the research work carried out by him, is accepted as the Research Thesis submission in partial fulfillment of the requirements for the award of degree of **Doctor of Philosophy**.

Dr. M.N. Satyanarayan
Research Guide

Prof. G. Umesh
Research Guide

Chairman-DRPC

To my family

ACKNOWLEDGEMENTS

Though only my name appears on the cover of this Thesis, a great number of people have contributed to this research. As is the custom, I would like to thank all those people without whose help and support, I would not have finished my PhD. I owe my gratitude to all individuals who have made this Thesis possible and it's them who have made my research experience something that I will cherish forever.

First and foremost, I would like to express my sincere and deep sense of gratitude to my research supervisors, **Dr. M.N. Satyanarayan** and **Prof. G. Umesh** for their constant help, guidance and support with both scientific and organizational problems. I have been amazingly fortunate to have advisors who gave me the freedom to explore on my own and the guidance to recover when my steps faltered. I am deeply indebted to their infinite patience, unfaltering encouragement and cheerfulness that kept me on track and helped me overcome many crisis situations and finish this Thesis.

I am infinitely grateful to my thesis committee members **Prof. A.V. Adhikari** and **Prof. Muralidhar Kulkarni**. Their insightful comments and constructive criticisms at different stages of my research were thought-provoking and they helped me focus my ideas.

Heartfelt gratitude to **The Head, Faculty and Non-Teaching Staff** of the **Department of Physics, NITK-Surathkal** for their timely support. I am very thankful for **Prof. M.S. Bhat** for giving me the opportunity to serve as a senior research fellow in his project.

I would like to express my deep gratitude to **Prof. K.L. Narasimhan**, for providing guidance during the initial stages of my PhD. I thank **Prof. V Jayathirtha Rao** and **Prof. Bhanuprakash** for supplying the novel materials during my PhD work. I am thankful to the **Prof. Subhasis Ghosh** who provided me the possibility to spend a period during the thesis activity into the Physics department of JNU Delhi. I have been very fortunate to have spent time in his laboratory. Special thanks to all my friends at JNU who made my stay successful.

I am also deeply grateful for the companionship of the fellow researchers in the Optoelectronics Laboratory and Department of Physics. All their names will be engraved in my memory forever. I would like to thank my seniors **Dr. Vikas** and **Dr. Manjunath** for training me and providing very fine technical details at an early stage of the research. I want to thank **Dr. Sadanand** for being a good companion. I want to thank **Dr. Garudachar** and **Dr. Ahipa** for synthesizing the molecules for my PhD work. Many thanks to **Mr. Raveendra Kiran** for his friendship inside and outside the work-time, for the time spent together during the experiments and for the infinite ways he helped me. I also thank **Ms. Ranjana, Ms. Jean, Mr. Achyutha** and **Mr. Makesh** for their timely help. It was a pleasure having **Mr. Shahshidhar** as a friend throughout this experience. I can honestly say that my experience at NITK has been better for working with him. Special thanks to **Mr. Krishna** and **Ms. Manasa** for assisting me in the optical measurements.

Most importantly, none of this would have been possible without the support and patience of parents and my brother for generously giving me all their love and support throughout all these years. They have been a constant source of love, concern and strength all these years. Without their hard work and dedication, I would not be where I am today. Last but not the least, I am very thankful for the continued support and encouragement from my loving wife. Her support has helped me stay on track mentally during this experience, and I couldn't ask for anything more.

Hidayath Ulla

ABSTRACT

Organic light-emitting devices (OLEDs) have been subject of intensive studies due to their great potential in display and lighting applications. The key point in OLEDs development for display and lighting applications is to find out materials emitting pure colours of red, green and blue with excellent emission efficiency and high stability. The efficiency of an OLED can be improved by balancing the transport of charge carriers in the device. Generally, this is done by including hole transporting and electron transporting materials in the OLED architecture. This thesis is focused on the study of electron transport materials for OLEDs based on novel naphthalimide and pyrene derivatives. This work improved the understanding on the physics of electron transport materials and the results of this study may be helpful for developing new devices and their applications. We observed that the naphthalimide derivatives have low-lying LUMO levels making them possess good electron-transporting and hole-blocking properties. The derivatives emitted in blue region with good chromaticity. In addition, they have high thermal stability and capable of forming good morphological films. Studies on the device properties of naphthalimide derivatives showed that they could be used as blue emitting electron transport materials. Also, the derivatives as host material in red OLEDs showed better performance than standard host material Alq₃ in terms of both chromaticity and efficiency. Investigations on the OLEDs based on novel pyrene derivatives as green emitting electron transport materials showed better performance than Alq₃. Temperature dependent electrical studies on the electron only devices showed that the pyrene derivatives have better electron mobilities than Alq₃.

Keywords: OLED, Naphthalimide, Pyrene, Electron-transport, Blue-emitting, Green-emitting.

CONTENTS

Declaration	
Certificate	
Acknowledgements	
Abstract	
Contents	i
Nomenclature	iv
Chapter 1 : Introduction	
1.1 Organic Electronics	1
1.2 Basics of Organic Molecular Semiconductors	1
1.2.1 Difference between Organic and Inorganic Semiconductors	4
1.2.2 Types of Organic Semiconductors	5
1.3 OLEDs – Timeline	7
1.4 OLED Design Concept and Operation	8
1.5 Performance of an OLED	13
1.5.1 Charge Carrier Injection	13
1.5.2 Charge Carrier Transport	15
1.5.3 Exciton Formation and its Decay	18
1.6 Materials for Organic Light Emitting Diodes	20
1.6.1 Anode Materials	21
1.6.2 Hole Injection Materials (HIM)	22
1.6.3 Hole Transport Materials (HTM)	23
1.6.4 Electron Transport Materials (ETM)	24
1.6.5 Electron Injection Materials (EIM)	25
1.6.6 Cathode Materials	25
1.6.7 Emissive or Light Emitting Materials (EML)	26
1.7 Major Challenges in the Field of OLEDs	27
1.7.1 Naphthalimide Derivatives	27
1.7.2 Pyrene Derivatives	30

1.8. Scope and Objectives of the Thesis	32
1.8.1 Scope of the Thesis	32
1.8.2 Objectives of the Thesis	33
1.9 Organization of the Thesis	34
Chapter 2: Materials and Experimental Techniques	
2.1 Materials used in this Work	35
2.2 Material Characterization Techniques	38
2.2.1 Single Crystal XRD	38
2.2.2 Photo-Physical Measurements	39
2.2.3 Electrochemical Measurements	40
2.2.4 Thermal Properties	41
2.2.5 Surface Morphology	41
2.3 Device Structures	42
2.4 Device Fabrication	43
2.4.1 Cleaning of Patterned ITO Coated Substrates	43
2.4.2 Device Fabrication and Parameters	44
2.5 Device Characterization	46
2.5.1 OLED Characterization	46
2.5.2 Electron Only Device Characterization	51
2.6 Conclusions	52
Chapter 3: Material Characterization of the Novel Naphthalimide Derivatives	
3.1 Introduction	53
3.2 Crystal Structure	55
3.3 Photo-Physical Properties	57
3.3.1 Steady-State Emission Measurements	57
3.3.2 Time-Resolved Photoluminescence Spectroscopy	70
3.4 Thermal Properties	72
3.5 Surface Morphology	74
3.6 Electrochemical Properties	74
3.7 Conclusions	77

Chapter 4: Naphthalimide Derivatives for Organic Light Emitting Diodes	
4.1 Introduction	79
4.2 OLEDs using Naphthalimides as Active Materials	80
4.2.1 Naphthalimide Derivative as Emissive Materials	80
4.2.2 Naphthalimide as ETL Material In Phosphorescent OLEDs	83
4.2.3 Naphthalimide Derivative as EL and ETL Material	85
4.3 OLEDs using Naphthalimides as Host Materials	90
4.4 Conclusions	96
Chapter 5: Pyrene Derivatives for Organic Light Emitting Diodes	
5.1 Introduction	97
5.2 Electroluminescence Studies	99
5.2.1 Pyrene Derivatives as Emissive Materials	99
5.2.2 Pyrene Derivatives as ETL Material for Phosphorescent OLEDs	103
5.2.3 Pyrene as both EL and ETL Materials	105
5.3 Electron Transport Studies on TBUT Pyrene	109
5.4 Conclusions	118
Chapter 6: Summary and Conclusions	
6.1 Summary	119
6.2 Conclusions	120
6.3 Scope for Future Work	121
References	123
List of Publications	145
Bio-Data	147

NOMENCLATURE

Ag	Silver
Al	Aluminum
Alq ₃	Tris(8-hydroxyquinoline)
Au	Gold
B	Brightness
BCP	Bathocuproine
BPhen	Bathophenanthroline
Ca	Calcium
cd	Candela
CIE	Commission Internationale d'Éclairage
Cu	Copper
CuPc	Copper phthalocyanine
CV	Cyclic Voltammetry
EA	Electron Affinity
EBM/EBL	Electron Blocking Material/Electron Blocking Layer
E _g ^{opt}	Optical band gap
EIM/EIL	Electron Injection Materials/Layers
EL	Electroluminescence
ETM/ETL	Electron Transport Material/Layer
F ₄ TCNQ	2,3,5,6-Tetrafluoro-7,7,8,8-tetracyanoquinodimethane
FWHM	Full Width at Half Maximum
<i>h</i>	Planck's constant
HIM/HIL	Hole Injection Material/Layer
HOMO	Highest Occupied Molecular Orbital
HTM/HTL	Hole Transport Material/Layer
IP	Ionization Potential
ITO	Indium Tin Oxide
J	Current density
L	Luminance
LCDs	Liquid Crystal Displays
LiF	Lithium Fluoride
LUMO	Lowest Unoccupied Molecular Orbital
Mg	Magnesium
MoO ₃	Molybdenum trioxide
N _v	Atomic density

OLED	Organic Light Emitting Diode
OMS	Organic Molecular Semiconductors
PANI	Poly(aniline)
PEDOT: PSS	Poly(3,4-ethylenedioxythiophene)-poly(styrenesulfonate)
PL	Photoluminescence
PLED	Polymer Light Emitting Diode
PMT	Photomultiplier tube
POS	Polymeric Organic Semiconductors
PPP	Poly(para-phenylene)
PPV	Poly(para-phenylene vinylene)
PT	Poly(thiophene)
PTCDA	3,4,9,10-perylenetetracarbonsaure dianhydride
q, e	Electronic charge
RGB	Red, Green and Blue
RMS	Root Mean Square
RS	Richardson-Schottky
SCLC	Space Charge Limited Current
TCSPC	Time Correlated Single Photon Counting
TPD	N,N' - (3-methylphenyl)-1,1' -biphenyl-4,4' -diamine
UV-Vis	Ultraviolet Visible
V	Voltage
V _{bi}	Built-in Voltage
VTE	Vacuum Thermal Evaporation
α	Absorption coefficient
α -NPD	4,4'-bis[N-(1-naphthyl-1)-Nphenyl-amino]-biphenyl
ϵ	Extinction coefficient
ϵ_0	Permittivity of free space
ϵ_r	Relative permittivity
λ_{Abs}	Absorbance maximum
λ_{PL}	Photoluminescence maximum
μ	Carrier mobility
v _{st}	Stokes' shift
τ	Fluorescence life time
Φ_{PL}	Photoluminescence Quantum yield

CHAPTER 1

INTRODUCTION

Overview

Chapter 1 presents a brief overview of the field of organic electronic devices, the materials used for making them and their characterization. It begins with a description of the relevant properties of organic molecular semiconductors (OMSs) focusing on the role of conjugation, types of OMSs and their differences from inorganic semiconductors. A brief description of the major milestones in organic light emitting diode (OLED) research and the working principle of OLEDs is presented. This is followed by a brief discussion on charge transport in disordered OMSs. Next, the nature of materials used for OLEDs and their characteristics is described. Lastly, the scope and objectives of the thesis are presented followed by a summary of all the chapters in the thesis.

1.1 ORGANIC ELECTRONICS

Organic electronics is a relatively new field of multidisciplinary research posing a series of conceptual, experimental and modeling challenges in making efficient electronic devices using carbon-based small molecules and polymers. This field is quite different, in many aspects, from conventional electronics wherein inorganic materials, such as silicon, gallium arsenide, etc., are used. One of the most important differences is that organic materials are highly disordered solids and, hence, the charge carriers exhibit “polaronic” nature. They have relatively low dielectric constant leading to a large exciton binding energy. In contrast to band transport in inorganics, in organic solids charge transport is dominated by “hopping” mechanism, which results in very low charge mobility. In the last few years, significant research has been focused on the study of high-performance OMSs and their use for the development of organic devices using new architectures for electronic components. The quest for more efficient, thinner, compact and flexible electronic systems require materials with new and improved characteristics, functionalities and new fabrication processes.

1.2 BASICS OF ORGANIC MOLECULAR SEMICONDUCTORS

Organic molecular semiconductors are materials belonging to the class of π -conjugated organic molecules wherein the carbon atoms are joined by alternating single and double bonds. In the carbon atom, there are six electrons, two in core and four in

the outer shell. Carbon atom, in the ground state, has the electronic configuration $1s^2 2s^2 2p^2$. The covalent binding energy for electron in the 2s state is 3~4 eV. It requires ~4 eV of energy to jump to 2p orbital. In the formation of organic molecules, one of the 2s electron is excited into an empty 2p orbital and forms hybrid bonds in this excited state. By forming this excited state, each carbon atom acquires four bonds and the electronic configuration of carbon atom is denoted as $1s^2 2s 2p^3$. The electronic and optical properties of these materials are due to carbon in its various hybridized state. Hybridization is a simple model in which mixing of orbitals takes place to form new hybridized orbital. The four electrons in the $n=2$ state of carbon can hybridize in three possible ways: sp , sp^2 , and sp^3 . In sp^3 configuration, all the four electrons participate in hybridization and form the strong “ σ bonds” with the neighbors, whereas, in sp^2 hybridization only three electrons (one in s orbital and other two electrons in p orbitals) participate in hybridization and hence form three σ bonds. The σ bond holds the molecule together. There is still one p_z electron left out which forms a weaker π bond with its neighbor. These p_z electrons forming the weaker π bonds are relatively free to move and are delocalized throughout the molecular backbone and, hence, are responsible for the electronic and optical properties. Therefore, the lowest electronic excitations of conjugated molecules are the π - π^* transitions with an energy gap typically between 1.5 and 3 eV, leading to light absorption or emission in the visible spectral range. The sp^2 hybridization results in alternate single and double bond formation and, hence, is responsible for the π -conjugated nature of the molecules, which leads to their semiconducting properties.

In OMSs, sp^2 hybridization is observed and as mentioned above the p_z electrons are responsible for the semiconducting nature of the materials. Figure 1.1 (a) shows sp^2 hybridization in the case of ethylene [Okamoto and Brenner 1964, Brütting 2005, Klauk 2006]. When a molecule comes close to its neighbor, the two p_z orbitals interact with each other forming π “bonding orbital” and π^* “anti-bonding orbital” [Okamoto and Brenner 1964]. Hence, the energy levels split due to hybridization and two energy states are formed as shown in Figure 1.1 (b). The lower state is called bonding orbital and is completely filled by two electrons, whereas, the upper state is completely empty and is called anti-bonding orbital. Figure 1.1 (b) shows bonding σ and anti-bonding σ^* states

formed from the overlap of hybridized sp^2 orbitals and bonding π and anti-bonding π^* states formed from the overlap of p_z orbitals.

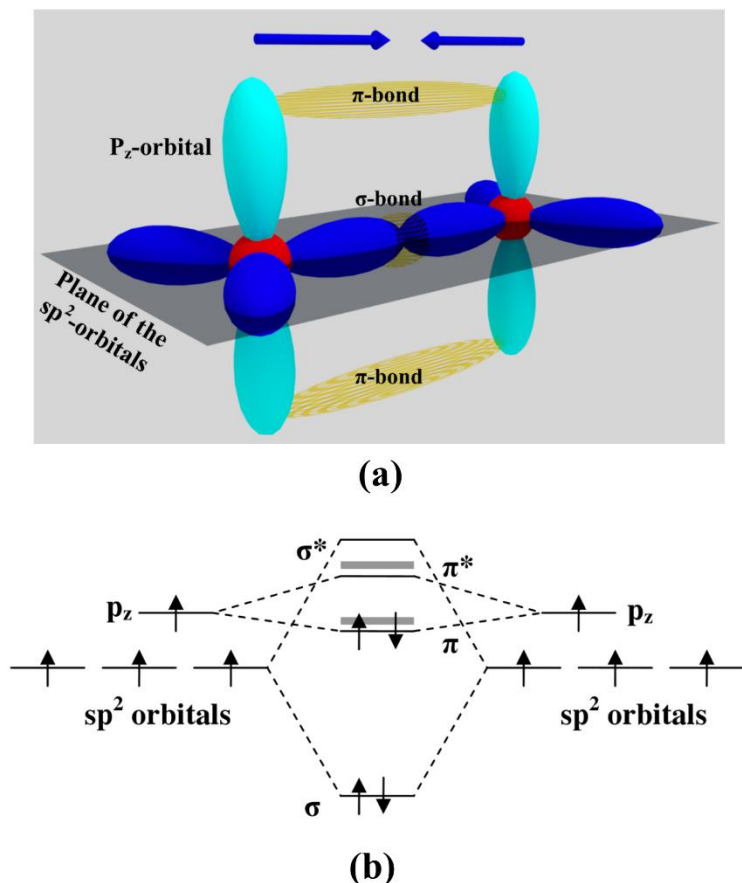


Figure 1.1 (a) Schematic presentation of σ and π bonds in ethylene (b) Schematic representation of the formation of bonding and anti-bonding orbitals (redrawn from [Okamoto and Brenner 1964]).

When several molecules join to form a crystalline solid, these two orbitals split into sub-orbitals leading to the formation of bands. The state possessing the highest energy of all the occupied (filled) orbitals is called highest occupied molecular orbital (HOMO) and is analogous to the top of the valence band for inorganic semiconductors. Lowest unoccupied molecular orbital (LUMO) is the state with the lowest energy of all the unoccupied (unfilled) molecular orbitals and is analogous to the bottom of the conduction band for inorganic semiconductors [Okamoto and Brenner 1964, Jain et al. 2007, So 2010]. The number of states in the two bands (HOMO and LUMO) increases as the number of molecules forming the system increases in organic materials.

Thus, the band gap of organic semiconductors corresponds to the HOMO-LUMO gap in their molecular orbitals.

The variations in the conjugation length, and in the interaction energies with surrounding molecules, give rise to locally varying polarization energies which lead to the formation of a broad Gaussian density of states (GDOS) [Bässler 1993, Brütting 2005] for bonding (occupied) and anti-bonding (unoccupied) orbitals of molecular sites as shown in Figure 1.2. This aspect is also a consequence of the disordered nature of organic molecular solids. In OMSs, the transport of charge carriers occur due to hopping of charge carriers between the HOMO or LUMO levels of comparable energies at different molecular sites. Thus the organic materials have several unique properties manifested by GDOS of the HOMO and LUMO levels.

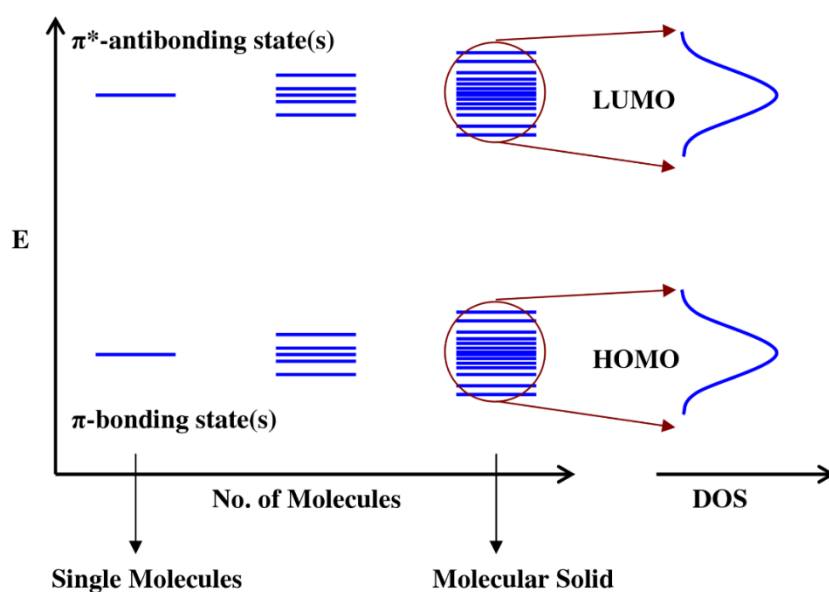


Figure 1.2 Bonding and anti-bonding levels in organic molecule. Disorder in OMSs leads to formation of HOMO and LUMO with GDOS [Okamoto and Brenner 1964]).

1.2.1 Difference between organic and inorganic semiconductors

OMSs are molecular solids and are very different from conventional inorganic semiconductors. Conventional semiconductors are held together either by strong covalent bonds, or ionic or covalent-ionic bonds, resulting in electronic bands that have extended energy states. On the other hand, OMSs are composed of organic molecules, held together loosely by weak intermolecular coupling (Van der Waals bonding) and

have localized energy states [Okamoto and Brenner 1964, So 2010]. However, the intramolecular coupling is strong, implying that electronic interactions among the molecules is weak and mean-free path of charge carriers is of the order of intermolecular spacing. The charge transport mechanism in inorganic semiconductors is band type with large carrier mobilities, while it is hopping type conduction in OMSs with low carrier mobilities [Okamoto and Brenner 1964]. The absence of long-range order leads to the localization of the electronic wave function and the formation of a broad GDOS for LUMO and HOMO bands. The charge transport, via thermally activated hops, results in the increase of charge carrier mobility μ with temperature T and electric field F in agreement with the universally observed [Kahn et al. 2003, Brütting 2005] Poole-Frenkel (PF) relation $\mu(F,T) = \mu(0,T) \exp[\gamma(T)F^{1/2}]$, where $\mu(0,T)$ and $\gamma(T)$ are temperature dependent quantities, known as zero field mobility and the field activation of the mobility, respectively. In these materials, hopping between two molecules having comparable energies describes the transport of charge carriers.

1.2.2 Types of organic semiconductors

OMSs are mainly divided into two categories according to their molecular weights (i) small π -conjugated OMSs and (ii) polymeric organic semiconductors (POSs) [Okamoto and Brenner 1964, Klauk 2006, Jain et al. 2007]. Small molecule OMSs are low molecular weight (\sim several hundred grams) organic molecules while POSs have high molecular weights (\sim several thousand grams) with a long chain of organic molecules in which a unit repeats many times (at least 20 and typically several hundred times) [Inzelt 2012]. POSs have been extensively studied due to the ease of device making using solution processing techniques such as, spin coating, dip coating, inkjet printing etc. [Brütting 2005, Jain et al. 2007, Inzelt 2012] making it suitable for flexible electronic systems. Small organic molecules i.e. π -conjugated oligomers, which have a well-defined chemical structure can be a better alternative. Highly ordered layers of small molecules can be obtained by using vapor deposition techniques [Tour 1996, Martin and Diederich 1999, Jain et al. 2007] and mobilities are generally several order of magnitude higher than that of solution processed polymer devices [Dimitrakopoulos and Malenfant 2002, Jain et al. 2007]. Some of the low weight conjugated organic molecule based OMSs, viz. 3,4,9,10-perylene-tetracarboxylic acid

dianhydride (PTCDA), copper phthalocyanine (CuPc), and tris(8-hydroxyquinoline) (Alq₃), pentacene, tetracene and anthracene, have structures as shown in Figure 1.3(a). The long chain POSs, poly(aniline) (PANI), poly(para-phenylene) (PPP), poly(para-phenylene vinylene) (PPV) and poly(thiophene) (PT) are shown in Figure 1.3(b).

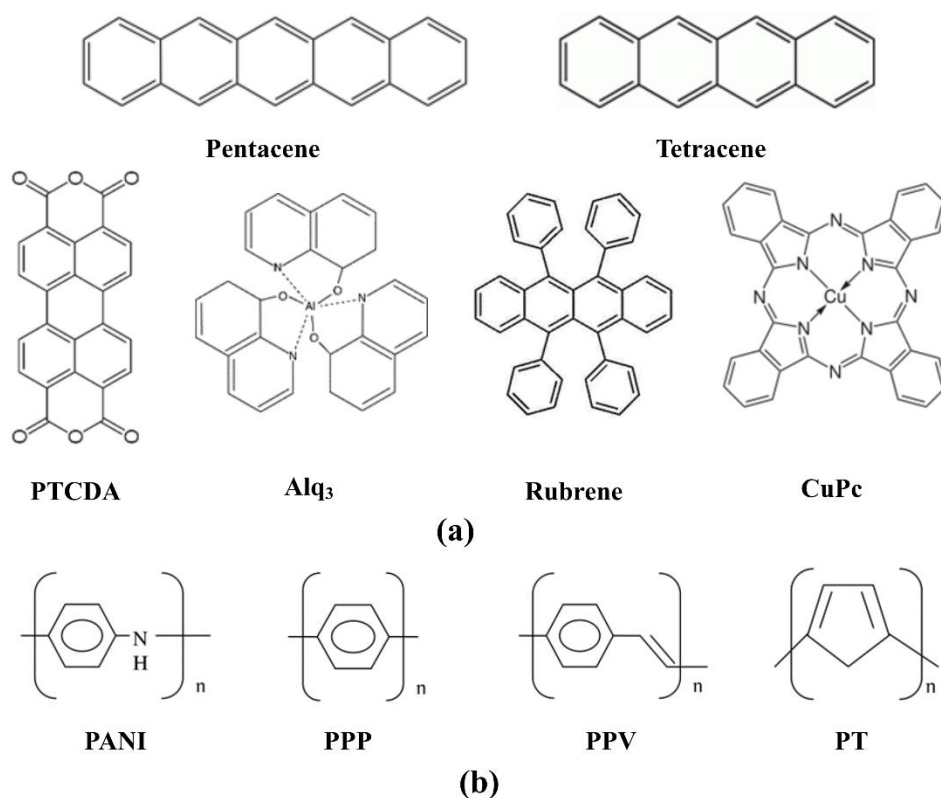


Figure 1.3 Some of the important (a) small molecule OMSs and (b) POSs

The discovery of electroluminescence (EL) from OMSs was a major breakthrough in the field of organic electronics [Pope et al. 1963, Tang and VanSlyke 1987, Burroughes et al. 1990, Baldo et al. 2000, Jain et al. 2007]. Based on this, many devices were developed for display and general lighting applications. The availability of a wide variety of organic materials and ease of fabrication of these devices makes it an ideal candidate for commercialization. Several devices are already in the market [Forrest et al. 1997, Klauk 2006, Jain et al. 2007, Seo et al. 2007]. The advantages of displays based on OLEDs over the conventional liquid crystal displays (LCDs) and cathode ray tubes include higher switching speed, wide viewing angle, feasibility for fabrication on flexible substrates [Brütting 2005, Klauk 2006, Jain et al. 2007] low power consumption, flat screen and light weight.

1.3 OLEDs – TIMELINE

Organic EL is an optoelectronic phenomenon wherein light is emitted from a device made of non-crystalline organic materials when it is forward biased. Initially organic EL was achieved by using molecular crystals of luminescent organic molecules. This phenomenon in alternating current mode (AC) was first observed and extensively studied way back in 1953 by Bernanose and his co-workers [1953]. In 1963, Pope and his group reported organic electroluminescence using direct current (DC) [1963]. The devices made by them were crystalline, operating voltages were very high (in the order of 400 V) and brightness was low for commercial applications. In 1965, Helfrich proposed the mechanism of double recombination radiation from anthracene (several microns thick) which led to the modern day hole-electron recombination of OLED devices [Helfrich and Schneider 1965]. However due to the large thickness of the material used, the onset of luminescence occurred above 100 V. Hence no practical application of this technology seemed possible due to the very large operating voltages. Later, thermally evaporated thin films of polycrystalline anthracene was used as the emitting material [P. S. Vincett 1982]. Due to imbalance in carrier injection, the efficiency of the device was poor.

The real breakthrough in organic EL, in the form of the first efficient low-voltage device, was demonstrated in 1987 by Ching Tang and Steve VanSlyke [1987] of Eastman Kodak Co. using an organic heterostructure, which is generally recognized as the most significant step forward in the development of OLED technology. They employed modern thin film deposition techniques with suitable materials and device structure to achieve moderately low bias voltages and highly improved luminance efficiency [Tang and VanSlyke 1987]. They reported an ITO/Diamine/ Alq₃/ Mg:Ag device. Diamine was used as a hole transporting material (HTM) and Alq₃ served as both the emitting and electron transport material (ETM). Though the amorphous nature of the film compromised the carrier transport in the film, the film itself was ultra-thin (135 nm) and, hence, the EL turn-on voltage was as low as 2.5 V. With operating voltage less than 10V, the light output was ~1000 cd/m². This simple design indicated the potential of organic molecules for lighting applications. Such *heterostructures* have become a standard design in OLED devices. This breakthrough also attracted many

chemists and engineers to focus on the further development of high performance OLEDs. In 1989, Tang and Vanslyke [1989] further proposed a guest-host system, in which efficient charge transport and luminescence were confined to two different materials, i.e. host and guest, respectively. This was achieved by doping organic light emitting films with small amounts of dopants. They inferred that the device efficiency can be increased, the emission color can be tuned and life time of the device can be improved [Tang et al. 1989, Slyke et al. 1996]. This work was also well recognized as another milestone in the OLED development. Shortly afterwards, using the knowledge of conductive polymers in 1977 by Nobel Laureates Alan Heeger, MacDiarmid and Shirakawa [1977], the Cambridge group of R.H. Friend announced, in 1990, a conducting polymer OLED (PLED) using poly(p-phenylene-vinylene) (PPV) [1990]. They reported EL from a single layer of spin-coated PPV. PLEDs can be easily fabricated by spin coating and inkjet printing [Bharathan and Yang 1998, Hebner et al. 1998], whereas small molecules based OLEDs (SMOLEDs) require the use of comparatively more expensive and elaborate vacuum thermal evaporation systems. Despite this, most of the OLEDs in production are SMOLEDs as they have higher efficiencies and longer lifetimes [Rakurthi 2010].

Since early 1990s, there has been increasing interest and intense research activities in this field by Engineers, condensed matter Physicists and Chemists. Significant efforts were directed towards improving color gamut, lifetime, luminance efficiency and reliability of the device through the design and synthesis of new materials as well as device engineering [Baldo et al. 2000, Jain et al. 2007, Helander et al. 2010, So 2010]. The growing interest is largely motivated by the promise of this technology in flat panel displays and solid-state lighting. As a consequence, OLEDs have evolved from a laboratory curiosity to practical devices for commercial production of large area displays and white light illuminators.

1.4 OLED DESIGN CONCEPT AND OPERATION

An OLED comprises of extremely thin layers of different organic materials sandwiched between two electrodes. It converts electrical energy into light energy. The basic principle of light emission in an OLED is electroluminescence. Figure 1.4 shows

the schematic of a simple single layer OLED with the organic layer sandwiched between a transparent anode and a metal cathode. A transparent and high work function material serves as anode, whereas low work function metals are used as cathode. The transparent anode helps in out-coupling the light from the OLED.

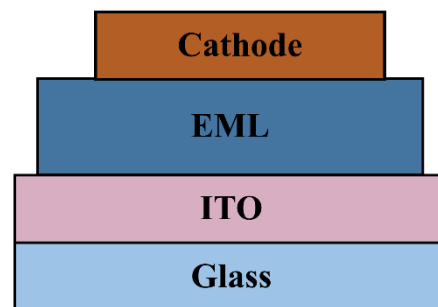


Figure 1.4 Schematic of a single-layer OLED device

Figure 1.5(a) ~ (d) illustrate the energy band diagrams that illustrate the principle of operation of the OLED. Before the electrical contact, the Fermi levels (E_F) of the three layers are not aligned as shown in Figure 1.5(a). The alignment of Fermi levels of anode and cathode occurs when the two electrodes are connected (shorted). The equalization of E_F leads to an equilibrium state due to which a built-in potential develops across the organic layer. Due to the built-in potential barrier (Figure 1.5(b)), charge injection into the organic layer is prevented. An electrical potential difference is applied between the anode and the cathode such that the anode is at a more positive electrical potential with respect to the cathode, i.e. the device is forward biased. When the applied forward bias voltage (V_{app}) equals built-in voltage (V_{bi}), a flat band condition is established as shown in Figure 1.5(c). At $V_{app}=V_{bi}$, charge carriers are ready to be injected into the organic layer as this is the minimum bias required for carrier injection. With further increase in the applied voltage V_{app} , an electric field develops across the device and charges are injected into the organic layer as shown in Figure 1.5(d). Holes are injected into the HOMO level of the OMS from the anode while electrons are injected into the LUMO level of the OMS from the cathode. Under the influence of applied bias voltage, the injected holes and electrons migrate towards the opposite electrodes. There exists the possibility of electron and hole recombination in the organic layer, the probability of which is maximum when electron and hole number densities are equal. The device is then said to operate under balanced current.

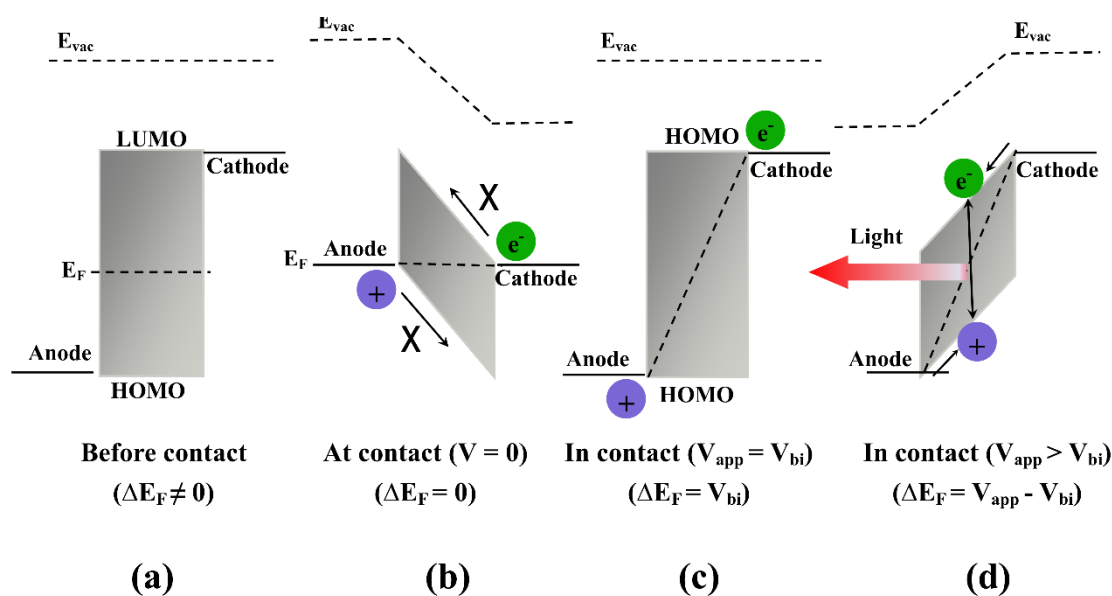


Figure 1.5 Schematic energy band diagrams about OLEDs operation (a) before the electrical contact, (b) after the electrical contact, (c) with $V_{app}=V_{bi}$ and (d) with $V_{app}>V_{bi}$ (redrawn from [So 2010])

Once both carrier types come near each other in the emission layer, they become a bound pair due to Coulombic interaction, which results in an excited state of organic molecule. The excited state, if long lived (e.g. triplet state), may get transferred to other molecules and its properties are conserved during the diffusion. In other words, the excitation of organic molecules leads to a bound state of an electron and a hole (e-h pair) termed as an exciton. The binding energy of an exciton in organic molecules is of the order of 0.5-1 eV [Barth and Bäessler 1997, Brütting 2005]. Such excitons generate a photon through the radiative relaxation in the organic layer, which is emitted through the anode and the substrate both of them designed to be optically transparent. The energy of the emitted photon depends on the energy of the excited organic molecule. The efficiency of an OLED is maximum when all the injected electrons and holes undergo recombination. The efficiency is less, even zero, if the electrons and holes do not meet each other within the same molecule and they migrate all the way to the opposite electrodes. This is normally the case in single layer, small molecule organic devices, as the electrons and holes usually have different mobility values for the same material. As a result, one of the injected carriers (e.g. hole) moves faster and reaches the opposite electrode without recombining with the other carrier (e.g. electron).

In 1987, Tang and VanSlyke demonstrated an effective way to prevent the leakage of injected carriers [1987], which revolutionized the field of organic electroluminescence. They fabricated a bilayer device with materials having different transport characteristics and complementary energy levels. Figure 1.6(a) shows the schematic of a bilayer device structure in which one of the organic layers is specifically chosen to transport holes and the other is specifically chosen to transport electrons. The interface between the two layers provides an efficient site for the recombination of the injected hole–electron pair resulting in electroluminescence. The energy band diagram of a bilayer OLED consisting of a hole-transport layer (HTL) and an electron transport layer (ETL) in forward bias condition is shown in Figure 1.6(b), where E_F denotes the Fermi level for the electrodes. The hetero-junction should be designed to facilitate hole-injection from the HTL into the ETL and to block electron injection in the opposite direction in order to enhance the probability of exciton formation and recombination near the interface region. As shown in Figure 1.6(b), the HOMO of the HTL is slightly above that of the ETL, so that holes can readily enter into the ETL, while the LUMO of the ETL is significantly below that of the HTL, so that electrons are confined in the ETL. Due to potentials barriers at the interface, the carriers pile up on either side of the organic-organic interface.

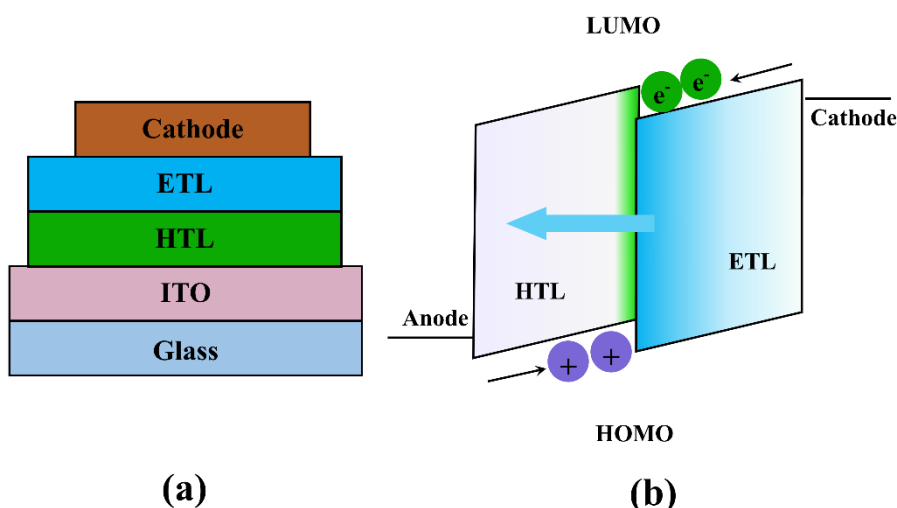


Figure 1.6 (a) Cross section of the first bi-layer OLED reported by Tang and Van Slyke and (b) Energy band diagram of a bilayer OLED under forward biased condition

Depending on energetics, an electron or hole tunnels through the barrier and exciton is formed in one of the layers. The low hole mobility in the ETL causes a build-up of hole density, and thus enhance the collisional capture process. Furthermore, this structure has one more advantage by which, due to sufficient spacing between the interface and the electrode, excitons are formed well away from the conductive contacts and hence the probability of quenching near the metallic surface is greatly reduced. In some special cases an electron and a hole can directly recombine to give rise to intermolecular excitons. Thus, the basic operation of OLEDs involves injection of carriers into the organic layer, then transportation through the organic layer and finally recombination of electron and hole at the HTL/ETL interface.

The bi-layer structure can be modified to a three-layer structure, in which an additional luminescent layer is introduced between the HTL and ETL to function primarily as the site for hole–electron recombination. Thus, the function of each individual organic layer is distinct from the other and can therefore, be optimized independently. Thus, the luminescent or recombination layer can be chosen to have a desirable EL color as well as high luminance efficiency. Likewise, the ETL and HTL can be optimized primarily for efficient carrier-transport property. To improve the OLED efficiency further, functionally distinct organic layers such as hole inducing, hole transporting, hole blocking, electron transporting, electron blocking, emissive layers etc., have also been used. Figure 1.7(a) shows a typical bottom emitting multilayer OLED structure. In this device, multiple organic layers are sandwiched between an anode and a cathode. Organic layers are stacked starting from hole injection layer (HIL) followed by HTL, electron blocking layer (EBL), emissive layer (EML), hole blocking layer (HBL), ETL and finally electron injection layer (EIL) [Justin Thomas et al. 2001, Kulkarni et al. 2004, Brütting 2005, Tung et al. 2005, Jain et al. 2007]. Figure 1.7(b) shows the schematic energy level diagram of a multilayer OLED. When the device is forward biased, holes are injected from anode and electrons from cathode. Holes traverse through HIL, HTL and EBL, and electrons traverse through EIL, ETL and HBL into the emissive layer where they recombine to form excitons, which further decay radiatively to emit light. The function of HIL and EIL is to lower the potential barrier for injection of holes and electrons, respectively [Chen and Wang

2004]. HTLs and ETLs are chosen to minimize barrier potential between injection and emission layer for hole and electron transport. Some of the electrons and holes pass through the emissive layer without recombination. These electrons and holes are blocked by EBL and HBL, respectively [Adamovich et al. 2003].

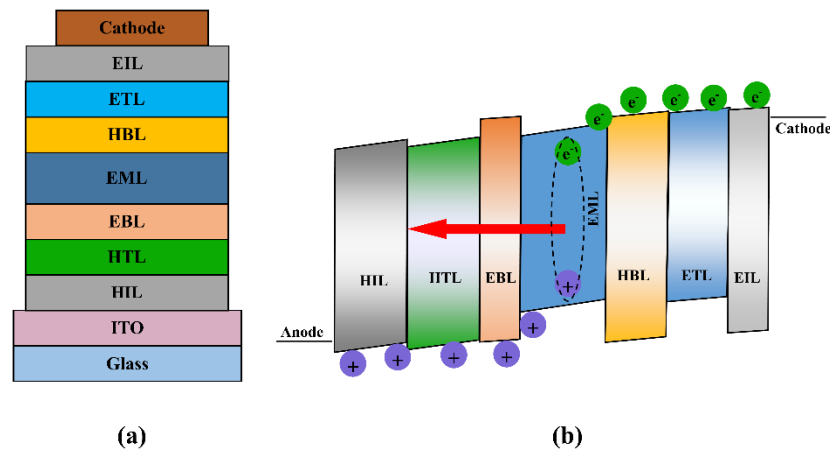


Figure 1.7 Schematic of (a) device structure and (b) energy levels diagram of multi-layer OLED

1.5 PERFORMANCE OF AN OLED

The basic electroluminescence mechanism can be explained following the steps shown in Figure 1.8. (1) Holes are injected by the anode and this injection depends, in the first approximation, on the energy difference (Φ_h) between the work function of the anode (χ_A) and the HOMO level of the organic material. On the other hand, electrons are injected by the cathode and the process depends on the energy difference (Φ_e) between the work function (χ_C) and the LUMO level. Once the carriers are injected into the organic material, they are transported by the applied electric field towards the opposite electrode (2), or they may form a singlet exciton (3). Such singlet excitons can subsequently decay emitting light (4). These mechanisms are discussed below in detail:

1.5.1 Charge carrier injection

When a metal/OMS junction is formed and voltage is applied across this junction, charge carriers are injected from metal Fermi level, E_F , into the HOMO/LUMO of OMS (electrons into LUMO and holes into HOMO). The density of charge carriers injected into OMS depends on applied voltage, and barrier height [Ishii

et al. 1999, Brütting 2005, Jain et al. 2007]. Classically, charge carrier injection into semiconductors is described by the thermionic emission theory [Brütting 2005, S.M.Sze 2008]. According to this theory, thermally activated carriers can overcome the energy barrier at metal/OMS interface.

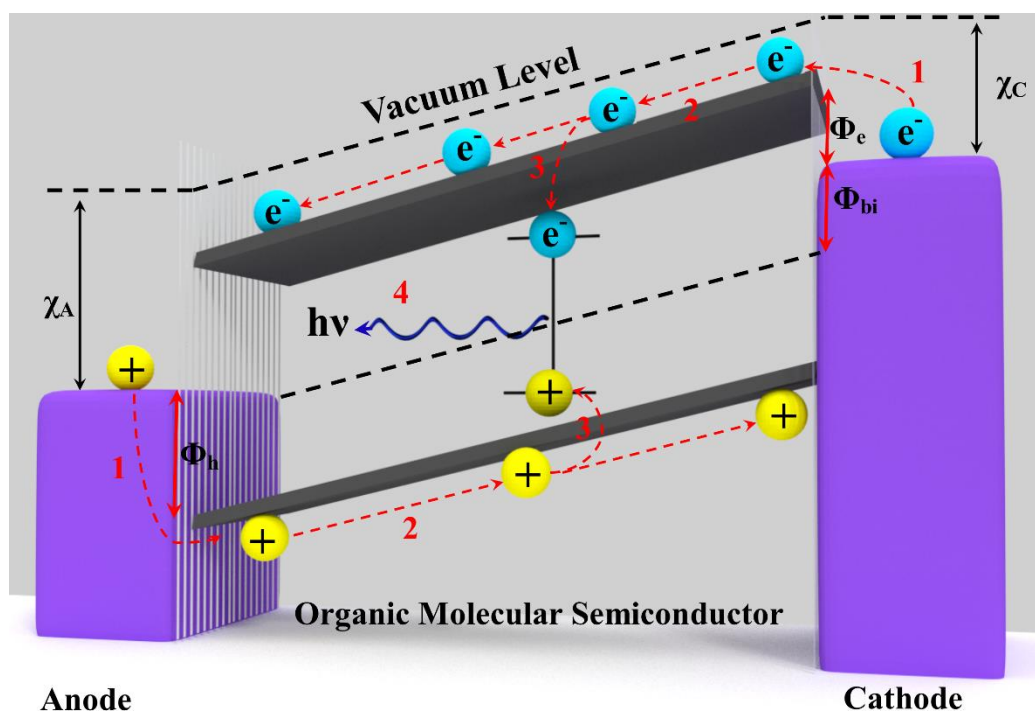


Figure 1.8 Band structure of an OLED operating in forward bias: (1) charge carrier injection, (2) charge carrier transport, (3) exciton formation, (4) radiative exciton decay (redrawn from [Brütting et al. 2001]).

Figure 1.9(a) shows the thermionic injection process showing the injection of electrons from Fermi level of the metal to LUMO of OMS. Charge carrier density injected into the semiconductor is given by [Brütting 2005, S.M.Sze 2008]

$$n = n_o \exp\left(-\frac{\Phi_b}{kT}\right) \quad (1.1)$$

where n_o is the charge carrier density in the bulk metal, Φ_b is the barrier height, k is Boltzmann's constant and T is the temperature of the device.

As barrier height increases, the thermally injected charge carriers into OMS decreases. At higher injection barrier, a considerable amount of charge carriers may be injected by quantum mechanical tunneling process also [Fowler and Nordheim 1928]

(Figure 1.9(b)). However, it was realized that these models are not directly applicable in OMSs due to the presence of localized energy states, low charge carrier mobilities and energy disorder [Scott and Malliaras 1999, 1999 Brütting 2005, 2005 Klauk 2006]. A number of modified models have been proposed to explain the charge carrier injection in metal/OMS, which are based on diffusion-limited injection [Scott and Malliaras 1999] and thermally assisted tunneling from the metal into a uniformly spaced chain of localized states [Abkowitz et al. 1995, Conwell and Wu 1997, Brütting 2005 So 2010].

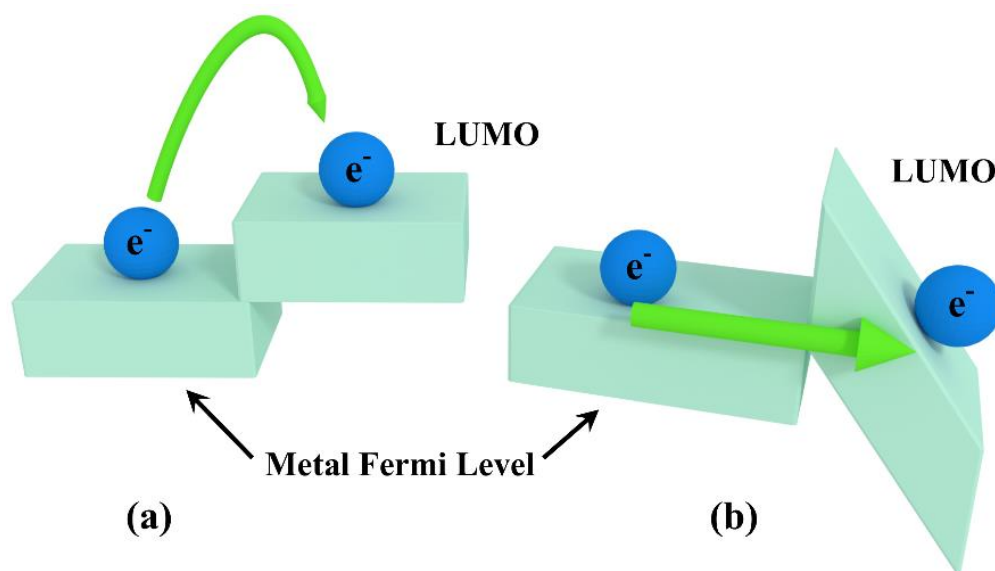


Figure 1.9 Schematic representation of (a) thermionic emission and (b) quantum mechanical tunneling process (redrawn from [Fowler and Nordheim 1928])

1.5.2 Charge carrier transport

Organic molecules in solid state form molecular solids in general and the charge transport mechanism in such materials differs from that in covalently bonded inorganic semiconductors [Roichman et al. 2004, S.M.Sze 2008]. The optimal performance of OLEDs depends on the charge carrier injection as well as the charge carrier transport inside the organic layers [Roichman et al. 2004]. There are several theories and mechanisms proposed for the charge carrier transport in OMS [Miller and Abrahams 1960, Simmons 1965, Emtage and O'Dwyer 1966, Brütting et al. 2001, Walker et al. 2002, Horowitz 2004, Roichman et al. 2004]. Here, we will discuss some of the widely used charge transport mechanisms briefly.

Space Charge Limited Transport: If the contact resistance between metal electrode and the OMS is much lower than the resistance of the bulk OMS material, then carriers will be easily injected into the organic material and the transport of charge will be dominated by the conductivity of the bulk material [Mark and Helfrich 1962, Walker et al. 2002, Brütting 2005]. In this case, the metal-OMS contact is termed as ohmic, which means that the electrode is an infinite reservoir of charge and can maintain a steady state space-charge limited current (SCLC) in the device as shown in Figure 1.10 [Mark and Helfrich 1962, Brütting et al. 2001]. In SCLC regime, the current conduction in the device is determined by the mobility of charge carriers. Due to low charge carrier mobilities in OMSs, a space charge region is formed throughout the OMS and the charge carrier movement is limited by this space charge [Brütting 2005]. The current density in SCLC regime is given by [Mark and Helfrich 1962, Brütting 2005]

$$J = \frac{9}{8} \mu \varepsilon \frac{V^2}{L^3} \quad (1.2)$$

where μ ($\text{m}^2 \text{V}^{-1} \text{s}^{-1}$) is the mobility of OMS, ε (F m^{-1}) is the permittivity of medium, L is the thickness (in m) of OMS layer and V is the applied voltage in volts.

Equation 1.2 shows that the current depends on square of the applied voltage in the space-charge regime. This relationship is called *Child's law* [Mark and Helfrich 1962], and it holds in materials where the presence of traps and defect states is low. However, trap states are commonly observed in OMSs due to impurities, dislocations and rough grain boundaries [Brütting et al. 2001]. The presence of these states influences the charge carrier transport within the OMS and the current density does not obey Child's law and deviates from Equation 1.2. In the presence of discrete trap states, the SCLC current density is given by [Brütting et al. 2001]

$$J = q^{1-l} \mu N_V \left(\frac{2l+1}{l+1} \right)^{l+1} \left(\frac{l}{l+1} \frac{\varepsilon_s \varepsilon_0}{H_b} \right)^l \frac{V^{l+1}}{d^{2l+1}} \quad (1.3)$$

where μ ($\text{m}^2 \text{V}^{-1} \text{s}^{-1}$) is the mobility of charge carriers, N_V is the atomic density ($\text{kg}^{-1} \text{mol}^{-1}$), H_b is trap density per unit energy (m^{-2}), $l = T_c/T$, T_c is critical temperature given by trap energy $E_t = kT_c$, ε_s is relative permittivity of the medium, ε_0 is the permittivity of free space (F m^{-1}), q (C) is the charge of an electron, V (volts) is applied voltage and d

(m) is the thickness of OMS layer. Additionally, the effective mobility in many disordered organic semiconducting materials is found to be electric field- dependent [Brütting et al. 2001], (i.e., $\mu = \mu_0 \exp(\gamma\sqrt{F})$) where μ_0 and γ are constants.

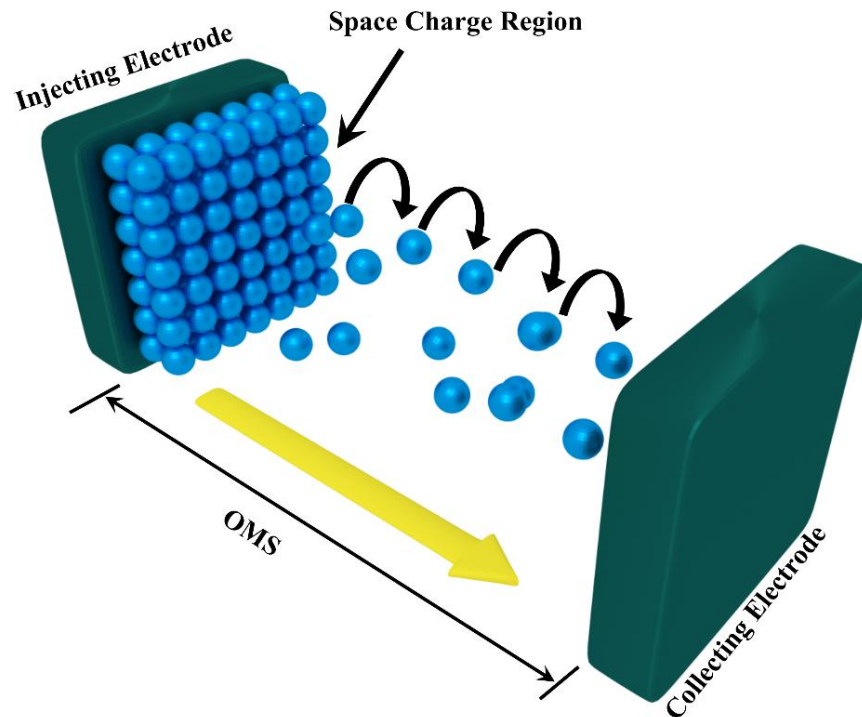


Figure 1.10: Schematic representation of space charge limited conduction in OMS (redrawn from [Mark and Helfrich 1962])

Injection Limited Transport: If the contact resistance is larger at the metal/OMS interface than the bulk resistance then the charge carrier transport is limited by the charge injection process [Horowitz 2004]. It occurs when energy barrier from the metal Fermi level to the HOMO/LUMO level of OMS is high (>0.5 eV) for charge carrier injection. Richardson-Schottky (RS) thermionic injection and Fowler-Nordheim (FN) tunneling mechanisms are the two models, which describe the charge carrier injection through metal/OMS interface [Fowler and Nordheim 1928, Simmons 1965].

RS mechanism is based on thermally assisted injection and is usually more significant at high temperatures where the carriers have sufficient thermal energy to overcome the energy barrier. This process is also assisted by field induced lowering of energy barrier [Simmons 1965, Emtage and O'Dwyer 1966, S.M.Sze 2008]. Hence, it is insignificant at low temperatures and for high potential barriers. In such situations,

carriers can be injected by quantum mechanical tunneling through the barrier as described in FN model, which is significant at high fields [Fowler and Nordheim 1928]. The J-V relation for such cases is given by the Fowler-Nordheim equation [Gao and Kahn 2001, Brütting 2005]:

$$J = AF^2 \exp\left(-\frac{K}{F}\right) \quad (1.4)$$

$$\text{where } A = \frac{q^3}{8\pi h\phi} \quad \text{and} \quad K = 8\pi \frac{\sqrt{2m}\phi^{3/2}}{3qh}$$

Here Φ is barrier height, m the effective mass of electrons in the active material, q the charge of an electron and h is Planck's constant. This treatment, which is purely quantum mechanical, also ignores the presence of localized states inside the OMS. In these models, the disordered nature of the semiconductor was ignored. In more recent models [Abkowitz et al. 1995, Conwell and Wu 1997, Arkhipov et al. 1999, Scott and Malliaras 1999, Wolf et al. 1999], hopping injection from the metallic electrode into OMSs has been taken into account.

1.5.3 Exciton formation and its decay

Generation of photon by the application of electric field in an OLED involves the field assisted carrier injection into the organic solids. The carriers transport by hopping between molecules under the influence of applied electric field. When electrons and holes come close to each other, they form excitons, after losing exciton binding energy [$E_b = e^2/(4\pi\epsilon\epsilon_0 r)$]. Excitons can be regarded as a bound electron hole pair coupled to lattice distortions. Radiative decay of an exciton gives rise to the emission of a photon [Ashcroft and Mermin 1976]. In OMSs, excitons are formed by either optical or electrical excitation. In optical excitation, atoms absorb photons due to optical pumping and as a result the electrons make transitions from HOMO to LUMO leaving a vacant state in HOMO [Atkins and Friedman 2010] that manifests as exciton. In OLEDs, exciton is formed by electrical pumping [Brütting 2005, Atkins and Friedman 2010]. In general there are three major types of excitons, known as Frenkel exciton, Wannier–Mott exciton and the charge-transfer exciton. The major differences in these excitons lie in their binding energy.

- i. **Frenkel Exciton:** In molecular solids with small dielectric constant, the coulombic interaction between electrons and holes is very strong (coulombic forces are inversely proportional to the dielectric constant) [Ashcroft and Mermin 1976]. This causes the exciton to be more tightly bound with large exciton binding energy (~ 100 meV - 1 eV). In most organic semiconductor, e^-h^+ pair is formed on the same molecule, analogous to molecular excited states (Figure 1.11) and the distance between this pair (radius of the exciton) is less than 1 nm. These small excitons are called Frenkel excitons. Due to large binding energy, they do not easily dissociate at room temperature. Therefore, they are useful for emission applications. Materials having Frenkel excitons are generally used for LED applications. Frenkel exciton have well - defined spin states (singlet and triplet), and their transport (diffusion) in solids is generally interpreted by Förster and Dexter energy transfer models [Ashcroft and Mermin 1976].
- ii. **Mott-Wannier Excitons:** In materials with large dielectric constant, the coulombic forces between electrons and holes are smaller and, hence, the size of exciton is larger [Ashcroft and Mermin 1976]. In this case, e^-h^+ pair is formed across two different molecules and, therefore the radius of the exciton is generally large (> 1 nm). This gives rise to a low exciton binding energy (< 100 meV) for this type of excitons. The electrons and holes are delocalized (Figure 1.11) and can be easily separated at room temperature, owing to the small Coulombic binding energy. The spin state of Mott-Wannier excitons is not well defined because of a rapid singlet–triplet exchange. The excitons generated in inorganic semiconductors are usually Mott-Wannier excitons. As they tend to dissociate very rapidly at room temperature, they play only a minor role in inorganic semiconductors.
- iii. **Charge transfer excitons:** These are intermediate between Frenkel type and Mott-Wannier type excitons. In such excitons, the electron and hole are separated but still tightly bound; the separated charges can be either localized or delocalized in relation to the lattice distortion. Sometimes Mott-Wannier excitons are also referred to as charge-transfer exciton (especially in case of organics used in photovoltaic applications). Charge transfer excitons are analogous to charge-transfer states observed in D-A molecules. They are often found in charge-transfer crystals, with electrons lying on one of the components and holes on the other component. On the other hand, they may also

be formed in solids consisting of only one organic compound. Therefore, materials having this type of excitons are useful for photovoltaic applications [Ashcroft and Mermin 1976].

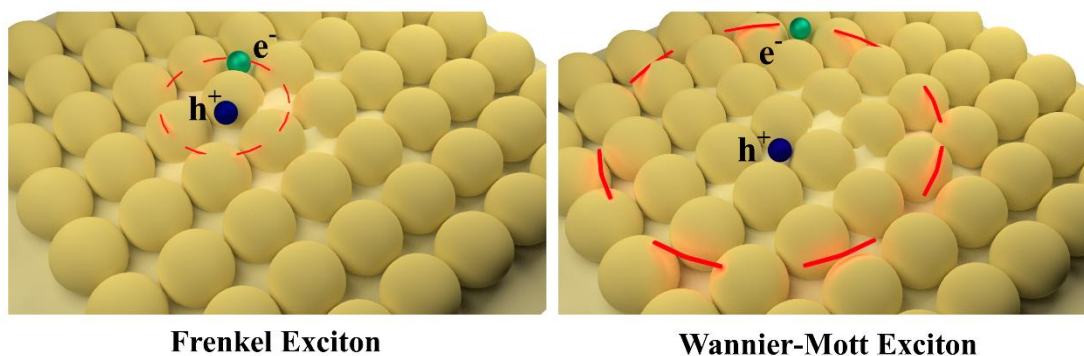


Figure 1.11 Schematic presentation of Frenkel and Mott-Wannier exciton
(redrawn from [Ashcroft and Mermin 1976])

1.6 MATERIALS FOR ORGANIC LIGHT EMITTING DIODES

The design of EL materials used in OLEDs is critical to device performance. Great strides have been made towards the development and improvement of molecular materials for display applications. Intense research in both academia and industry over the last decade has yielded OLEDs with remarkable color fidelity, device efficiencies and operational stability. The position of the HOMO and LUMO levels of the molecular layers is of special importance for their use in OLEDs. For a low drive voltage of the OLED device, the energy levels of all materials should be well matched to avoid barriers for charge carrier injection and for charge carrier transport at the interfaces of two materials. Furthermore, the mobility for majority carriers must be high in electron and hole transport materials. Further, for OLED device made by thermal evaporation, the small molecule materials used must necessarily have high thermal stability. Besides the thermal stability, most materials used in OLEDs have stable amorphous phase at the processing temperature, as it is beneficial for the morphological stability of the device [Schmechel and Seggernvon 2005]. The crystallization is believed to be a major lifetime limiting process for OLEDs, because it roughens the surface, which may result in contact delamination. In addition, by forming uniform films, amorphous materials

help to avoid grain boundaries, which may act as trap states during transport of charges [Schmechel and Seggern von 2005].

1.6.1 Anode Materials

The materials selected for anode should be high work function materials capable of injecting holes into the HOMO of the organic molecules. The general requirements for the material to be used as anode in OLED are

- i. High electrical conductivity so as to minimize contact resistance.
- ii. Must form good quality film with good ‘wetting’ when coated on organic materials so as to ensure good ohmic contact with the organic material.
- iii. Good thermal and chemical stability.
- iv. Must be transparent in visible region for ‘cathode on top’ configuration or highly reflective for ‘top emitting’ or transparent cathode device and
- v. High work function ($\Phi > 4.1$ eV) for efficient hole injection.

Clearly, in any light-emitting device, the light must couple out from the device. In most OLEDs the anode, usually made of a transparent conductor, is designed to act as such exit window for the device. ITO coated onto a glass or plastic substrate is the most frequently used anode material particularly in OLEDs with ‘cathode on top’ (i.e., bottom emitting) configuration. ITO is a highly degenerate n-type semiconductor with high conductivity. It is highly transparent in the visible region due to its band gap of 4 eV. It can make good “contact” with many organic materials. The work function of ITO is typically 4.5 eV, but can be increased up to 5.1 by surface treatment and it also depends on the oxygen content. This facilitates efficient injection of holes. Although other transparent and conductive electrode materials do exist (e.g., fluorine doped tin oxide, aluminum-doped zinc oxide), the commercial availability of glass substrates, pre-coated and (as needed) pre-patterned with ITO due to its extensive use in liquid crystal display (LCD) screens make ITO the most commonly used material [Brütting 2005, Klauk 2006, Jain et al. 2007, So 2010].

Besides ITO, other materials such as Poly (3,4-ethylene dioxy -2,4-thiophene)-polystyrene sulfonate (PEDOT: PSS) [Huh et al. 2008], noble metals like gold and platinum [Salaneck et al. 2001], aluminum, indium-doped zinc oxide, magnesium indium oxide and nickel tungsten oxide have been studied as anode materials for OLEDs. PEDOT: PSS is a conducting polymer and its thin films are transparent to the visible spectrum. It makes an emulsion in water. It can be easily spin coated as a film onto plastic or glass substrate to function as a transparent anode. When PEDOT: PSS is coated on top of ITO, the contact is ohmic for hole injection into many organic materials. Thin films (<1 nm) of gold and platinum are also transparent to the visible spectrum. The work function of gold and platinum are 5.1 eV and 5.6 eV respectively, and hence thin evaporated films can be used as anode. Often, a thin layer (< 10Å) of these noble metals are coated over a conventional anode like ITO, which then increases the work function and retains good transparency. Anode materials are typically deposited by evaporation, sputtering, or chemical vapor deposition methods. Other methods such as screen-printing, laser ablation, electrochemical deposition, etc., have also been employed [Brütting 2005, Klauk 2006, Jain et al. 2007, So 2010].

1.6.2 Hole Injection Materials (HIM)

Hole injection materials (HIM) are used to ‘modify’ the anode to improve the hole injection from anode to HTM. For multilayer OLEDs, the interfacial structure at the organic-metal and organic-organic interfaces plays an important role. A very thin film (1-2 nm) of HIM acts as an interface connection layer between the anode and the HTM, so as to improve the film formation and to facilitate efficient hole injection from anode to the HTM. The use of HIM decreases the operating voltage and improves the lifetime of the devices [Brütting 2005, Klauk 2006, Jain et al. 2007, So 2010].

The commonly used HIMs are copper phthalocyanine (CuPc), PEDOT: PSS, F₄TCNQ, ZnPc, or various inorganic buffer layers like TiO₂ and MoO₃ [Zhi-Feng et al. 2003]. CuPc layer has proved to be an effective HIM on ITO anode [Li 2015]. PSS rich PEDOT is also a preferred option for HIM [Jain et al. 2007, Li 2015]. The exact mechanism operating in PEDOT: PSS as HIM is still unclear, but the most accepted one is the creation of interfacial dipoles on the surface of PEDOT: PSS that helps in the

injection of holes to the HTM [Hwang et al. 2006, Li 2015]. Large roughness and spikes on bare ITO surfaces are undesirable and are effectively smoothed by PEDOT: PSS layer. On the negative side, commercially available PEDOT: PSS solutions used for the application have very short shelf-life. On the other hand, F₄TCNQ, an electron acceptor material, is now being widely used as HIM on ITO anode [Jain et al. 2007, Li 2015]. More recently, inorganic compounds like ZnO have also been used as thin buffer layer between ITO and HTM [Brütting 2005, Klauk 2006, Jain et al. 2007, So 2010].

1.6.3 Hole Transport Materials (HTM)

A thick layer (40-100 nm) of a HTM on top of ITO with or without HIM layer serves as an interface with the emitting layer and efficiently provides holes for exciton formation. It also creates an energy barrier for electrons and confines them to the emissive layer, well away from the anode. The general requirements for organic materials to be used as HTM are:

- i. High mobility values for holes.
- ii. The material should be easily oxidizable i.e., their HOMO level in the thin film should be close to the work function of the anode for easy hole injection.
- iii. High glass transition temperature and high thermal stability.
- iv. Reversible cyclic voltammogram for oxidation indicating stability of the cation radical.
- v. Large optical band gap

The frequently used hole-transporting materials in OLEDs such as N,N'- (3-methylphenyl)-1,1'-biphenyl-4,4'-diamine (TPD) and 4,4'-bis[N-(1-naphthyl-1)-Nphenyl-amino]-biphenyl (α -NPD) belong to the triarylamine family. The hole mobility values for TPD and NPD are 2×10^{-3} and 3×10^{-4} cm²V⁻¹s⁻¹ respectively. These molecules have low LUMO energy values (2-2.5 eV) and hence they also function as electron blocking material. Other than triarylamine family, CuPc, PEDOT: PSS and PTCDA: MoO₃ are also widely used HTM materials [Brütting 2005, Klauk 2006, Jain et al. 2007, So 2010, Li 2015].

1.6.4 Electron Transport Materials (ETM)

A thin layer (~ **6-10** nm) of ETM between the emissive layer and cathode promotes the electron injection during the device operation. This layer in contact with the cathode receives the electrons from the cathode and transports them to the recombination zone or anode. The electron mobility of organic molecules is less than hole mobility. In most cases, it is difficult to have an organic material with good mobility for both electrons and holes. The ETM also confines the holes within the emissive layer due to its large work-function. For the molecule to be used as ETM, the following criteria have to be met:

- i. High mobility values for electrons,
- ii. Energy of the LUMO level close to the work-function of cathode (low electron affinity) for easy electron transport and/or injection,
- iii. High glass transition temperature and high thermal stability
- iv. Stable under chemically reduced state,
- v. Large optical band gap

Common ETMs are based on electron deficient heterocycles, like oxadiazoles, triazoles, pyridine, pyrimidine, imidazole or triazine. Among ETMs, BCP, BPhen, TPBI and the metal chelate Alq₃ are the most commonly used materials [Brütting 2005, Klauk 2006, Jain et al. 2007, So 2010, Li 2015] Alq₃ is one of the most widely used electron transporting material since its first use in OLEDs [Tang and VanSlyke 1987] simply because it has a suitable LUMO level of ~ 3 eV to facilitate electron injection from the cathode. The value of electron mobility in Alq₃ is $1.4 \times 10^{-6} \text{ cm}^2 \text{V}^{-1} \text{s}^{-1}$ and hole mobility is $2 \times 10^{-8} \text{ cm}^2 \text{V}^{-1} \text{s}^{-1}$ [Brütting 2005, Klauk 2006, Jain et al. 2007, So 2010, Li 2015]. The origin of higher electron mobility than hole mobility in Alq₃ is due to specific arrangement of Alq₃ molecules in the solid state [Lin and Cheng 2005]. Besides working as an ETM, it also acts as emitting layer in green OLEDs. The electron mobility of TPBI is higher than that of Alq₃ and is of the order of 10^{-6} – $10^{-5} \text{ cm}^2 \text{V}^{-1} \text{s}^{-1}$ [Wong et al. 2001]. The value of electron mobility of BCP and BPhen is of the order of

$10^{-5} \text{ cm}^2\text{V}^{-1}\text{s}^{-1}$ [Jain et al. 2007, Gao et al. 2015]. BCP is also suitable as hole blocking material due to its low HOMO level of 6.5 eV [Adamovich et al. 2003, Brütting 2005, Klauk 2006, Jain et al. 2007, So 2010, Li 2015].

1.6.5 Electron Injection Materials (EIM)

A thin layer ($\sim 1 \text{ nm}$) of a EIM in contact with the cathode lowers the work-function of the cathode (e.g. Al) and hence facilitates electron injection into the ETM. The commonly used materials are LiF, CsF, Li_2O , MoO_3 [Li 2015]. One of the widely used EIM is LiF with Al as cathode and Alq_3 as ETM [Mishra et al. 2006]. The electron injection barrier has been shown to be closer by 0.4 eV in the case of $\text{Alq}_3/\text{LiF}/\text{Al}$ than Alq_3/Al [Mishra et al. 2006]. The mechanism of electron injection using EIM is still being debated. Nevertheless, the use of EIM with Al is as good as using low work function cathodes like Ca (2.87 eV) and Mg (3.66 eV) [Jain et al. 2007, So 2010].

1.6.6 Cathode Materials

The constraints on the cathode materials are fewer than those for the anode materials, because, usually cathodes need not be transparent to light. In certain instances, where a completely transparent OLED is needed (windshield and heads-up displays), ITO may also be used as the cathode with suitable modifications. In general, cathode materials are pure metals or metal alloys. Typically, they are low work-function elements such as Ca, Al, Cu, Ag, Au etc. Clearly, a low work-function facilitates electron injection into the lowest unoccupied molecular orbital (LUMO) level of the ETL material. However, low work-function also implies high chemical reactivity and problems can arise due to direct chemical reduction of organic materials in contact with such low work-function metals. Although production of such species may be detrimental to device performance, it may, in favorable circumstances, actually assist charge injection. Ease of oxidation of low work-function metals and alloys can also lead to difficulties in device processing due to sensitive to moisture and oxygen contaminants [Klauk 2006, Jain et al. 2007].

The requirements for the cathode materials are as follows:

- i. High conductivity

- ii. Low work-function to promote electron injection
- iii. Good film-forming and wetting properties to ensure good contact with adjacent organic layers,
- iv. Good thermal stability,
- v. Transparent if used in “top-emitting” OLEDs and highly reflective if used in “bottom-emitting” OLEDs

A frequently used cathode material is Al. Other popular cathode materials are LiF/Al (3.6-3.8 eV), Ca/Al, Mg/Ag (2.9 eV), and Ba/Al (2.6) [Klauk 2006, Li 2015]. Although even lower work-function can be achieved with Yb (2.4 eV), for example, the low optical reflectivity of the latter makes it less suitable for OLED applications. Very low work-function materials such as Cs, Ca (2.60 eV) etc. will have to be accompanied with another metal such as Al, Ag etc. to prevent reaction with atmosphere and, hence, increase the device lifetime. It is worth noting that the work-function of the metals depends on their purity, the deposition method and the surface structure, and the crystalline nature of the deposited films. Research on cathode materials has been focused on reduction of the high chemical activity of the low work-function metals (e.g., Ca/Al), the increase of chemical stability, and improvement of the sticking coefficient of the interlayer materials (e.g., LiF/Al).

1.6.7 Emissive or Light Emitting Materials (EML)

The most important material in any OLED is the emissive layer which generates the photons. The important requirements of light emitting materials are as follows:

- i. Must have high photo-luminescence quantum yield in the thin film form.
- ii. HOMO-LUMO energy levels must be compatible with those of the neighboring layers for efficient electron and hole injection from electrodes.
- iii. High glass transition temperature,
- iv. Large Stokes shift to avoid reabsorption of the emitted photon

- v. Good film forming property,
- vi. Efficient energy transfer from the host in a guest-host system.

The emitting layer may consist of a host material doped with another highly luminescent molecule as guest molecule. Energy transfer from the host (primary exciton) to guest (secondary exciton) makes possible to change the color of emission and/or increase EL efficiency, which is a common practice on phosphorescent OLEDs [Li 2015].

1.7 MAJOR CHALLENGES IN THE FIELD OF OLEDs

The recent studies of OLEDs are mainly focused both on optimizations of EL structures and on developing new optoelectronic emitting materials. The key point in OLEDs development for display and lighting applications is to find out materials emitting pure colors of red, green and blue (RGB) with excellent emission efficiency and high stability. Numerous materials with brightness RGB emission have been designed and developed to meet the requirements. Also, for using organic materials in device applications, the primary hurdle is still poor stability, short lifetime and low efficiency. The efficiency of an OLED can be improved by balancing the transport of charge carriers in the device. This is because optimum formation of excitons inside the emissive layer of an OLED requires the balancing of electrons and holes in this layer. Generally this is done by including HTL and ETL in the OLED architecture. A large number of materials showing both charge transport as well as emitting properties have been reported [Klauk 2006, Jain et al. 2007, So 2010]. Among these, derivatives based on naphthalimide and pyrene have been studied extensively because of their relatively high electron affinity values and better thermal stability [Justin Thomas et al. 2001, Liao et al. 2007, Oelgemöller and Kramer 2010, Thomas and Tyagi 2010, Liang et al. 2011, Hu et al. 2013, Marinova et al. 2013, Wang et al. 2014, Triboni et al. 2015].

1.7.1 Naphthalimide derivatives

Naphthalimide derivatives are an attractive class of organic materials for OLEDs, and are the most frequently studied materials as they hold great promise as efficient emitters [Grayshan et al. 1974, Ding et al. 2008, Bojinov et al. 2009,

Oelgemöller and Kramer 2010, Liu et al. 2012, Zhang et al. 2012, Lee et al. 2013, Wang et al. 2014, Triboni et al. 2015]. They have high electron affinities, wide energy gaps and low reduction potentials and making them good candidates for use as electron transport materials in OLEDs [Alexiou et al. 1990, Demeter et al. 1993, Wintgens et al. 1996, Oelgemöller and Kramer 2010, Wang et al. 2010] Their excited-state properties can be drastically changed by proper choice of the substituent on the aromatic ring [Grabchev et al. 1995, Martin et al. 1996, Cacialli et al. 1998, Niu et al. 2006, Wang et al. 2014]. Though many naphthalimides have been studied experimentally and theoretically in recent years, a very few reports on OLEDs based on naphthalimide derivatives are available [Grabchev et al. 1995, Cacialli et al. 1998, Niu et al. 2006, Bojinov et al. 2009, Wang et al. 2014, Jin and Tang 2013, Marinova et al. 2013, Arunchai et al. 2015, Jin and Ahmad 2015, Triboni et al. 2015]. Some of the recent significant reports on OLEDs based on naphthalimide derivatives are given below.

Xiao et al. [2012] studied an orange-red light material emitting dopant based on naphthalimide (TNGT). The device with the configuration: ITO/PVK: TNGT (20 wt%) (70 nm)/BCP (5 nm)/Alq3 (30 nm)/LiF (0.5 nm)/Al (100 nm) showed maximum luminance and efficiency of 6600 cd/m² and 4.57 cd/A, respectively.

Liu et al. [2012] reported novel blue light-emitting sextuple hydrogen-bonding self-assembly molecular duplexes bearing 4- phenoxy-1,8-naphthalimide fluorophores (PhNIHB). Employing PhNIHB as emitting materials, they fabricated solution-processed devices with structure of ITO/PEDOT: PSS (40 nm)/PVK (40 nm)/ PhNIHB (70–80 nm)/CsF (1.5 nm)/Al (120 nm). The devices emitted in blue-green region with maximum luminance and efficiencies of 73 cd/m², 0.37 cd/A (η_C) and 0.35% (η_{EQE}).

Wang et al. [2015] used a novel naphthalimide derivative 4-(N,N-dimethylamino)-N-(2'-fluorenyl)-1,8-naphthalimide (DFN) as electron-transporting electroluminescent material. The OLED device: ITO/ α -NPD/DFN/Al showed yellow-green emission with maximum luminance and efficiencies of 3563 cd/m², 0.2% (η_{EQE}) and 0.55 lm/W (η_p).

Triboni et al. [2015] studied 4-(2-fenoxy-p-xileno)-N-methyl-1,8-naphthalimide (NPOX) for blue OLEDs. Using the SCLC model, they obtained the value of the

mobility of the positive charge carriers ($\mu \sim 5 \times 10^{-5} \text{ cm}^2 \text{V}^{-1} \text{s}^{-1}$) for hole only device: ITO/ PEDOT:PSS (60 nm) / NPOX (170 nm)/ Al (120 nm). They used NPOX as the emitting layer in OLED with structure: ITO/ PEDOT:PSS (60 nm)/ NPOX (100 nm)/ Al (120 nm). the device showed emission in the blue region with maximum at 465 nm.

Arunchai et al. [2015] reported triphenylamino naphthalimides (TPN) derivatives as yellowish green emitting materials. They fabricated non-optimized OLED devices with ITO and LiF/Al as electrodes using PEDOT-PSS as the hole-injection layer which led to poor device performances. They inferred that the performance is the result of an improper barrier for electron migration at the interface between emissive layer and the LiF/Al electrode. They incorporated BCP as hole-blocking material in the device configuration: ITO/ PEDOT:PSS/ TPN:CBP/ BCP/ LiF/ Al with 6% TPN doped in CBP. The devices showed maximum luminance and efficiencies of 10,404 cd/m^2 at 14 V, 3.77 cd/A (η_c) and 1.11% (η_{EQE}).

Luo et al. [2015] reported novel derivatives based on naphthalimides (N1) for OLED applications. Using N1 as the dopant, a heavily doped standard-red organic light-emitting diode (OLED) with the device configuration of ITO/MoO₃ (1 nm)/TCTA (40 nm)/CzPhONI:N1 (14 wt%) (20 nm)/TPBI (45 nm)/LiF (1 nm)/Al (80 nm) was fabricated. The devices showed maximum external quantum efficiency and maximum current efficiency 1.8% and 0.7 cd/A , respectively.

Wang et al. [2015] studied the role of naphthalimide derivatives (CzPhONI) as host materials in fluorescent and phosphorescent OLEDs. They found that both efficient energy transfer and triplet energy up-conversion were involved in the emission mechanisms of CzPhONI-based fluorescent and phosphorescent OLEDs, while the characteristics of single-carrier devices proved that charge trapping followed by direct exciton formation in phosphorescent OLEDs. The devices had a structure of ITO (100 nm)/ NPB (30 nm)/ TCTA (10 nm)/ CzPhONI: dyes (20 nm)/ Bphen (40 nm)/ Mg: Ag (100 nm). The devices with rubrene and DCJTb as fluorescent dyes showed maximum luminance and current efficiency of 19,500 cd/m^2 and 15.0 cd/A , respectively. The devices with phosphorescent dyes (t-bt)2Ir(acac) and Ir(piq)₃ showed maximum luminance and current efficiency of 41,710 cd/m^2 and 44.2 cd/A , respectively.

1.7.2 Pyrene derivatives

Pyrene consists of four fused benzene rings, resulting in a large, flat aromatic system. Pyrene has been the subject of tremendous investigation. It exhibits a set of many interesting electrochemical and photophysical attributes [Tao et al. 2005, Tang et al. 2006, Thomas and Tyagi 2010, Figueira-Duarte and Müllen 2011, Liu et al. 2011, Krotkus et al. 2012], which have results in its utilization in a variety of scientific areas particularly in the field of organic electronics. Pyrene derivatives have been developed as RGB emitters in OLEDs because of their promising fluorescent properties [Jiang et al. 2001, Justin Thomas et al. 2001, Balaganesan et al. 2003, Liao et al. 2007]. In particular, these materials have a strong π -electron delocalization character and they can be substituted with a range of functional groups, which could be used for OLEDs materials with tunable wavelength. To date, various pyrene-based light-emitting materials have been disclosed in recent literatures [Justin Thomas et al. 2001, Balaganesan et al. 2003, Liao et al. 2007, Thomas and Tyagi 2010, Liang et al. 2011, Hu et al. 2013, Idzik et al. 2014, Ledwon et al. 2014, Peng et al. 2014]. Some of the recent significant reports on pyrene derivatives are given below.

Xing et al. [2005] reported ethynyl-linked carbazole-pyrene-based organic emitters (ECP) for OLED applications. The single layer OLEDs fabricated by doping ECP into PVK (10:1 w/w %). The device (ITO/PVK: ECP/Al) showed maximum luminance and efficiencies of 60 cd/m² 0.023 lm/W. To improve the device performance, they added an additional electron-transporting layer (TPBI) in the device configuration: ITO/PVK: ECP (60 nm)/TPBI (30 nm)/Al (100 nm). The performance of the device improved with maximum luminance and efficiency of 1000 cd/m² and 1.1 lm/W.

Sun and co-workers [Yang et al. 2007] reported dipyrenylbenzenes (dPB) as emitting materials for highly efficient OLEDs. The devices: ITO/NPB (50 nm)/dPB (30 nm)/BCP (10 nm)/Alq₃ (30 nm)/LiF (1 nm)/Al showed bluish green emission with maximum luminance efficiencies of ~1459 cd/m², and ~5.18 lm/W, respectively.

Moorthy et al. [2007] reported tetraarylpyrene derivatives for OLED applications. They studied the functional behaviour the derivatives as pure blue host

emitting materials in OLEDs with the configuration: ITO/NPB (40 nm)/AP (10 nm)/TPBI (40 nm)/LiF (1 nm)/Al (150 nm). The devices showed maximum luminance and efficiencies of 4730 cd/m², 2.7 cd/A (η_c) and 3.3% (η_{EQE}). The maximum luminance efficiency of 2.7 cd/A achieved underscores the fact that the attachment of sterically hindered substituents to the pyrene does indeed lead to suppression of face-to-face aggregation.

Cheng and co-workers [Wu et al. 2008] reported derivatives based on dipyranylbenzene (PPP). A bilayer device using PPP as the hole transporter and Alq₃ as the emitter emits green light at 513 nm, which can comparable to the common Alq₃-based devices using NPB as the hole transporter, indicated PPP as an excellent hole transporter. Furthermore, as emitter materials, the devices: ITO/CuPc (10 nm)/NPB (50 nm)/PPP (30 nm)/TPBI (40 nm)/ Mg:Ag/Ag showed blue emission with maximum luminance efficiencies of ~40400 cd/m² and ~ 5.2 %.

Lee and co-workers [Oh et al. 2009] reported pyrene-based electron transport materials (ANP): 1,6-di(pyridin-3-yl)-3,8-di-(naphthalen-1-yl)pyrene and 1,6-di(pyridin-3-yl)-3,8-di(naphthalen-2-yl)pyrene. They fabricated OLEDs with the standard device configuration with pyrene derivatives as ETMs and compared them with Alq₃ as ETM. The external quantum efficiencies of the devices with pyrene as ETMs increase by more than 50% at 1 mA/cm² compared with those of the device with representative Alq₃ as ETM. The enhanced quantum efficiencies are due to the balanced charge recombination in an emissive layer. The electron mobilities of the derivatives was $\sim 4 \times 10^{-5} \text{ cm}^2 (\text{Vs})^{-1}$ which is three times higher than that of Alq₃. The devices showed maximum efficiencies of ~2.0 lm/W.

Sellinger and co-workers [Sonar et al. 2010] reported 1,3,6,8-tetraarylpyrenes (TAP) for OLED applications. The fabricated blue OLEDs: ITO/PEDOT: PSS (50 nm)/TAP (50 nm)/TPBI (20 nm)/Ca (20 nm)/Ag (100 nm) showed maximum luminance and efficiency of 5015 cd/m² and 2.56 cd/A, respectively. The turn-on voltage for the device of around 3 V is quite low, suggesting that the barrier for hole injection from PEDOT: PSS is low.

Tao et al. [2010] reported new carbazole/fluorene/pyrene-composed organic light emitting hybrids (CFP). Tri-layer OLEDs with CFP as emitter materials were studied using the configuration: ITO/NPB (50 nm)/CFP (20 nm)/TPBI (30 nm)/LiF (0.5 nm)/MgAg (100 nm). The devices emitted in deep-blue region with turn-on voltage of < 3.5 V. The device showed maximum luminance and current efficiency of 7332 cd/m^2 4.4 cd/A (at 3.1 lm/W).

Peng et al. [2014] reported phenanthroimidazole derivatives (PPP) bearing terminal pyrene unit. The devices with configuration: ITO/NPB (45 nm)/PPP (15 nm)/TPBI (40 nm)/LiF/Al showed green emission with maximum luminance and current efficiency of 1149 cd/m^2 and 0.92 cd/A , respectively.

Tao et al. [2005] reported a series of fluorene derivatives (FP) in which pyrenyl groups are introduced. Using these derivatives as host emitters, blue-light-emitting OLEDs were fabricated in the configuration of ITO/CuPc (15 nm)/NPB (50 nm)/FP (30 nm)/Alq₃ (50 nm)/Mg:Ag (200 nm). The devices showed turn-on voltages of ~ 5.8 V with maximum luminance and efficiencies of 14300 cd/m^2 and 5.0 , respectively. The studied devices using a hole-blocking layer to confine and enhance electron-hole recombination in the EML with the configuration: ITO/CuPc (15 nm)/NPB (50 nm)/FP (30 nm)/TPBI (50 nm)/Mg:Ag. Compared to the Alq₃-based device, the TPBI-based device showed higher efficiency of 5.3 cd/A with a lower turn-on voltage of 5.2 V.

1.8. SCOPE AND OBJECTIVES OF THE THESIS

1.8.1 Scope of the Thesis

As already stated, the efficiency of OLEDs can be improved by balancing the charges in the OLED structures. The charge carrier balancing depends upon the electron mobility in ETL and hole mobility in HTL and their respective film-thicknesses. Their mobilities and thicknesses must necessarily be optimized in order to obtain equal number of electrons and holes inside the emissive layer. However, the hole mobility in HTL is usually much higher than the electron mobility in ETL under the same electric field. For example, the electron mobility of the most widely used ETL material, i.e., Alq₃, is $\sim 10^{-6} \text{ cm}^2/\text{Vs}$ [Kepler et al. 1995, Naka et al. 2000], while the hole mobility of the most widely used HTL, i.e., α -NPD, is $\sim 10^{-4} \text{ cm}^2/\text{Vs}$ [Naka et al. 2000, Brütting

2005]. Currently, search is on to find new electron transporting emitters with a high ionization potential values or to find ways to increase the mobility of the existing ETLs by some means. Though a large number of thermally stable and efficient hole-transporting materials are available, only a few efficient electron transport materials having good mobility and thermal properties have been discovered [Justin Thomas et al. 2001, Kulkarni et al. 2004, Tung et al. 2005]. Materials like Alq₃ and Bphen are generally used as electron transport materials but they have rather low charge carrier mobility [Justin Thomas et al. 2001, Kulkarni et al. 2004, Tung et al. 2005]. Hence, research efforts have focused on exploring electron transport properties of novel n-type materials for use as electron transport materials in the development of high efficiency OLEDs. Naphthalimide and Pyrene derivatives have been extensively studied as emitting materials with good charge transport abilities. In view of that, it is imperative to study the role of these derivatives in OLEDs as emitting materials as well electron-transporting materials. Moreover, it is also essential to study the charge carrier mechanism in these derivatives. Accordingly, this thesis work has been carried out with the following objectives.

1.8.2 Objectives of the Thesis

- i. To study the photo-physical, thermal, morphological and electrochemical properties of novel naphthalimide derivatives.
- ii. To fabricate OLEDs and demonstrate the electron transport and electroluminescent properties of naphthalimide derivatives and compare it with standard electron transport material, Alq₃.
- iii. To study the role of naphthalimide derivatives as host material in red OLEDs using red dopant DCM with Rubrene as assistive dopant and compare with standard host material, Alq₃.
- iv. To fabricate OLEDs and demonstrate electron transport and electroluminescent properties of pyrene derivatives and compare with standard Alq₃.
- v. To study the charge transport mechanism in pyrene derivatives.

1.9 ORGANIZATION OF THE THESIS

The contents presented in the thesis have been broadly divided into six chapters with several sections in each chapter.

Chapter 1 presents a brief overview of the field of organic electronic devices. This is followed with materials used for making them and their characterization. A review of the earlier work on organic semiconductors and their application in organic light emitting diodes is presented. Lastly, the motivations, scope and objectives of the thesis are presented followed by a summary of all the chapters in the thesis.

Chapter 2 discusses the various organic materials, device structures, device fabrication and characterization techniques used during this work. A brief description of each of these is provided.

Chapter 3 discusses the material protocols of novel naphthalimide derivatives obtained by the substitution of electron donating phenoxy groups at the C-4 position. A detailed discussion on experimental results is presented.

Chapter 4 presents the suitability of naphthalimides as blue light emitting electron transporter materials for organic light emitting diodes. This is realized by fabricating OLEDs with naphthalimides as electroluminescent materials, electron transporting materials and electron transporting emitters using different device configurations. Also, naphthalimides as host materials for Red OLEDs is included.

Chapter 5 presents the application of pyrene derivatives in organic light emitting diodes. This is realized by fabricating OLEDs with pyrene as electroluminescent materials, electron transporting materials and electron transporting emitters using different device configurations. Further, the transport mechanism pyrene has been investigated by analyzing its temperature dependence in electron only devices.

Chapter 6 outlines the summary of the work presented in the thesis along with important conclusions drawn from the study. Scope for further research has also been included in this chapter.

References used have been listed at the end followed by the Bio-data.

CHAPTER 2

MATERIALS AND EXPERIMENTAL TECHNIQUES

Overview

Chapter 2 discusses the various organic materials, device structures, device fabrication and characterization techniques used during this work. A brief description of each of these is provided. It starts with a brief description of relevant materials, classified according to their functionalities and their properties. This is followed with the description of the material characterization techniques used for study of photo-physical, electrochemical, morphological, thermal properties as well as description of other instruments used to analyze the materials. Different device structures, the fabrication techniques and the devices characterizations that were employed are explained.

2.1 MATERIALS USED IN THIS WORK

The materials used in the study are based on small molecular OMSs which are grouped according to their functionalities such as hole injection, hole transport, light emission, hole blocking, electron transport, electron injection and electrodes. Several new electron-transporting electroluminescent molecules are described in Chapter 3 and Chapter 5. The molecular formulae of the organic materials used in this work are presented in Figure 2.1. The corrected chemical designation of each organic compound can be found in Table 2.1. The lowest unoccupied molecular orbital (LUMO) and the highest occupied molecular orbital (HOMO) of most of these materials are depicted in Figure 2.2. F₄TCNQ, α -NPD, Alq₃, BCP, CBP, Ir(ppy)₃, DCM, Rubrene, LiF and Al were obtained from commercial sources. Naphthalimide derivatives were synthesized in the Department of Chemistry, National Institute of Technology, Surathkal (India) and Pyrene derivatives were obtained from Indian Institute of Chemical Technology, Hyderabad (India). All these materials were used as received. The materials used for the various layers of the OLED device are described below:

Anode: Glass substrates with patterned Indium Tin Oxide (ITO, 120 nm), procured from M/S Xin Yan Technology Ltd., Hong Kong, having a sheet resistance of 15 Ω/\square were used as Anode for hole injection. The work function of ITO varies from 4.4 eV to 4.9 eV and depends on the method employed for depositing the ITO film and

subsequent surface treatment carried out prior to deposition of the organic layers [Brütting 2005, Klauk 2006, So 2010].

Table 2.1 Chemical description of the organic materials used in this thesis

Abbreviation	Chemical description
F ₄ TCNQ	2,3,5,6-tetrafluoro-7,7,8,8-tetracyano quinodimethane
α -NPD	N,N'-di(1-naphthyl)-N,N'-diphenyl-[1,1'-biphenyl]-4,4'-diamine
Alq ₃	Tris-(8-hydroxyquinoline)aluminum
LiF	Lithium Fluoride
BCP	2,9 dimethyl 4,7 diphenyl 1,10 phenanthroline
Ir(ppy) ₃	Tris[2-phenylpyridinato-C ² ,N]iridium(III)
CBP	4,4'-Bis(N-carbazolyl)-1,1'-biphenyl
DCM	4-(Dicyanomethylene)-2-methyl-6-(4-dimethylaminostyryl)-4H-pyran
Rubrene	5,6,11,12-Tetraphenylnaphthacene

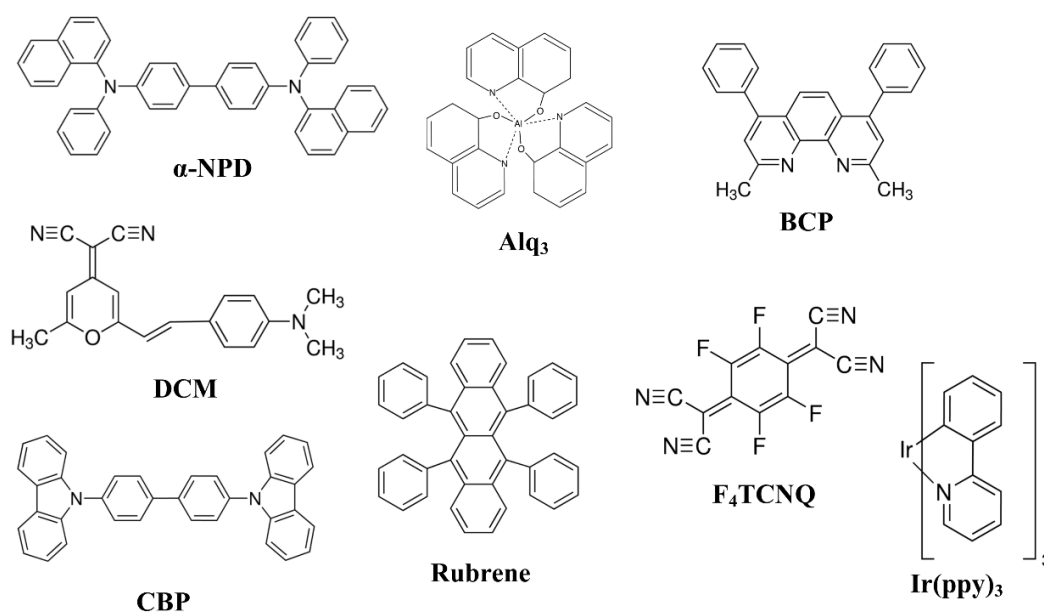


Figure 2.1 The molecular structure of the organic materials used in this work.

Hole Injection Material: The acceptor molecule 2,3,5,6-tetrafluoro-7,7,8,8-tetracyano quinodimethane (F₄TCNQ, Lumtec Taiwan, Sublimed grade purity >99%) is one of the most efficient hole injection materials (HIM). It acts as a p-type dopant in order to increase the conductivity of hole transport materials (HTMs). LUMO of F₄TCNQ (~5.1

eV) matches with HOMO of the HTM used in this study. Therefore, electron transfer from HOMO of HTMs to LUMO of F₄TCNQ generates a hole in HOMO of HTMs, thereby, increasing the carrier concentration in HTM [Brütting 2005, Klauk 2006, So 2010].

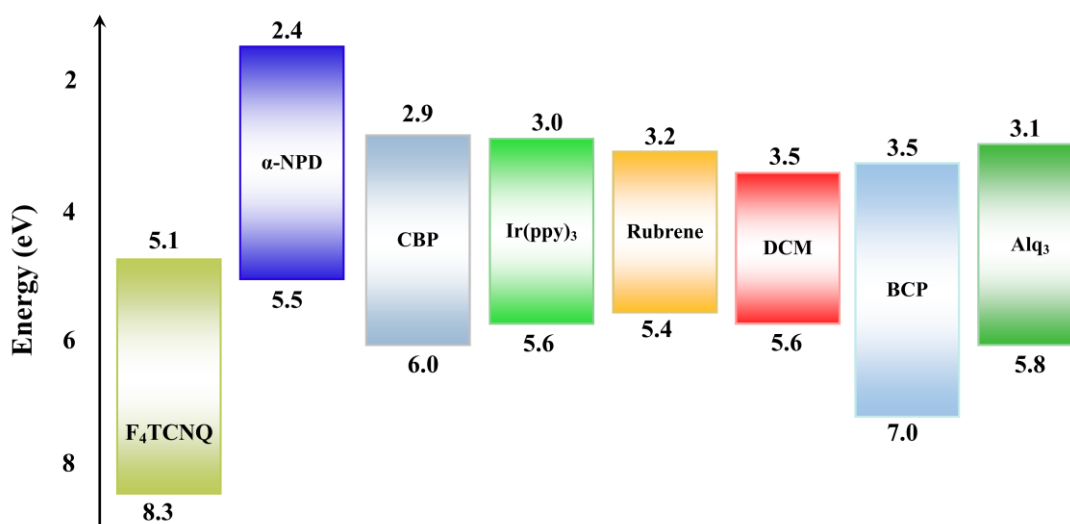


Figure 2.2 The HOMO and LUMO energy levels of most organic semiconducting materials used in the work [Brütting 2005, Klauk 2006, Jain et al. 2007, So 2010].

Hole Transport Material: In the present study, N,N'-di(1-naphthyl)-N,N'-diphenyl-[1,1'-biphenyl]-4,4'-diamine (α -NPD, Sigma Aldrich, Sublimed grade purity >99%) was used as hole transport material (HTM); it is one of the most widely used HTMs in OLEDs. One of the reasons for its popularity is because sublimed α -NPD can be manufactured readily and is thus abundantly available. However, the rather low glass transition temperature (T_g) of 95 °C may affect its morphological stability at high operating temperature. It has HOMO level of ~5.4 eV which ensures an efficient hole injecting contact [Brütting 2005, Klauk 2006, So 2010].

Electron Transport Material: In this study, Tris-(8-hydroxyquinoline) aluminum (Alq₃, Sigma Aldrich, Sublimed grade purity >99.99%) was used as ETM. It has LUMO values close to work function of Aluminum, used as the cathode in this work. Alq₃ act as both green emitter material and electron transport material. Alq₃ is a very good material for OLED devices because it possesses three important properties, viz., a large Stokes-shift (leading to negligible re-absorption of emitted light), relatively high

electron mobility and appropriate values of the HOMO (~5.7 eV) and LUMO (~3.0 eV) energy levels [Brütting 2005, Klauk 2006, So 2010].

Emissive Materials: The emissive materials used in this work are of two types: fluorescent and phosphorescent materials. Ir(ppy)₃ doped CBP (Sigma Aldrich, Sublimed grade purity >99.99%) was used as a green phosphorescent emissive material. For red OLEDs, DCM and Rubrene were used as dopants. Novel naphthalimide derivatives (see Chapter 3) and novel pyrene derivatives (see Chapter 5) were used as fluorescent materials. Alq₃ was also used as green fluorescent material.

Hole Blocking Material: 2,9 dimethyl 4,7 diphenyl 1,10 phenanthroline (BCP, Sigma Aldrich, Sublimed grade purity >99.99%) was used as hole blocking material. Its basic functionality is to block extra holes, which pass through the emissive layer without recombination. The high HOMO value of BCP (~6.5 eV) satisfies this requirement by confining the holes to the emissive region [Brütting 2005, Klauk 2006 So 2010].

Electron Injection Material: Lithium Fluoride (LiF, Sigma Aldrich, Anhydrous >99.99%) was used as an electron injection material, because LiF may n-dope the organic/Al interfaces and thereby can make the contact more ohmic [Brütting 2005, Klauk 2006 So 2010].

Cathode: Aluminum (Al, Alfa Aesar, purity >99.99%) was used as cathode. It has a work function of approximately 3.7 eV [Krishna et al. 2009]. We have coated Al electrodes for our study under normal vacuum (1×10^{-5} – 4×10^{-6} torr). After formation of an oxide layer it is much less reactive, which makes it attractive for commercial applications [Brütting 2005, Klauk 2006, So 2010].

2.2 MATERIAL CHARACTERIZATION TECHNIQUES

2.2.1 Single crystal XRD

Single crystal X-ray Diffraction (XRD) data was obtained using the BRUKER APEX II Duo CCD single Crystal X-ray Diffractometer equipped with a micro-focus Mo K α radiation ($\lambda = 0.71073 \text{ \AA}$) at room temperature. The ORTEP diagram and packing diagram were created using Mercury 3.1 software.

2.2.2 Photo-physical measurements

UV-Vis Absorbance: Absorption of chromophores are generally determined using UV-Vis absorption spectroscopy. Absorption spectra of molecules in solution taken in a quartz cuvette of 1 cm path length as well as a thin solid film were recorded using UV-Visible spectrophotometer (Ocean Optics Inc. SD 2000) having 0.6 nm resolution. Absorption spectra were corrected for the absorption of blank substrates or pure solvents in a reference cuvette.

Steady state Photoluminescence measurements: Steady state photoluminescence (PL) spectrometry is widely employed to explore the excited state property of the molecule. Room temperature PL spectra of the thin films and the solutions of the derivatives in different solvents were taken by exciting the samples using light of particular wavelength (usually the wavelength of peak absorption). Steady state PL spectra and quantum yield measurements in the visible region have been recorded on Fluoromax-4 TCSPC spectrophotometer (Horiba Jobin Yvon) at room temperature. This instrument is equipped with a steady state and transient excitation source and a Photomultiplier Tube (PMT). The spectrophotometer has been corrected for the wavelength dependence of the sensitivity of the detectors and throughput of the monochromators. Figure 2.3 shows a photograph of this system. The spectrometer uses a 150 W xenon lamp as the excitation source (light source) with a broad-spectrum emission. The detector used was R-928 PMT operating at a voltage of 950 V) in photon counting mode. The excitation and emission slit widths were 5 nm. The spectral data were collected using FluorEscence software and data analysis was done using OriginPro 6.0 software. A monochromator placed before the sample chamber selects the wavelength used to excite the sample. Right angle geometry was used for the measurements in the case of solutions taken in cuvettes. For solid thin films, the measurement was done with the 'front-face' arrangement. In this arrangement, the emission from the sample is collected at an angle of 45° to the excitation light beam. The emission spectra data were also corrected for the spectral sensitivity of the photomultiplier PMT (R-928). Different cutoff filters were used in the monochromator, whenever required, to prevent overtones. The fluorescence quantum yield (Φ) of the derivatives was determined on the basis of absorption and PL spectra in chloroform

(CHCl₃) by a comparative method using 9,10-diphenylanthracene ($\Phi_{ref} = 0.90$ in cyclohexane) as a standard [Brütting 2005, Klauk 2006, So 2010].



Figure 2.3 Fluoromax-4 TCSPC spectrophotometer for steady state and time resolved photoluminescence measurements

Time resolved photoluminescence decay and spectra: Room temperature fluorescence lifetime measurements were done using a Fluoromax-4 TCSPC Spectrophotometer (Horiba Jobin Yvon) attached with a NanoLED excitation source using the time-correlated single-photon counting (TCSPC) technique. A 350 nm pulsed NanoLED was used as excitation source for all the measurements. The fluorescence decay was acquired with a peak preset of 5,000 counts with a repetition rate of 1 MHz and coaxial delay of 60 ns. The decay data was analyzed using Data Analysis Software 6 (DAS6). TCSPC technique was used for measuring the photoluminescence intensity decays from the excited organic molecules in solution and thin film. In this method, the sample is excited by NanoLED pulses at high repetition rate, and the time difference between the excitation pulse and the arrival time of the ‘single’ fluorescence photon at the detector during excitation is measured [Brütting 2005, Klauk 2006, So 2010].

2.2.3 Electrochemical measurements

Electrochemistry was used to determine the oxidation and/or reduction potential of the new molecules in polar solutions. The linear correlation of electrochemical oxidation and reduction potential of organic molecules were determined in a solvent such as acetonitrile. The ionization potential and electron affinity of the molecules in solid state are well established [Wang et al. 2010]. The electrochemical studies of the naphthalimide derivatives, to obtain the energies of the HOMO and LUMO levels, were

performed experimentally using Cyclic Voltammetry (CV) measurements. CV using a conventional three-electrode cell system is the preferred electrochemical method for such studies. All the CV experiments were performed using AUTOLAB PGSTAT-30 electrochemical analyzer (scanning rate of 10 mV s^{-1}) at room temperature. The measurements were done in acetonitrile (10^{-3} M) solutions of the samples with tetrabutyl ammonium hexafluoro phosphate solution (0.1 M in acetonitrile) as supporting electrolyte [Wang et al. 2010]. All solutions in the cell were purged with ultra-pure N_2 for 10-15 min before each experiment, and a blanket of nitrogen was used during the experiment. Ag/AgNO_3 in 0.1 M acetonitrile was used as reference electrode. Platinum was used as the working electrode as well as counter electrode. Each measurement was calibrated with ferrocene/ferrocenium (Fc/Fc^+) redox system as internal standard [Wang et al. 2010]. The experimental error in the determination of oxidation potential using CV is about $\pm 10 \text{ mV}$. CV determines the oxidation potential (E_{ox}) as the energy that is necessary to remove an electron from the molecule when it is surrounded by the solvent and in the presence of an electrolyte.

2.2.4 Thermal Properties

Thermo Gravimetric Analysis (TGA) and Differential Thermal Analysis (DTA) were carried out up to $600 \text{ }^\circ\text{C}$ on EXSTAR 6000, TG/DTA 6300 thermal analyzer. Melting points were estimated using open capillary method and Differential Scanning Calorimetry (DSC). DSC measurements were performed using a SHIMADZU DSC-60. A constant heating rate of $10 \text{ }^\circ\text{C min}^{-1}$ was used to melt and decompose the derivatives under nitrogen atmosphere at a flow rate of 30 mL min^{-1} for both DSC and TGA.

2.2.5 Surface Morphology

The roughness of the organic films was determined from the topography image of the surface obtained using Atomic Force Microscope (AFM). The effect of the deposition rate on the morphological properties of organic thin films were assessed by AFM. Atomic Force Microscope from M/S Park Systems (XE-70 AFM), shown in Figure 2.4, is used to characterize the surface morphology of the thermally deposited OMS thin films on the substrates. The AFM images were taken in the non-contact mode under ambient conditions.

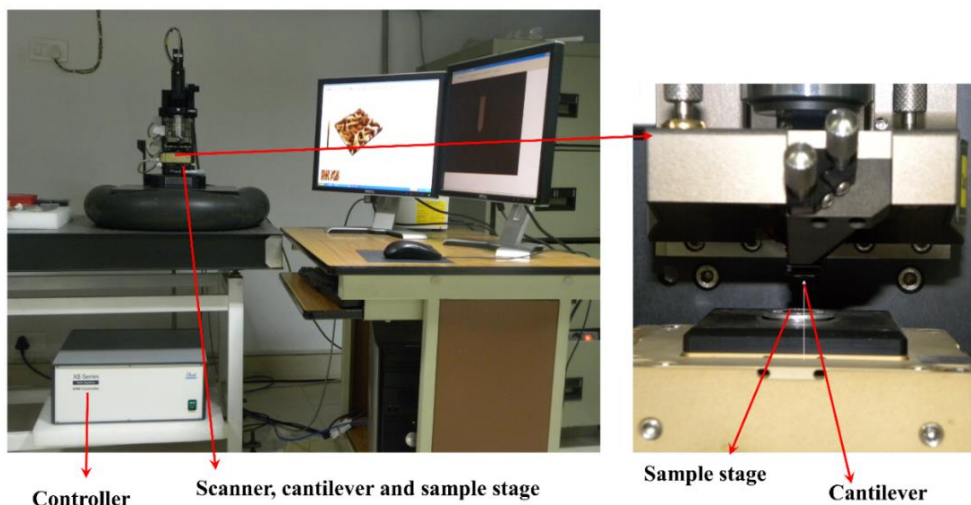


Figure 2.4 Park Systems XE-70 AFM

2.3 DEVICE STRUCTURES

In the present work, two types of devices were fabricated: electron only devices and light emitting devices. In this section, the device structures are described.

Electron Only devices: In order to study the electron transport in electron transport materials (ETMs) used in our OLEDs (discussed in chapter 5), electron only devices were fabricated. A thin film of the ETM material is sandwiched between low work function metal (aluminum) to fabricate electron only devices. If the energy barrier for electron injection is quite low in comparison to the energy barrier for hole injection, then the current in the device will be only due to the electrons. Figure 2.5 shows the schematic device structure used for the electron transport study.

Organic Light Emitting Device: Figure 2.6 shows the structure of a typical multi-layer OLED, fabricated for our investigations. In this device, multiple organic layers are deposited over a transparent electrode on a glass substrate. ITO is used as an anode, which is transparent to visible light. The other layers of the OLED are in the order of HIL, HTL, EML, HBL, ETL and EIL. Finally, a metal with low work function is deposited over these organic layers and it works as a cathode. F₄TCNQ was used as HIL, α -NPD was used as HTL, naphthalimide/pyrene derivatives were used as EL, Alq₃ was used as both EL and ETL, and LiF was used as EIL. Al is generally used as cathode.

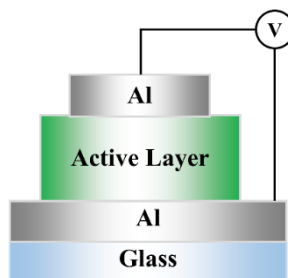


Figure 2.5 Schematic device structure of the electron only devices

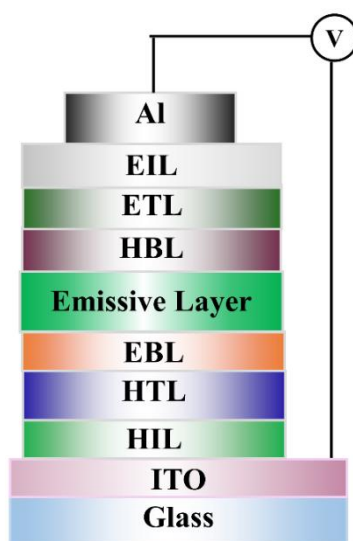


Figure 2.6 Typical device structure of a multi-layer OLED used in this study.

2.4 DEVICE FABRICATION

In this section, the steps used in the device fabrication are discussed. The fabrication steps are

2.4.1 Cleaning of patterned ITO coated substrates

The cleanliness of the substrate is very crucial for successful performance of the devices. Using unclean substrate leads to electrical shorting of the devices and also the contaminated area spreads to the whole device very quickly. Hence, before film deposition the substrates are thoroughly cleaned. Commercially, available patterned ITO coated glass substrates having a sheet resistance of 20 Ω /square and thickness of 120 nm are cut into pieces of size 1x1". Each piece has four ITO strips (2 mm x 25 mm) separated by 2 mm gap. The patterned ITO coated glass substrates are first washed with labolene solution and then rinsed well using distilled water. The substrates are then

ultrasonicated in labolene (to remove oil), deionized water (to remove the detergent), trichloroethylene, acetone (to remove most of the chemical contaminants), and then with IPA sequentially for 20 minutes each. Finally they are cleaned thrice ultrasonically with de-ionized water, each for 10 min, then dried using pure N₂ gas. The substrates were degreased with acetone. Cleaned substrates were then dried in a vacuum oven for 10 min at temperature 120°C. The cleaned ITO substrates were then treated by UV-generated ozone for 15 min. The ozone treatment of ITO serves in the removal of volatile impurities from the surface and increase in the work function of ITO from 4.5 eV upto 5.1 eV [Brütting 2005, Klauk 2006, So 2010].

2.4.2 Device Fabrication and Parameters

In the present work, films were deposited using Vacuum Thermal Evaporation (VTE) technique. This is a commonly used technique to make thin films of small organic molecules, which can sublime at high temperature in high vacuum and are thermally stable. This process is based on the sublimation of molecules, kept in a boat, which is resistively heated under high vacuum ($\sim 10^{-6}$ Torr). Separate VTEs were used for the fabrication of electron only devices and for OLEDs.

Fabrication of OLEDs: The fabrication of the OLEDs discussed in this thesis was done using an appropriately designed complete oil free VTE system equipped with turbo molecular pump as shown in Figure 2.7. The system is capable of evaporating six materials at a time with a rotatory filament arrangement. The organic materials in granular or powder form used for the deposition were put into small molybdenum boats. For deposition of cathode, Al wire was placed in a tungsten filament. The pre-cleaned ITO substrate was fixed to substrate holder kept at a distance of ~ 50 cm from the boat. The entire chamber was pumped down and evacuated using a turbo-molecular pump backed by roots pump to a base pressure of $\sim 10^{-6}$ Torr. The source boat/filament was heated by passing electrical current through it. The current flow through the boat/filament was controlled manually by a variac such that the evaporation rates for organic materials, LiF and Al metal electrode, were set to 0.5-1 Å/sec, 0.1 Å/sec and 5-6 Å/sec, respectively. The evaporated materials condense onto the surface of the substrate. The effective device area was ~ 1.6 mm².

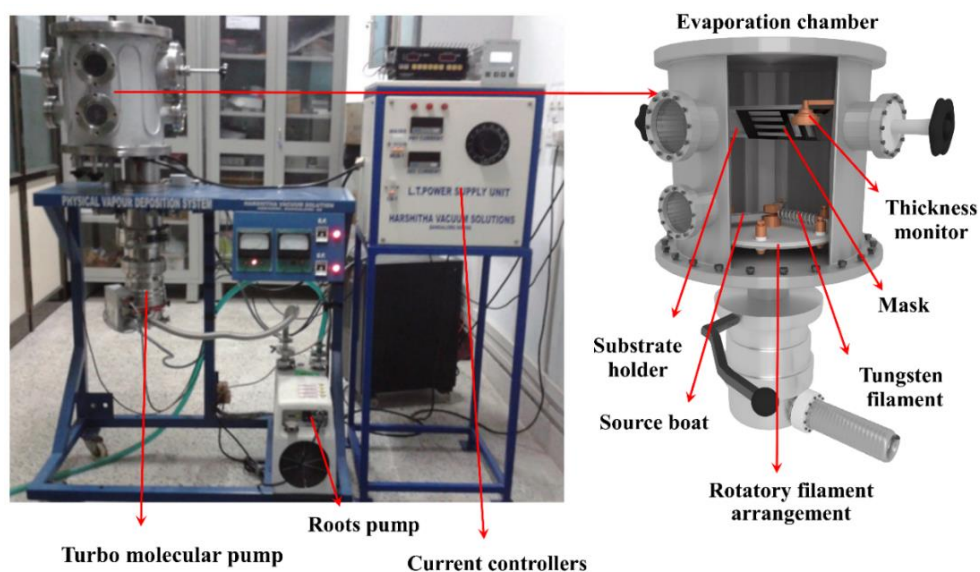


Figure 2.7 Physical vapor deposition system equipped with a turbo-molecular pump used for the fabrication of OLEDs

All the layers are coated without breaking the vacuum. The film thickness and the deposition rates were monitored in situ by a quartz crystal balance. The substrate holder can be rotated to move the substrate away from the vapor stream preventing further deposition of the film. Thus, the film deposition duration can be controlled by quick start/stop operation. Multilayer film deposition is done by keeping different materials in different boats and heating them in a proper sequence. Between successive depositions the chamber was pumped down to high vacuum and kept in that condition for typically 15 min for organic materials to avoid any contamination from material used in the preceding deposition step. LiF evaporation was done using molybdenum boat. After the deposition of LiF, a mask is slid on the substrate in order to coat Al through the mask, thereby creating a pixel cathode pattern.

Fabrication of electron only devices: The fabrication of the electron only devices discussed in this thesis was done using VTE system shown in Figure 2.8. Extra-dry piston pump for roughing vacuum (10^{-2} mbar) and turbo molecular pump for high vacuum (10^{-6} mbar) are used to make it completely oil free. The substrate temperature can be varied from 30°C to 250°C. Organic materials were evaporated using a molybdenum boat and Al was evaporated from tungsten filament. The temperature of the boat/filament is controlled by the resistive heating of the boat with a variable voltage

source.

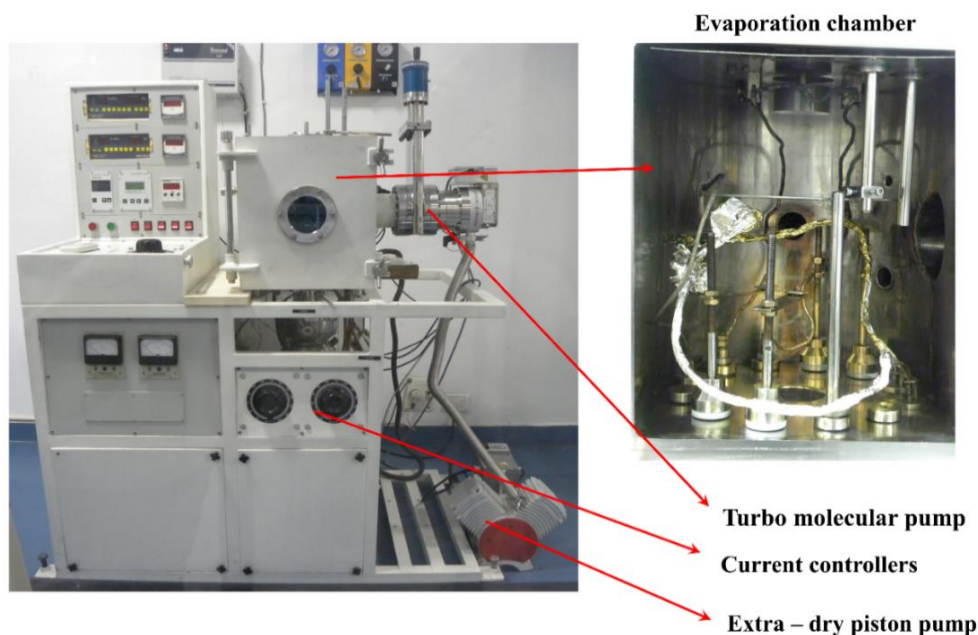


Figure 2.8 Oil free thermal evaporation system used for the fabrication of electron only devices

2.5 DEVICE CHARACTERIZATION

2.5.1 OLED characterization

The fabricated devices were characterized employing various techniques. Figure 2.9 shows schematic of the OLED characterization system. The characterization techniques are described below.

Current-voltage characterization: The current-voltage characteristics were measured using a Keithley source meter (2400). It has a built-in voltage source, which can supply ± 100 V and a current measuring range from 10 pA to 2mA and can be interfaced to a computer using IEEE card. Labtracer software was used to operate the source meter through computer.

Electroluminescence spectrum: Electroluminescence (EL) spectra were recorded using the Horiba Jobin Yvon iHR 320 spectrometer connected to a CCD (Synapse Horiba Jobin Yvon). The device was placed in a dark chamber to avoid external stray light. The pixel surface of the device was placed normal to the detector and voltage was

then applied to illuminate the pixel. EL spectrum was acquired using the SynerJY software.

Electroluminescence intensity: The EL intensity of the OLEDs was measured using a large area (10 mm diameter) calibrated Si photodiode (SM1PD2A) connected to Keithley 6485 Pico ammeter. The Si detector was placed at a fixed distance of 5 mm directly below the ITO side of the OLED device.

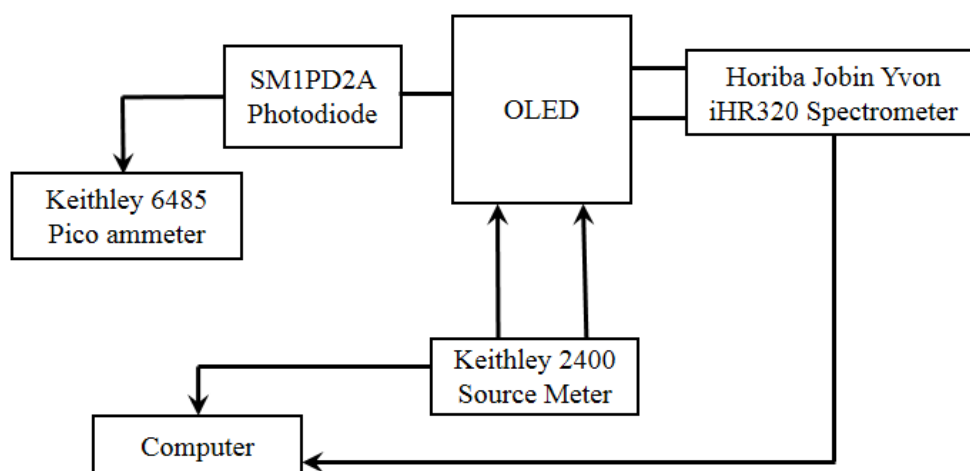


Figure 2.9 Schematic diagram for electrical and luminescence measurement setup for OLED characterizations

Calculation of EL brightness, Current and Power efficiency: Brightness of a display or light emitting device is quantified in units of candela and lumen. This requires conversion of intensity and spectral data measured by photodetectors. However, human eye is capable of detecting the electromagnetic radiation in visible region its responsivity varies significantly across the visible spectrum. Light intensity as measured by a calibrated Si detector gives photocurrent, which is converted to optical Watt using calibration data supplied by the manufacturer. Candela is the preferred unit of light intensity emitted by OLED for display purposes. Candela is lumen per steradian, lumen being the luminous power, which depends upon the sensitivity of the human eye. The standardized response of the eye of light is known as *photopic curve* [Hammond and Mason 1971], which is shown in Figure 2.10. By definition, an eye has a maximum efficiency of 683 lumens per incident optical Watt at a wavelength of 555

nm. From the *photopic curve* it is possible to calculate the responsivity (Φ) of the eye to a given EL spectrum in the visible region, $I_{EL}(\lambda)$ using the equation

$$\Phi = \frac{\int I_{EL}(\lambda)P(\lambda) d\lambda}{\int I_{EL}(\lambda) d\lambda} \quad (\text{lm/W}) \quad (2.1)$$

where $P(\lambda)$ (lm/W) is the photopic response.

The photocurrent I_{photo} (A) generated by EL at the Si diode can be converted to lumens by using the relation [Brütting 2005, Klauk 2006, So 2010],

$$B = \left(\frac{\Phi}{R_{det}} \right) I_{photo} \quad \text{lm} \quad (2.2)$$

and

$$R_{det} = \frac{\int I_{EL}(\lambda)R(\lambda)d\lambda}{\int I_{EL}(\lambda)d\lambda} \quad \text{A/W} \quad (2.3)$$

where $I_{EL}(\lambda)$ is the EL spectrum and $R(\lambda)$ is taken from the calibration curve (A/W) of the Si detector as supplied by the manufacturer.

The luminance (L , cd/m^2) of the device is calculated as B divided by the device area (A) and the solid angle (Ω). The current efficiency (η_c , cd/A) of the device is calculated by dividing brightness by current density (J , A/m^2). Power efficiency (η_p , lm/W) was calculated by dividing B by the electrical power ($V \times i_d$), where V is the applied voltage and i_d is the current through the device. The luminance and efficiencies are given by the expressions [Brütting 2005, Klauk 2006, So 2010]

$$\text{Luminance,} \quad L = \frac{B}{A \times \Omega} \quad \text{cd/m}^2$$

$$\text{Current Efficiency,} \quad \eta_c = \frac{L}{J_d} \quad \text{cd/A}$$

$$\text{Power Efficiency,} \quad \eta_p = \frac{B}{V \times i_d} \quad \text{lm/W}$$

Color coordinates: Electroluminescence (EL) spectra provide information about the exciton formation and recombination regions in the device. By examining EL spectra

and comparing them with spectral signatures of the materials constituting the layers of a hybrid structure, one can determine which of the materials contribute the most to the LED emission. Consequently, EL measurements provide an extremely important device design tool. Analogous to PL measurements, emission is collected into a spectrometer but the excitation of the emission in this case is electrical rather than optical. During the EL measurements, a voltage source is connected to a LED which results in current passing through the device and hence, exciton formation and recombination. It is apparent from the previous section, that the overlap of a LED EL spectrum with the standard luminosity function largely determines the perceived luminous efficacy or power efficiency. The position and shape of an EL spectrum also determines the color purity of a LED emission. According to the International 1931 Convention on illumination (Commission Internationale d'Eclairage (CIE)), all the colors can be plotted on the CIE color space defined by the CIE standard observer color matching functions. The CIE coordinates take into account the spectral response of three different color receptive cells in the eye, shown in Figure 2.11. It is possible to calculate the color coordinates of any light source. The coordinates (x, y) are calculated as [Brütting 2005, Klauk 2006, So 2010]

$$x = \frac{x'}{x' + y' + z'}$$

$$y = \frac{y'}{x' + y' + z'}$$

where

$$x' = \int I_{EL}(\lambda) X(\lambda) d\lambda,$$

$$y' = \int I_{EL}(\lambda) Y(\lambda) d\lambda,$$

$$z' = \int I_{EL}(\lambda) Z(\lambda) d\lambda$$

$I_{EL}(\lambda)$ is the EL spectrum of an LED

$X(\lambda)$, $Y(\lambda)$, $Z(\lambda)$ being the responsivity of the three receptors.

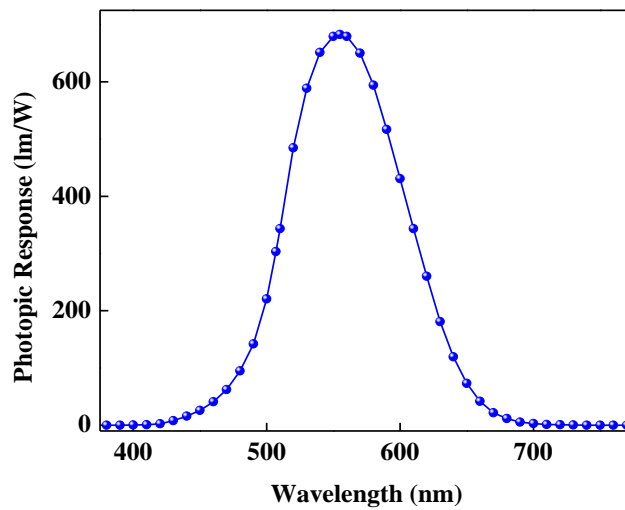


Figure 2.10 Photopic response of the cone photoreceptor cells in human eye.

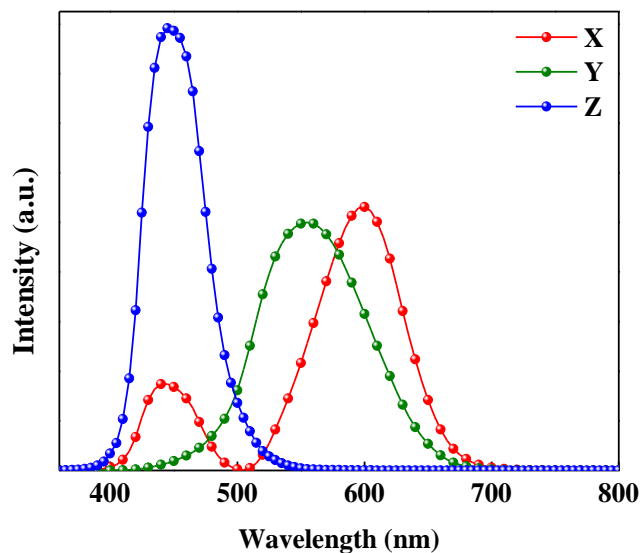


Figure 2.11 The standardized response of the three color-sensitive photoreceptors in eye [Hammond and Mason 1971, Klauk 2006, So 2010]

The CIE coordinates for an OLED is shown on a color map (Figure 2.12) to give an impression of the color sensed by human eye for a particular EL spectrum. The outer curve of a CIE color space is defined by the monochromatic sources at different wavelengths. For every light source, one can now find a corresponding point in the CIE diagram. The corners of the color space correspond to the pure red, pure green and pure blue colors. It is possible to obtain any color with arbitrary color coordinates by simply mixing the light from the pure sources. Consequently, when designing LEDs for display

applications it is desirable to create colors with CIE (x,y) coordinates close to the corners of chromaticity diagram [Brütting 2005, Klauk 2006, So 2010].

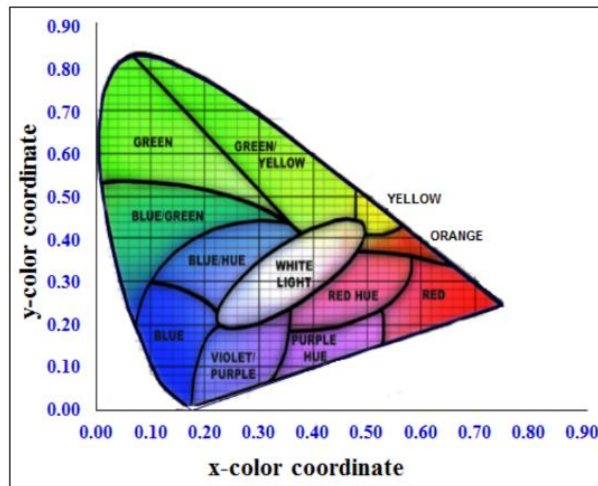


Figure 2.12 The CIE chromaticity diagram [Hammond and Mason 1971, So 2010]

2.5.2 Electron only device characterization

All the current-voltage measurements for electron only devices were performed using Keithley voltage sources and pico-ammeter interfaced via National Instruments GPIB 488.2 board as shown in Figure 2.13. The temperature dependence measurements were done inside a CTI-Cryogenics close cycle cryostat and temperature is controlled with Lakeshore temperature controller. Figure 2.14 shows snapshots of measurement setup and sample holder with a device mounted on it.

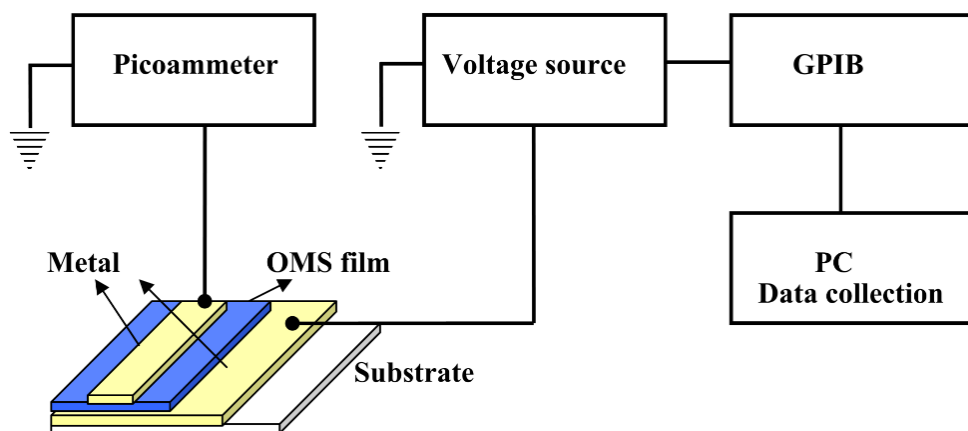


Figure 2.13 Schematic diagrams for I-V measurement setup for electron only devices.

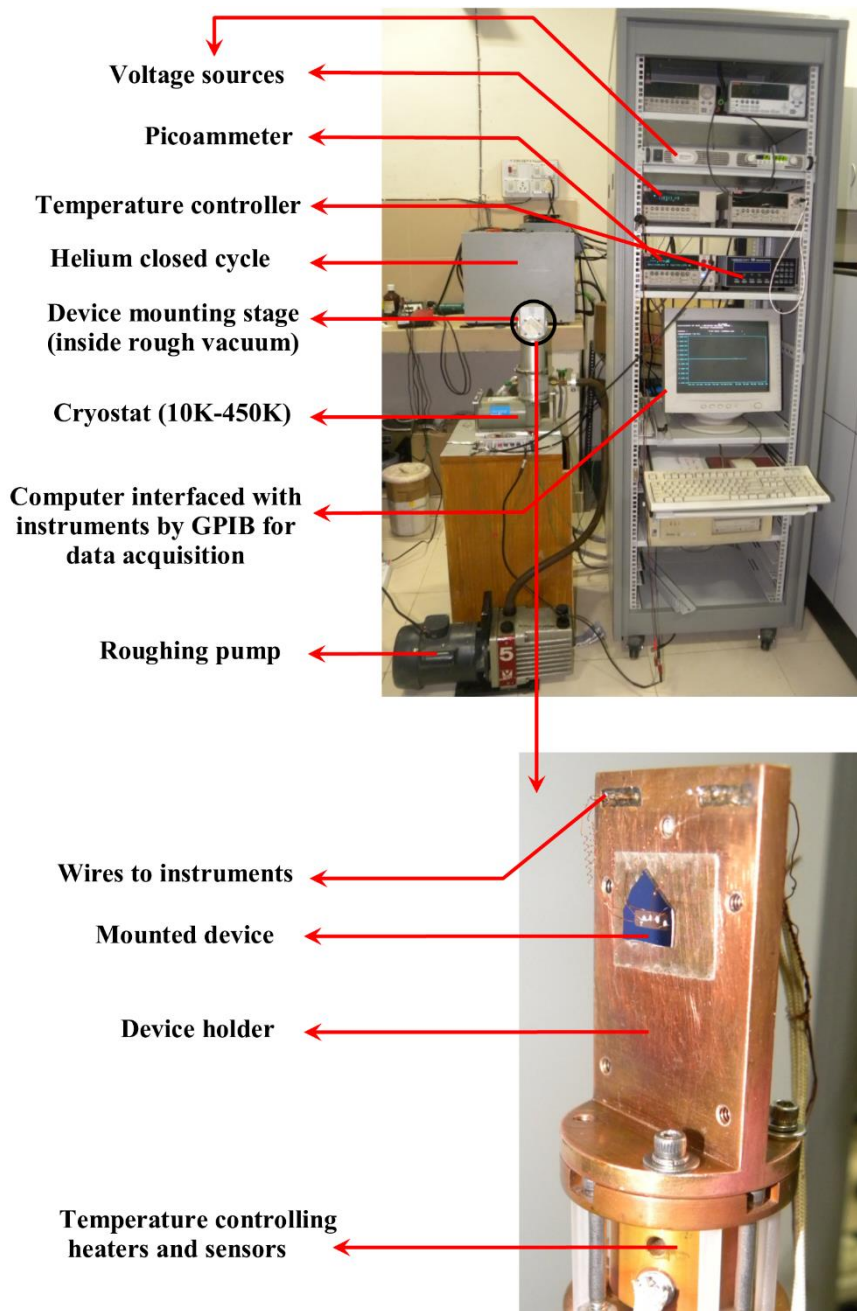


Figure 2.14: Measurement setup with sample holder used for temperature dependent electrical characterizations

2.6 CONCLUSIONS

A brief introduction of the materials used in the thesis was discussed. The various techniques to characterize the materials was presented. In addition, the fabrication techniques and characterizations of electron only devices and OLEDs was explained in detail.

CHAPTER 3

MATERIAL CHARACTERIZATION OF THE NOVEL NAPHTHALIMIDE DERIVATIVES

Overview

Chapter 3 describes the material protocols of twelve novel naphthalimide derivatives obtained by the substitution of electron donating phenoxy groups at the C-4 position. It involves the study of their photo-physical properties using UV-visible, steady-state emission and time-resolved photoluminescence spectroscopic techniques to explore their linear optical behavior. Further it covers the thermal, morphological and electrochemical properties of the derivatives. In addition, it deals with single crystal structural analysis of the selected material. A detailed discussion on experimental results is presented.

3.1 INTRODUCTION

1,8-naphthalimides show considerable promise in organic electronics, especially in OLEDs, and are the most frequently studied materials as they hold great promise as efficient emitters [Grayshan et al. 1974, Oelgemöller and Kramer 2010, Wang et al. 2010, Zhang et al. 2012, Lee et al. 2013, Triboni et al. 2015]. These derivatives are a special class of versatile photoluminescent materials, which possess unique photophysical properties. They are of great interest owing to their excellent PL quantum efficiency, good photo-stability and film-forming properties as well as desirable chemical and thermal stabilities [Ding et al. 2008, Bojinov et al. 2009, Oelgemöller and Kramer 2010, Liu et al. 2012, Zhang et al. 2012, Lee et al. 2013, Wang et al. 2014]. Naphthalimides possess wide energy band-gaps and low reduction potentials [Alexiou et al. 1990, Demeter et al. 1993, Wintgens et al. 1996, Oelgemöller and Kramer 2010, Wang et al. 2010] and their excited-state properties can be drastically changed by proper choice of the substituent on the aromatic ring [Grabchev et al. 1995, Martin et al. 1996, Cacialli et al. 1998, Niu et al. 2006, Wang et al. 2014]. In addition, the electronic absorption and emission in these materials depend on the properties of the surrounding medium.

The charge transfer (CT) characteristics of naphthalimide derivatives in excited states and their spectral properties have attracted considerable attention due to their relevance in organic photo-electronics [Grabchev et al. 1995, Martin et al. 1996, Cacialli et al. 1998, Niu et al. 2006, Wang et al. 2014]. In OLEDs, the advantage of C-

4 substituted naphthalimides is due to their low reduction potential and wide energy gaps, along with the high PL efficiency. Emission from intramolecular CT states contributes substantially to the EL of these devices. It has been reported that the presence of an electron-deficient center generally makes these derivatives acquire high electron affinity. Hence, it validates the presence of electron-transporting or hole-blocking capabilities that are appropriate for balanced carrier injection in OLEDs [Cacialli et al. 1998, Tian et al. 2000, RudenVon et al. 2010, Yang and Wang 2012]. One possibility to achieve this is by the substitution of electron donating groups at the C-4 position of 1,8-naphthalimide [Wang et al. 2010]. Without any substituents at the C-4 position, a nonpolar π - π^* state occurs in the parent NI. Introduction of electron-donating/electron-withdrawing substituents, such as N-substituted groups, C-substituted groups, and O-substituted groups, induces a polar CT excited state [Alexiou et al. 1990, Distanov et al. 1997, Bojinov et al. 2003, Islam et al. 2005, Yang et al. 2005a, 2005b, Magalhães et al. 2006].

The materials with CT character are especially interesting due to their strong oxidizing or reducing capacity. In general, non-substituted 1,8-naphthalimides present low PL quantum yield. Substitution of electron-donating groups usually increases the PL emission and hence PL quantum yield [Gan et al. 2004, Ding et al. 2008, RudenVon et al. 2010, Wang et al. 2010]. The PL emission color of these derivatives can be readily tuned from yellowish green wavelengths to pure blue by the introduction of different electron-donating substituents at the C-4 position of the naphthalimide moiety [Karamancheva et al. 1998, Grabchev et al. 2002, Gan et al. 2004, Ding et al. 2008, RudenVon et al. 2010, Wang et al. 2010]. By employing naphthalimide derivatives as emitters, efficient OLEDs have been obtained, such emitters having employed C-substituted groups (e.g. arylalkynyl, arylalkenyl) or N-substituted groups (e.g. arylamino, alkylamino) in the C-4 position. Thus, EL colors varying from greenish blue to orange have been generated [Gan et al. 2004, Islam et al. 2005, Wang et al. 2005, Liu et al. 2008, Mikroyannidis et al. 2009]

In this chapter, a detailed material characterization of twelve novel naphthalimide derivatives has been investigated. The molecular structures of the derivatives are shown in Table 3.1. The derivatives (**NI-x**) were obtained using 6-

bromo-2-(2-hydroxyethyl)-1H-benzo[de]isoquinoline-1,3(2H)-dione (**BNI**) as starting material by the substitution of electron donating phenoxy groups at the C-4 position. By the acetylation of derivatives **NI-x**, we obtained derivatives **NA-x**. The photophysical, thermal, electrochemical properties of all the derivatives were studied. As all the derivatives showed similar solvatochromic behavior, PL lifetime and morphological studies, only the results of **NI-Cl** and **NA-Cl** are included.

3.2 CRYSTAL STRUCTURE

To confirm the structures of the derivatives, single crystal XRD of **NI-Br** (a typical sample) was performed. Single crystals of **NI-Br** suitable for X-ray diffraction analysis were grown using its solution in methanol at room temperature. The solvent was evaporated slowly by passing through a parafilm plastic containing pinholes and a good quality crystal was obtained. Single crystal XRD analysis was carried out to determine its molecular structure and it tallied with that shown in Table 3.1. Crystallographic data of **NI-Br** are listed in Table 3.2. The ORTEP diagram with labeling and packing pattern of **NI-Br** are depicted in Figure 3.1. As can be seen from Figure 3.1, derivative **NI-Br** crystallizes in the triclinic space group *P*-1 with cell parameters $a = 7.7810(3) \text{ \AA}$, $b = 8.8770(3) \text{ \AA}$, $c = 12.6940(4) \text{ \AA}$, $V = 841.12(5) \text{ \AA}^3$ and $Z = 2$. The extensive $\pi \cdots \pi$ stacking interactions result in the head to tail arrangement of molecules.

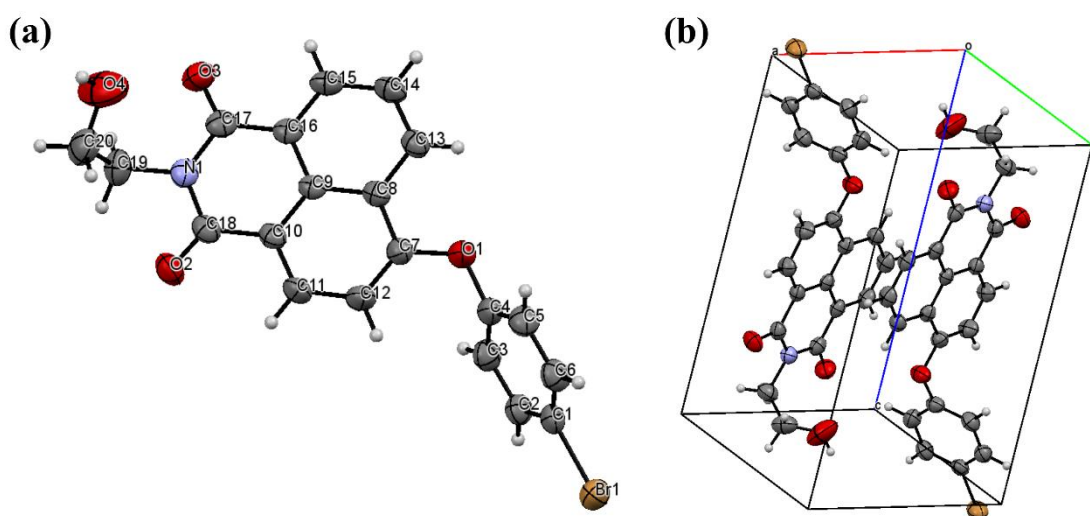


Figure 3.1 (a) ORTEP diagram and (b) packing pattern of the naphthalimide **NI-Br**

Table 3.1 Molecular formula, molecular weights, chemical name and chemical structure of the naphthalimide derivatives

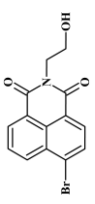
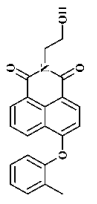
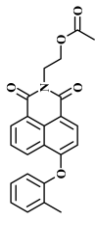
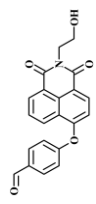
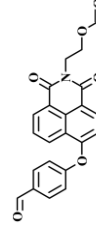
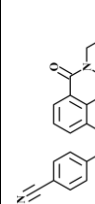
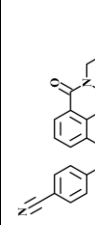
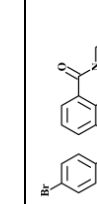
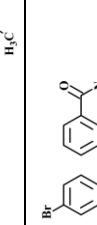
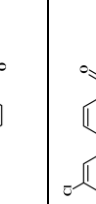
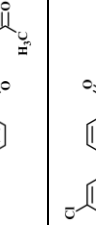
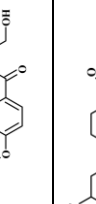
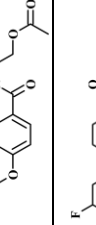
Compound	Product	Chemical Name	Chemical Name	Compound	Product Structure	Chemical Name
BNI		6-bromo-2-(2-hydroxyethyl)-1H-benzo[de]isoquinoline-1,3(2H)-dione				
NI – CH₃ C ₂₁ H ₁₇ NO ₄ 347.36 g		2-(2-hydroxyethyl)-6-(2-methylphenoxy)-1H-benzo[de]isoquinoline-1,3(2H)-dione		NA – CH₃ C ₂₃ H ₁₉ NO ₅ 389.40 g		2-[6-(2-methylphenoxy)-1,3-dioxo-1H-benzo[de]isoquinolin-2(3H)-yl]ethyl acetate
NI – CHO C ₂₁ H ₁₅ NO ₅ 361.34 g		4-([2-(2-hydroxyethyl)-1,3-dioxo-2,3-dihydro-1H-benzo[de]isoquinolin-6-yl]oxy) benzaldehyde		NA – CHO C ₂₃ H ₁₇ NO ₆ 403.38 g		2-[6-(4-formylphenoxy)-1,3-dioxo-1H-benzo[de]isoquinolin-2(3H)-yl]ethyl acetate
NI – CN C ₂₁ H ₁₄ N ₂ O ₄ 358.34 g		4-([2-(2-hydroxyethyl)-1,3-dioxo-2,3-dihydro-1H-benzo[de]isoquinoline-6-yl]oxy) benzonitrile		NA – CN C ₂₃ H ₁₆ N ₂ O ₅ 400.38 g		2-[6-(4-cyanophenoxy)-1,3-dioxo-1H-benzo[de]isoquinolin-2(3H)-yl]ethyl acetate
NI – Br C ₂₀ H ₁₄ BrNO ₄ 412.23 g		6-(4-bromophenoxy)-2-(2-hydroxyethyl)-1H-benzo[de]isoquinoline-1,3(2H)-dione		NA – Br C ₂₂ H ₁₆ BrNO ₅ 454.27 g		2-[6-(4-bromophenoxy)-1,3-dioxo-1H-benzo[de]isoquinolin-2(3H)-yl]ethyl acetate
NI – Cl C ₂₀ H ₁₄ ClNO ₄ 367.78 g		6-(4-chlorophenoxy)-2-(2-hydroxyethyl)-1H-benzo[de]isoquinoline-1,3(2H)-dione		NA – Cl C ₂₂ H ₁₆ ClNO ₅ 409.81 g		2-[6-(4-chlorophenoxy)-1,3-dioxo-1H-benzo[de]isoquinolin-2(3H)-yl]ethyl acetate
NI – F C ₂₀ H ₁₄ FNO ₄ 351.32 g		6-(4-fluorophenoxy)-2-(2-hydroxyethyl)-1H-benzo[de]isoquinoline-1,3(2H)-dione		NA – F C ₂₂ H ₁₆ FNO ₅ 393.36 g		2-[6-(4-fluorophenoxy)-1,3-dioxo-1H-benzo[de]isoquinolin-2(3H)-yl]ethyl acetate

Table 3.2 Crystallographic data for **NI-Br**

Compound	NI-Br
Molecular formula	C ₂₀ H ₁₄ BrNO ₄
Formula weight	412.23
Radiation wavelength (Å)	0.71073
Radiation type	Mo K _α
Crystal form/ Color	Block/ Colorless
Crystal system	Triclinic
Space group	P-1
a, b, c [Å]	7.7810(3), 8.8770(3), 12.6940(4)
α, β, γ [deg]	78.64
Volume [Å ³] & Temperature (K)	841.12(5), 296 K
Z	2
<i>F</i> (000)	416
Density, ρ _{calc} [Mg/m ³]	1.628
μ [mm ⁻¹]	2.47
Crystal dimension/size (mm)	0.30 × 0.27 × 0.23
θ range for data collection (°)	2.8 – 26.9
θ _{max} / θ _{min} (°)	26.4/ 1.7
Limiting indices	-9 ≤ h ≤ 9, -11 ≤ k ≤ 11, -15 ≤ l ≤ 15
Reflections collected	12581
Independent reflections	3444
<i>R</i> _{int}	0.039
Goodness-of-fit on F ²	0.90
Final R indices [I > 2σ (I)]	R = 0.040, wR = 0.126
CCDC no.	978898

3.3 PHOTO-PHYSICAL PROPERTIES

3.3.1 Steady-state emission measurements

Studying the photophysical properties is vital for understanding the functioning of organic materials when they are used in device applications. Under

irradiation, the photophysical properties of naphthalimides are generally related to the polarization of their chromophoric system and are governed by the nature of the substituents [Duke et al. 2010]. With the absorption of light, the connected electron donating groups at C-4 position of the naphthalic ring creates a *push-pull* electronic configuration. This generates an internal CT excited state resulting in the donor-acceptor (D- π -A) interactions between the electron-donating substituents at the C-4 position and the electron-accepting carbonyl groups [Cao et al. 2002, Srikun et al. 2008]. These interactions may be influenced by environmental effect of different media, especially the polarity of organic solvents [Liu et al. 2006, Gasiorski et al. 2012, Kityk 2012]. In order to investigate the effect of the solvent polarity on the phenoxy substitution at the C-4 position of the 1,8 naphthalimide, the photo-physical characteristics of the derivatives were recorded in both protic and aprotic organic solvents (10^{-5} M) of varying polarity and thin solid films [Banerjee et al. 2012, 2013] using UV-Vis absorption and PL spectroscopy. Basic photo-physical characteristics such as the wavelength of absorption maximum, PL maximum, molar extinction coefficient, optical band gap, full width at half maximum, Stokes' shift, oscillator strength, PL quantum yield, energy yield, and the energy of the lowest singlet-excited state of the materials were determined. The results are summarized in Table 3.3. As seen from Figure 3.2, the absorption and PL spectra of the derivatives in CHCl_3 and thin solid films have bands with a single maximum. As we know, the shift can be described as hypsochromic or bathochromic depending on whether the absorption maximum occurs at a shorter or longer wavelength. The absorption curve is more or less a mirror image of the PL curve. The overlap of the absorption and PL spectra is small.

At room temperature, **BNI** that has an electron-withdrawing bromo group at C-4 position, shows absorption maximum wavelength of 340 nm (shoulder peak at 354 nm) in CHCl_3 solution [Wang et al. 2010]. The replacement of the bromo group in the **BNI** with electron-donating phenoxy groups (derivatives **NI-x** and **NA-x**) lead to bathochromic absorption peak shifts (λ_{Abs}) of ~ 20 nm, thus indicating that the lowest singlet excited state of the derivatives has CT character. The CT process is possible due to the electron-donating ability of the phenoxy groups at C-4 position.

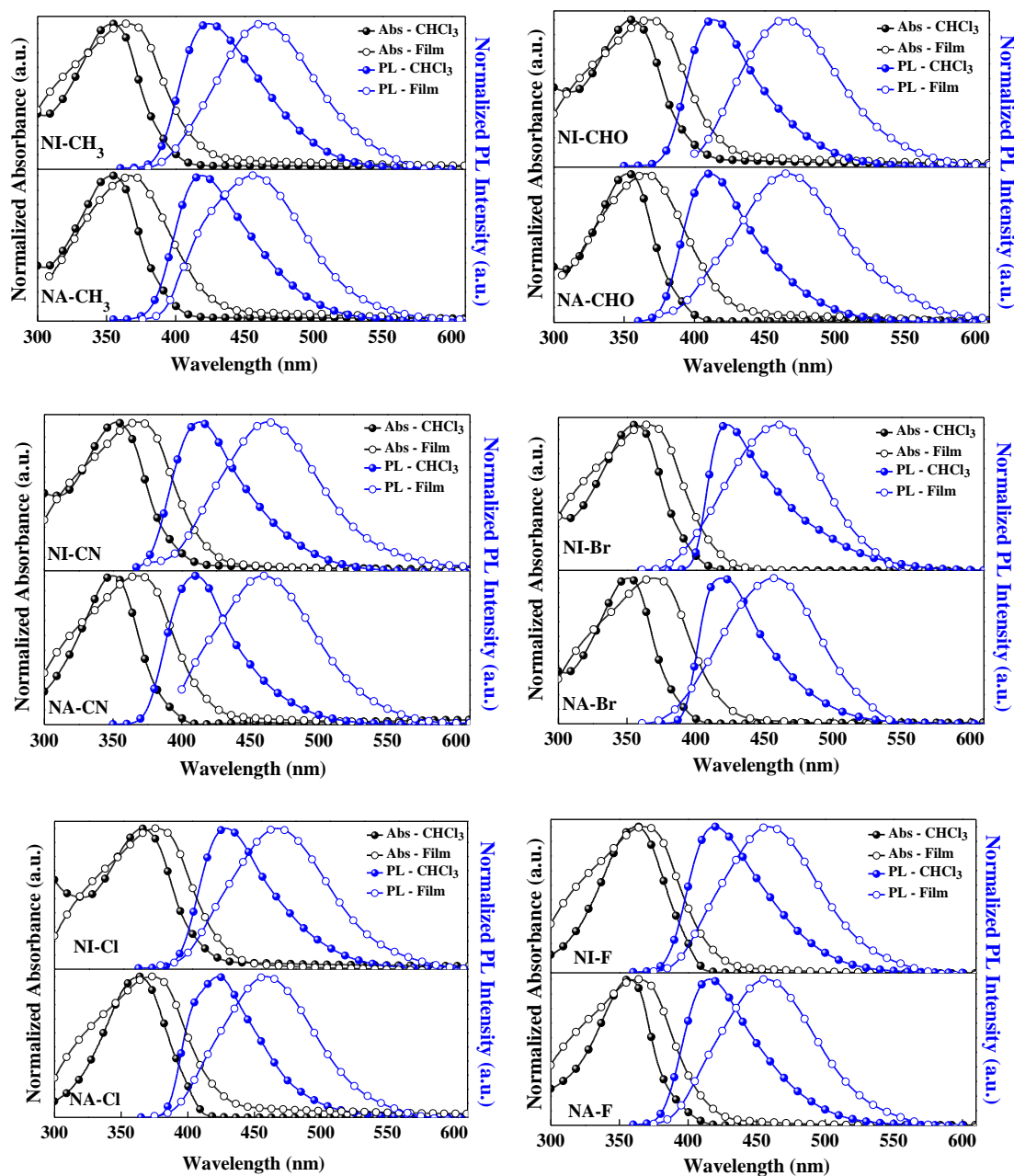


Figure 3.2 UV-Vis absorption and PL spectra of the naphthalimides in CHCl_3 and thin solid film form

The change in λ_{abs} may be due to the different electron-donating abilities of the substituents at C-4 position and nature of the lowest excited state of the systems. The presence of the electron donating groups increases the electron density at the C-4 position, and hence the respective absorption maximum undergoes a bathochromic shift. All the derivatives have quite similar broadband UV-Vis absorption

characteristics (Figure 3.2) with λ_{Abs} in the range 351-360 nm. This can be attributed to the π - π^* electronic transitions in the naphthalimide moiety from the electron donating phenoxy substituents at the C-4 position to the electron accepting carbonyl groups. The absorption is clearly due to the naphthalimide moiety. The lowest excited state is prevalent in π - π^* character for 1,8-naphthalimides [Bojinov and Simeonov 2010, Marinova et al. 2013]. A slight bathochromic shift (~ 10 nm) is observed in λ_{Abs} of the thin films (Figure 3.2) compared to that in CHCl_3 solution, with λ_{Abs} shifting to 360-374 nm. The observed mild shift indicates that the π - π^* interaction between the molecules in the solid thin film state is weak due to some intermolecular aggregation in condensed state. Here, it is also noteworthy that the π - π^* absorption transitions of derivatives **NA-x** are slightly hypsochromic shifted (1-5 nm) compared to **NI-x**.

The optical energy band gaps (E_g^{opt}) of the derivatives are calculated using Tauc plots (Figure 3.3), from the solid-state absorption spectra. Here, direct allowed transitions ($(ah\nu)^2$ versus $h\nu$) are considered and the calculated E_g^{opt} values are in the range 2.98 to 3.14 eV as given in Table 3.3. The molar extinction coefficients ($\log \epsilon$) of the derivatives are high and in the range 4.109-4.384 $\text{l mol}^{-1} \text{cm}^{-1}$ indicating that the long wavelength band of the absorption spectrum has a CT nature, due to the π - π^* character of the $S_0 \rightarrow S_1$ transition. The value of $\log \epsilon$ for the derivatives are in the desirable range since the obtained values are two-fold larger than those for analogous 1,8-naphthalimides [Wintgens et al. 1996, Grabchev et al. 2001] suggesting absence of ground state interaction between the 1,8-naphthalimide chromophoric units [Barros et al. 1995].

The derivatives displayed intense blue PL emission corresponding to $S_1 \rightarrow S_0$ transition in CHCl_3 solution and in thin solid film form. This may be ascribed to the CT interaction from the substituent group donors at the C-4 position to carbonyl group acceptors in the 1,8-naphthalimide moiety. Due to the presence of electron-withdrawing bromo-substituent at the C-4 position, **BNI** exhibits weak PL with λ_{PL} at 406 nm in CHCl_3 solution [Wang et al. 2010]. On substituting bromo group in the **BNI** with the electron donating phenoxy groups at the C-4 position (**NI-x** and **NA-x**), the PL intensity improved with bathochromic shifts (~ 20 nm) in the emission wavelength towards pure blue (λ_{PL} : 410-426 nm) with narrow full width at half maximum (FWHM) of 39-47 nm

as shown in Figure 3.2. The observed shifts (Table 3.3) can be attributed to the formation of D- π -A molecular structures with the introduction of the substituents. All the derivatives displayed similar PL spectra, which can be attributed to the similarity in molecular structure. Similar to UV-Vis absorption, the λ_{PL} of **NA-x** are hypsochromic shifted (3-5 nm) compared to derivatives **NI-x**. Studying PL of the derivatives in thin film state is important from the point of view of practical device applications. The PL emission spectra of the derivatives in thin solid films are analogous to those recorded in CHCl_3 solution, with λ_{PL} in the region 457-468 nm with FWHM ranging from 58-64 nm. These peaks are bathochromic shifted by 36-54 nm when compared to PL in CHCl_3 solution. The observed shifts confirm the presence of aggregation in solid state. The narrow FWHM in PL spectra imply that the derivatives are capable of blue emission with good chromaticity.

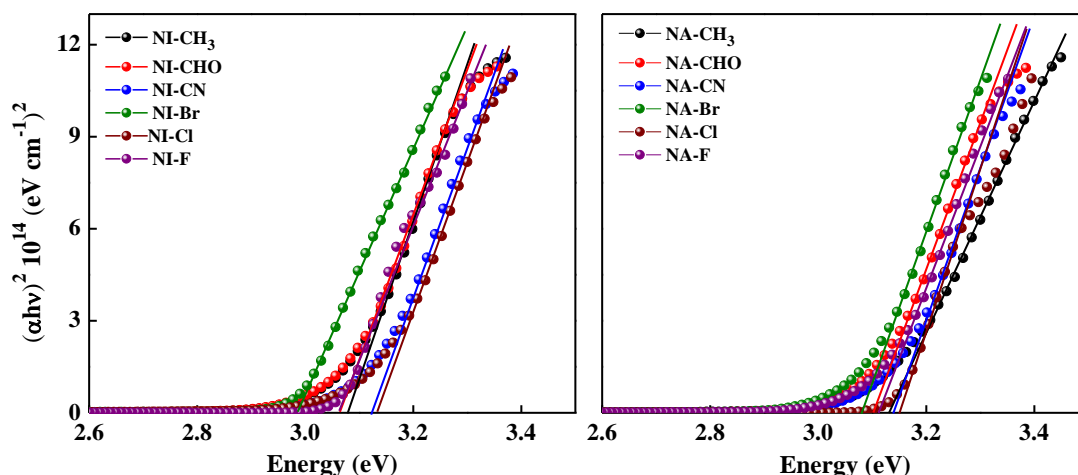


Figure 3.3 Optical band-gap determination of the naphthalimides by Tauc plots.

The energy of activation of the first excited state (E_{S1}) obtained from the point of intersection of absorption and PL spectra in CHCl_3 solution at the corresponding wavelength λ_{S1} , has the values of 310-326 kJ mol^{-1} . Stokes' shift (ν_{st}) and oscillator strength (f) are important parameters of PL materials. The Stokes' shift indicates the difference in the structure and properties of the PL molecules in the ground state S_0 and the first excited state S_1 [Gordon and Gregory 1987, Tonzola et al. 2003]. Stokes' shift was calculated as the difference between absorption and emission maxima obtained from the corrected spectra on the wavenumber scale using Equation 3.1. The Stokes' shifts of the derivatives are high (Table 3.3), in the range 3895-4623 cm^{-1} (in CHCl_3)

and 5093-5982 cm^{-1} (thin film). Thus ensuring that there is no re-absorption of the emitted radiation. The oscillator strength reveals the strength of transition and is proportional to the area under the absorption band. It gives the effective number of the electrons, which take part in the transition between the ground state and the excited state. The oscillator strength values were determined by Equation 3.2, where $\Delta\nu_{1/2}$ is the width of the absorption band (in cm^{-1}) at half of ϵ_{max} [Gordon and Gregory 1987, Tonzola et al. 2003]. The derivatives have oscillator strength values in the range 0.272-0.311. Both Stokes shift and oscillator strength values for the derivatives are comparable with reported values for 1,8-naphthalimides [Grabchev et al. 1995, Cosnard and Wintgens 1998, May et al. 1999, Bojinov and Simeonov 2010, Marinova et al. 2013] and for other blue emitting heterocyclic compounds [Kumar and Thomas 2011, Mahajan et al. 2012, Singh et al. 2012].

$$\nu_{st} = (\nu_{Abs} - \nu_{PL}) = \left(\frac{1}{\lambda_{Abs}} - \frac{1}{\lambda_{PL}} \right) \times 10^7 \quad (3.1)$$

$$f = 4.32 \times 10^{-9} \Delta\nu_{1/2} \epsilon_{max} \quad (3.2)$$

The ability of the derivatives to emit the absorbed light, i.e., PL efficiency, is quantitatively characterized by measuring the PL quantum yield (Φ_{PL}) which is an important parameter for the quantitative characterization of fluorophores. The PL quantum yield has been estimated from the absorption and PL spectra of the derivatives using Equation 3.3 with 9,10-diphenylanthracene ($\Phi_{ref} = 0.90$ in cyclohexane) as standard [Dawson and Windsor 1968, Hamai and Hirayama 1983, Gordon and Gregory 1987, Gan et al. 2004].

$$\Phi_{PL} = \Phi_{ref} \left(\frac{S_{sample}}{S_{ref}} \right) \left(\frac{A_{ref}}{A_{sample}} \right) \left(\frac{n_{sample}^2}{n_{ref}^2} \right) \quad (3.3)$$

where S_{ref} , A_{ref} , n_{ref} and S_{sample} , A_{sample} , n_{sample} represent the integrated emission band area, the absorbance at the excited wavelength, and the refractive index of the solvent, respectively for the standard reference and the sample. The PL quantum yields of the derivatives are in the range 0.11-0.55. The calculated energy yield of PL (E_{PL}) using Equation 3.4 are in the range 0.09-0.47, which can also be used instead of Φ_{PL} [Grabchev et al. 2001]. There is a slight decrease in both Φ_{PL} and E_{PL} values for the

acetylated versions **NA-x** compared to **NI-x**. This can be attributed to the presence of the acetyl functional group. The values of Φ_{PL} and E_{PL} are higher than their analogous derivatives [May et al. 1999, Grabchev et al. 2001, Wang et al. 2005, Marinova et al. 2013].

$$E_{PL} = \Phi_{PL} \frac{\lambda_{Abs}}{\lambda_{PL}} \quad (3.4)$$

The performance of the materials in the EL devices can be evaluated by comparing the emission color by means of color coordinates. The *Commission Internationale de L'Éclairage (CIE)* chromaticity coordinates (Table 3.3) are determined using the emission spectra of the derivatives excited at 330 nm (in CHCl_3) and 360 nm (thin films). The CIE coordinates are located in the deep blue region of the chromaticity diagram (Figure 3.4). The variations in the color coordinates (x , y) may be due to different phenoxy-groups at the C-4 position of the naphthalimide backbone. From the CIE coordinate data presented in the Table 3.3, it is clear that, the acetylated versions (**NA-x**) have higher x -coordinate values and lower y -coordinate values compared to their respective counterparts (**NI-x**) as these act as electron deficient centers. Furthermore, the thin films of all the derivatives show decrease in the x -coordinate values and increase in the y -coordinate values from that in CHCl_3 solution. This can be attributed to the molecular aggregation in thin solid film form. The results indicate that the derivatives are potential materials for the fabrication of blue OLEDs.

Solvatochromism is the ability of a chemical substance to change color due to a change in solvent polarity. Solvent effects can play a significant role in the photophysics of excited states [Reichardt 1994, Suppan and Ghoneim 1997]. In photophysical studies of 1,8-naphthalimide derivatives, it had been reported [Martin et al. 1996] that the absorption and PL maxima of these molecules had a bathochromic/hypsochromic shifts with varying dielectric constant of the solvents. This fact takes place in electronic transitions of the type $\pi \rightarrow \pi^*$ with a higher dipole moment in the excited state S_1 than in the ground state S_0 [Hossain et al. 2005]. Table 3.4 summarizes the absorption maxima, emission maxima and Stokes' shift of the derivatives **NI-Cl** and **NA-Cl** in the solvents investigated.

Table 3.3 Photophysical data of the novel naphthalimide derivatives

Compound	λ_{Abs} (nm) ^{a,b}	λ_{Em} (nm) ^{a,b}	Φ_{PL}^c	FWHM (nm) ^{a,b}	$\log \varepsilon^d$	E_{st}^e	ν_{st} (cm^{-1}) ^{a,b}	f^f	E_{PL}^g	$E_{\text{g}}^{\text{opt}}$ (eV) ^h	CIE coordinates ^{a,b}		
											x	y	z
NI - CH ₃	355 (365)	424 (462)	0.27	47 (61)	4.317	318	4616 (5737)	0.301	0.22	3.08	0.151 (0.146)	0.059 (0.167)	
NI - CHO	355 (368)	414 (468)	0.19	39 (59)	4.358	321	4022 (5799)	0.283	0.16	3.06	0.153 (0.148)	0.054 (0.166)	
NI - CN	352 (368)	413 (463)	0.55	40 (60)	4.347	323	4164 (5546)	0.311	0.47	3.12	0.156 (0.151)	0.053 (0.162)	
NI - Br	356 (363)	423 (461)	0.25	39 (63)	4.171	311	4450 (5856)	0.303	0.21	2.98	0.153 (0.145)	0.081 (0.131)	
NI - 4Cl	363 (374)	426 (462)	0.28	44 (59)	4.339	312	4074 (5093)	0.307	0.33	3.04	0.155 (0.144)	0.050 (0.143)	
NI - F	360 (367)	420 (459)	0.38	43 (60)	4.384	310	3968 (5462)	0.294	0.33	3.07	0.153 (0.151)	0.051 (0.147)	
NA - CH ₃	352 (363)	419 (457)	0.12	43 (64)	4.282	319	4567 (5682)	0.296	0.10	3.13	0.153 (0.152)	0.052 (0.125)	
NA - CHO	353 (364)	411 (465)	0.11	40 (62)	4.259	324	4014 (5982)	0.272	0.09	3.10	0.155 (0.150)	0.045 (0.161)	
NA - CN	351 (368)	410 (460)	0.37	39 (61)	4.214	326	4132 (5457)	0.302	0.32	3.14	0.156 (0.157)	0.038 (0.139)	
NA - Br	351 (360)	419 (458)	0.24	39 (62)	4.109	316	4623 (5944)	0.291	0.20	3.08	0.154 (0.145)	0.047 (0.121)	
NA - 4Cl	362 (371)	422 (458)	0.26	46 (58)	4.268	316	3928 (5120)	0.298	0.21	2.99	0.155 (0.145)	0.044 (0.129)	
NA - F	358 (363)	416 (457)	0.28	40 (60)	4.293	318	3895 (5666)	0.285	0.24	3.11	0.154 (0.151)	0.046 (0.140)	

^a Recorded in 10^{-5} mol L⁻¹ CHCl₃ Solution, ^b Values in parantheses are recorded in thin solid film state, ^c Relative PL quantum yield (Φ_{PL}) of naphthalimide solution in 10^{-5} mol L⁻¹ CHCl₃ using 9,10-diphenylanthracene in cyclohexane ($\Phi_{\text{ref}}=0.90$) as standard, ^d Molar extinction coefficients ($1 \text{ mol}^{-1} \text{ cm}^{-1}$), ^e Energy state of activation of the first excited state (kJ mol^{-1}), ^f Oscillator strength, ^g Energy yields of fluorescence, ^h Optical band gap by Tauc plots of solid state absorption spectra.

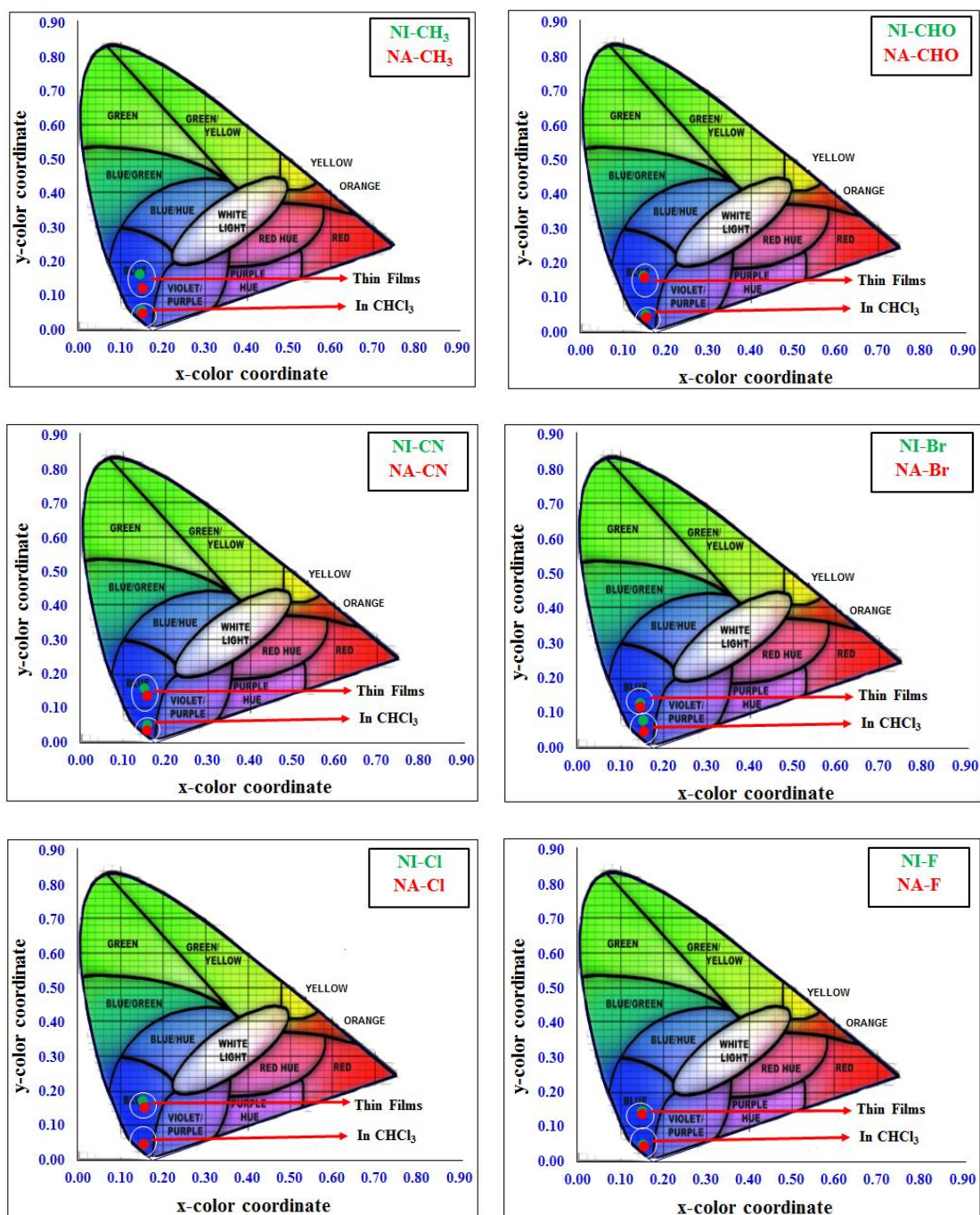


Figure 3.4 Chromaticity diagrams of the naphthalimide derivatives.

The absorption spectral data of the derivatives **NI-Cl** and **NA-Cl** showed a very small change in λ_{abs} for the derivatives when the solvent was changed indicating no evidence of strong solvent effect in the ground state as reported for other 1,8-naphthalimides [Magalhães et al. 2006, Bojinov et al. 2008]. The absorption is slightly extended to the visible region for Thin films in all solvents in this study. The absorption spectra of

the derivatives (Figure 3.5) in hexane and cyclohexane are well structured. Use of polar solvents results in the disappearance of the vibrational structure. In polar solvents, λ_{abs} is shifted to higher wavelengths but the absorption profile has a single peak. A bathochromic shift in λ_{abs} was noticed for derivatives dissolved in various solvents from hexane (~ 338 nm) to water (~ 361 nm), signifying a red shift in λ_{abs} for polar solvents [Patra and Barakat 2011]. However, the position of λ_{abs} peak remains immune to the varying polarity of the polar protic and polar aprotic solvents, indicating that solvent polarity has little impact on the absorption spectra of the derivatives. The absence of any specific effects in protic solvents indicates lack of intermolecular H-bond formation in the molecules' ground state [Georgiev and Bojinov 2010].

The PL emission spectra (Figure 3.6) demonstrate solvent dependent shifts in emission maxima as the 1,8-naphthalimide chromophoric system is very sensitive to the solvent polarity. The specific chromophore–solvent interaction, causing a change in the polarization of the 1,8-naphthalimide system also affects the PL maxima. Similar to the absorption characteristics, the derivatives **NI-CI** and **NA-CI** showed structured emission in non-polar solvents like hexane and cyclohexane; whereas in the case of moderate and high polarity solvents, the derivatives exhibited broadband emission without any clear vibrational structure [Patra and Barakat 2011]. As can be seen in Figure 3.6, an increase in solvent polarity, i.e., from non-polar to polar solvents, resulted in bathochromic shifts. For instance, an enormous bathochromic shift of 77 nm was observed in the case of **NI-CI** when changing the solvents from hexane to water, which was not noticed in the absorption spectra. This shift indicates that the stabilization of the solvent is more prominent in the excited states when compared to the ground states [Murphy et al. 2014]. As can be seen from Table 3.4, there was a remarkable increase in the Stokes' shift of **NI-CI** from 3570 cm^{-1} in hexane to 6997 cm^{-1} in water. Similar kind of behavior was also observed for other reported 1,8-naphthalimides [Bojinov et al. 2003, Magalhães et al. 2006, Marinova et al. 2013]. In polar solvent, the large Stokes shift is due to major stabilization of S_1 state with contribution of an intramolecular CT effect [Bojinov 2004, Martín et al. 2005, Georgiev and Bojinov 2010].

Table 3.4 Absorption maxima, PL maxima and Stokes' shift of **NI-CI** and **NA-CI** in organic solvents of different polarity

Solvents	NI-CI			NA-CI		
	λ_{abs} (nm)	λ_{PL} (nm)	ν_{st} (cm^{-1})	λ_{abs} (nm)	λ_{PL} (nm)	ν_{st} (cm^{-1})
Hexane	340, 354	387, 406	3570	338, 351	383, 403	3561
Cyclohexane	342, 356	388, 409	3640	339, 353	385, 404	3576
Toluene	360	422	4081	358	417	3952
Chlorobenzene	362	428	4240	363	422	3880
Benzene	358	422	4245	357	418	4075
DCM	362	429	4349	359	424	4301
Propanol	355	432	5052	357	431	4825
1-butanol	358	433	4818	358	431	4740
THF	357	423	4358	356	421	4305
Chloroform	363	426	4074	362	422	3928
Ethyl Acetate	353	422	4620	355	420	4361
Dioxane	352	419	4538	356	418	4190
Acetone	355	428	4836	356	427	4665
Methanol	358	433	4847	356	433	4961
Ethanol	358	432	4793	357	433	4904
Acetonitrile	355	432	5022	356	429	4774
N,N-DMF	355	433	5105	357	434	4985
DMSO	358	436	5006	360	437	4916
Water	361	483	6997	362	475	6572

To comprehend the effect of polarity on naphthalimides in various solvents, solvent dependent spectral shifts were investigated. The response of the derivatives to solvent polarity can be analyzed in terms of the difference in the dipole moments in the ground and excited states. This can be estimated from Lippert–Mataga (LM) equation given below. Equation 3.5 shows the dependence of the Stokes' shift of the PL spectra of the molecules on the dielectric constant and the refractive index of the solvents being used [Mataga et al. 1956, Lippert 1957, Reichardt 1994, Degheili et al. 2009].

$$v_{st} = (\bar{\nu}_{Abs} - \bar{\nu}_{PL}) = \frac{2\Delta f}{hca^3} \Delta\mu^2 \quad (3.5)$$

where f and $\Delta\mu$ is given by

$$f = \frac{\varepsilon - 1}{2\varepsilon + 1} - \frac{n^2 - 1}{2n^2 + 1} \quad \text{and} \quad \Delta\mu = \mu_E - \mu_G$$

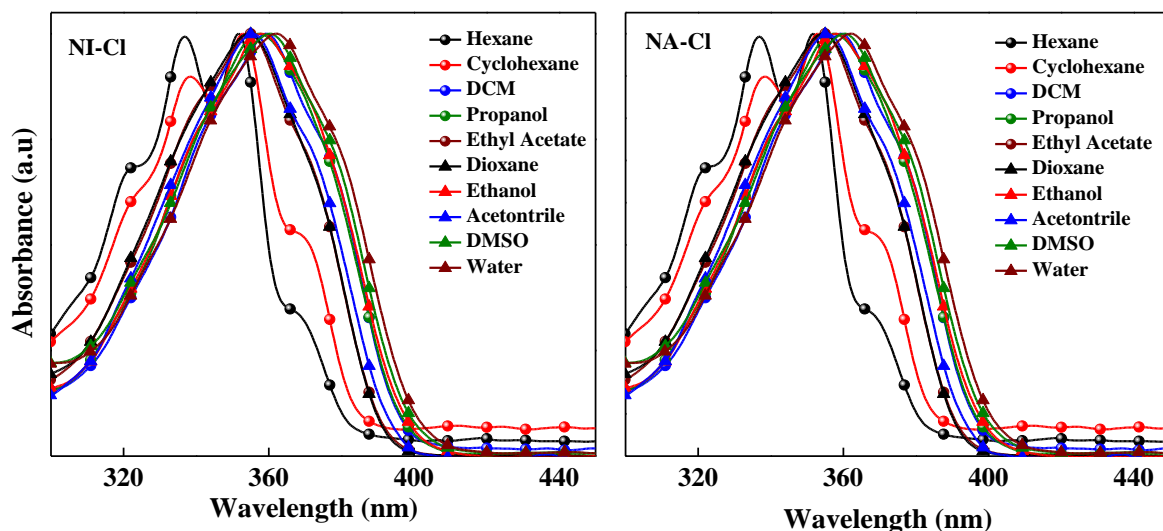


Figure 3.5 UV-Vis absorption spectra of the derivatives in different solvents (10^{-5} M) carried out at ambient temperature.

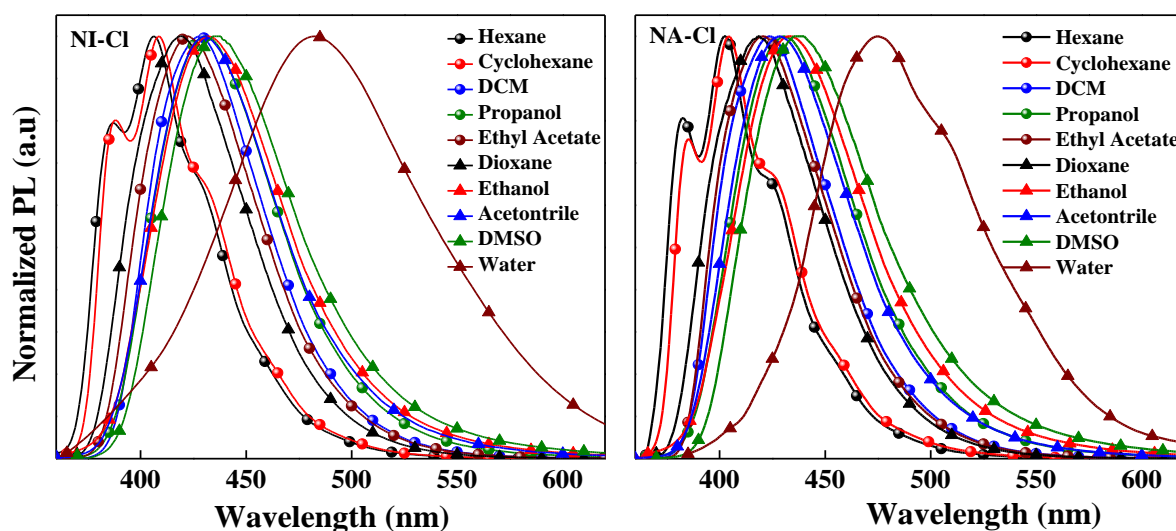


Figure 3.6 PL spectra of the derivatives in different solvents (10^{-5} M) carried out at ambient temperature.

Here $\bar{\nu}_{\text{Abs}}$ and $\bar{\nu}_{\text{PL}}$ are the wave numbers (cm^{-1}) of the absorbance and PL emission respectively, h is Planck's constant, c is the speed of light in vacuum, a is the Onsager radius of the cavity in which the fluorophore resides [Edward 1970], $\Delta\mu$ represent the variation between the dipole moments of the excited (μ_E) and ground states (μ_G) of the fluorophore [Lakowicz 2007], and Δf is the solvent polarity parameter also known as the orientation polarizability, which involves the dielectric constant (ϵ) and refractive index (n) of the solvents. Orientation polarizability of the solvent is the result of both the mobility of the electrons in the solvent and the dipole moment of the solvent. The LM plot can be obtained by plotting the Stokes' shift versus orientation polarizability of the solvent. Figure 3.7 represents the LM plot of the derivatives **NI-Cl** and **NA-Cl** in different solvents.

In the case of charge transfer in a molecule, the gross solvent polarity indicator scale such as empirical parameter of solvent polarity $E_{\text{T}}30$ is more relevant [Reichardt 1994]. Figure 3.8 shows plots of Stokes' shift versus the $E_{\text{T}}30$ values of the solvents. Similar trend is seen for both protic and aprotic solvents. Clearly, the polarity of the solvents significantly influences the spectral properties of the derivatives **NI-Cl** and **NA-Cl**. Changes in the position of the CT band of the derivatives dissolved in various solvents are brought about by the solvatochromic effect of the solvent [Grabchev et al. 2001]. The linear dependence of the characteristics indicates that dipole-dipole interactions dominate in the dye solution.

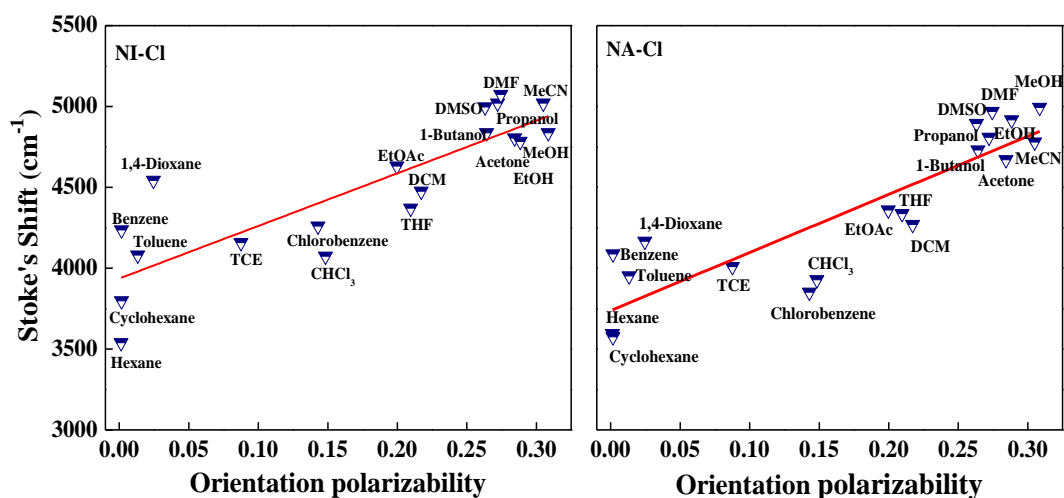


Figure 3.7 Lippert - Mataga plots of **NI-Cl** and **NA-Cl** in different solvents

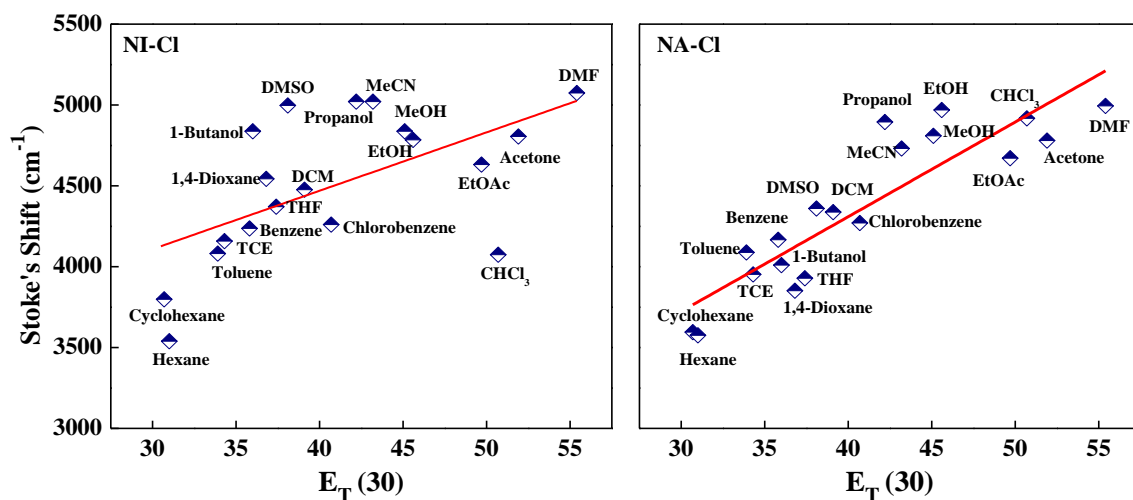


Figure 3.8 Correlation of solvent induced Stokes' shift of **NI-Cl** and **NA-Cl** with $E_T(30)$ parameter

3.3.2 Time-Resolved Photoluminescence Spectroscopy

In order to investigate the emission mechanism, studying the PL decay lifetime is vital as it is an extremely important parameter, which decides the suitability of the material for device applications. The radiative recombination efficiency is directly proportional to the particular transition decay time. With the intention of gaining more information about the excited state electron-transfer dynamics of the derivatives, time resolved PL spectroscopy was employed to study PL decay spectrum of the derivatives dissolved in CHCl_3 at room temperature at their respective PL maxima for blue emission by time correlated single photon counting technique using a 350 nm pulsed NanoLED source for excitation. The obtained results are reported in Table 3.5 and the decay profiles of the derivatives are plotted in Figure 3.9. The lifetime data obtained for the derivatives were fitted to a double exponential function given below using DAS 6 software.

$$F(t) = A_1 \exp\left(-\frac{t}{\tau_1}\right) + A_2 \exp\left(-\frac{t}{\tau_2}\right) \quad (3.6)$$

Here τ_1 and τ_2 are the decay lifetimes of the luminescence with amplitudes A_1 and A_2 , respectively. The observed lifetimes are $\tau_1 \sim 0.54$ ns and $\tau_2 \sim 2.38$ ns for derivative **NI-Cl**; and $\tau_1 \sim 0.91$ ns and $\tau_2 \sim 3.63$ ns for derivative **NA-Cl**. For double-exponential decay, the average lifetime, τ_{av} , is typically tailored to replace the various

parameters of the luminescence lifetime, which is given by [Fujii et al. 1997, Murakami et al. 2000, Gupta et al. 2011, Kumar et al. 2013]

$$\tau_{av} = \frac{(A_1\tau_1^2 + A_2\tau_2^2)}{(A_1\tau_1 + A_2\tau_2)} \quad (3.7)$$

Table 3.5 Time-Resolved PL Spectroscopy data for derivatives **NI-Cl** and **NA-Cl**

Compound	Decay time (τ) with relative amplitude (A)				τ_{av} (ns)
	τ_1 (ns)	A1 (%)	τ_2 (ns)	A2 (%)	
NI-Cl	0.54	59.9	2.38	40.1	1.91
NA-Cl	0.91	43.2	3.63	56.8	3.19

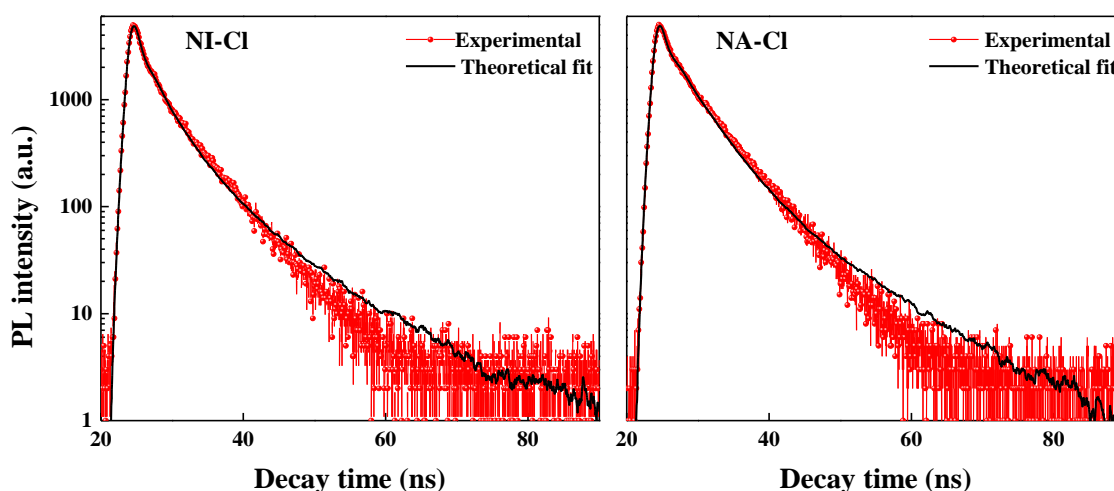


Figure 3.9 Time resolved PL spectra of **NI-Cl** and **NA-Cl** in chloroform.

The calculated average lifetime for the derivatives are 1.91 ns for **NI-Cl** and 3.19 ns for **NA-Cl**. The nature of the bi-exponential decay curve is well described in literature and is ascribed to two processes: (i) a fast process due to the relaxation of the carriers into the unoccupied ground state, and (ii) a slow process associated with the radiative recombination of electron-hole pair. Depending on the acceptor concentration, these two processes contribute to the energy transfer [Singh et al. 2011]. It can also be noted from the decay profile that the triplet energy transfer is totally suppressed in both the derivatives [Kumar et al. 2013]. The presence of double exponential decay component indicates the presence of at least two electronically excited species. The

obtained results are highly suitable for OLED device applications as well as many other optical display applications.

3.4 THERMAL PROPERTIES

In order to be used in optoelectronic devices, organic materials should possess very good thermal stability to withstand temperature rise as high as 80 °C [Dawson and Windsor 1968, Hamai and Hirayama 1983, Mahajan et al. 2012]. Thermal stability is a key requirement for practical applications of organic fluorophores in EL devices. The stability and the lifetime of the devices can be improved by possessing materials with high thermal stability and melting point. The thermal properties such as melting points (T_m), decomposition temperatures (T_d) and decomposition rates (T_{max}) of the derivatives were investigated by TGA, DTG and DSC. The TGA and DTG were employed to determine the thermal stabilities and were carried out in the temperature range 30-600 °C. The melting points of the derivatives were determined using DSC. In order to melt and decompose the derivatives, a constant heating rate of 10 °C min⁻¹ under nitrogen atmosphere (flow rate: 30 mL min⁻¹) was maintained. The results are summarized in Table 3.6.

The TGA thermograms (Figure 3.10) and the data presented in Table 3.6 reveal that all the derivatives exhibited high thermal decomposition temperatures with a single step in the thermal decomposition process. No weight loss was observed at lower temperatures. The step starts at ~ 235 °C followed by a rapid weight loss of ~ 60% of the mass between 235 °C and 330 °C. This can be ascribed to the loss of the side chains of the derivatives. On further heating, a gradual weight loss was observed due to the decomposition of the backbone. The derivatives have decomposition temperatures in the range of 260-284 °C (5% weight loss, T_5) and 278-308 °C (10% weight loss, T_{10}). A slight weight loss is observed at around 150 °C for some derivatives, which might be due to some volatile impurities or moisture present in the material; and is not due to the decomposition of the derivatives. It may also be noted from Figure 3.10 that, although these derivatives have a similar structure, their TGA plots are different. The derivative thermogram curves (Figure 3.11) show narrow derivative peaks, indicating a high decomposition rate with T_{max} in the range 320-381 °C. The DSC scans (Figure 3.12)

show that all the derivatives exhibit clear endothermic melting. The melting points of the derivatives are relatively high and are in the range 135-271 °C. The trend of melting point depressions provided by DSC are in good agreement with that of melting points measured by capillary method. The decomposition and melting temperatures of the derivatives are relatively higher than the reported naphthalimides analogues [Grabchev et al. 2001, Martín et al. 2005, Georgiev and Bojinov 2010, Wang et al. 2010]. Despite being relatively low molecular weight molecules, the derivatives exhibited high decomposition temperatures indicating that they are stable at high temperatures, which is highly desirable for applications in OLEDs. These materials are stable enough to withstand the temperature at which vacuum vapor deposition would be carried out.

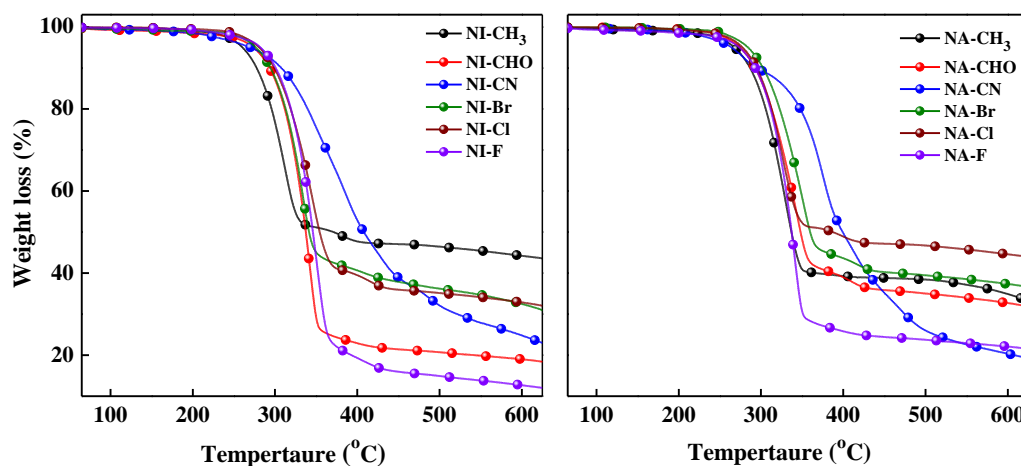


Figure 3.10 TGA thermograms of the naphthalimides under nitrogen atmosphere

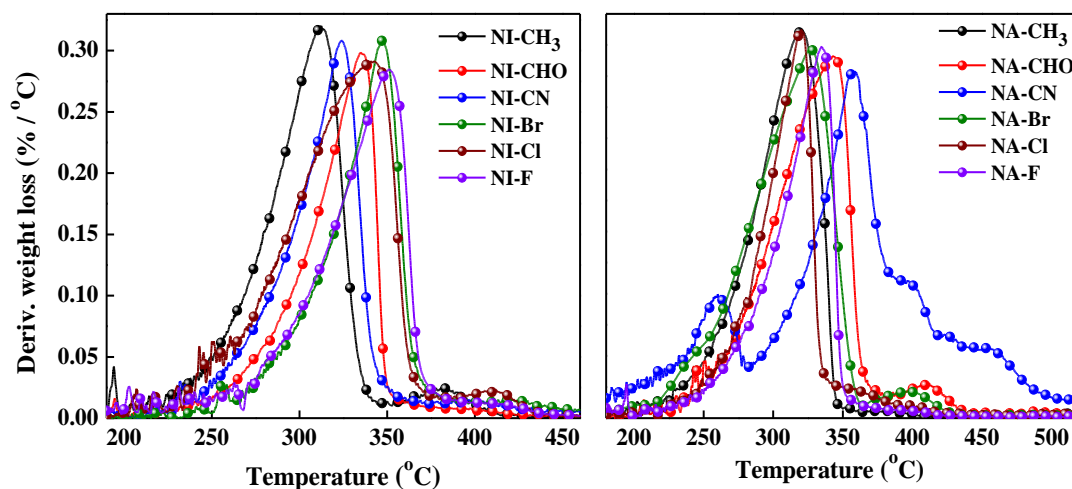


Figure 3.11 Derivative weight loss of the naphthalimides under nitrogen atmosphere

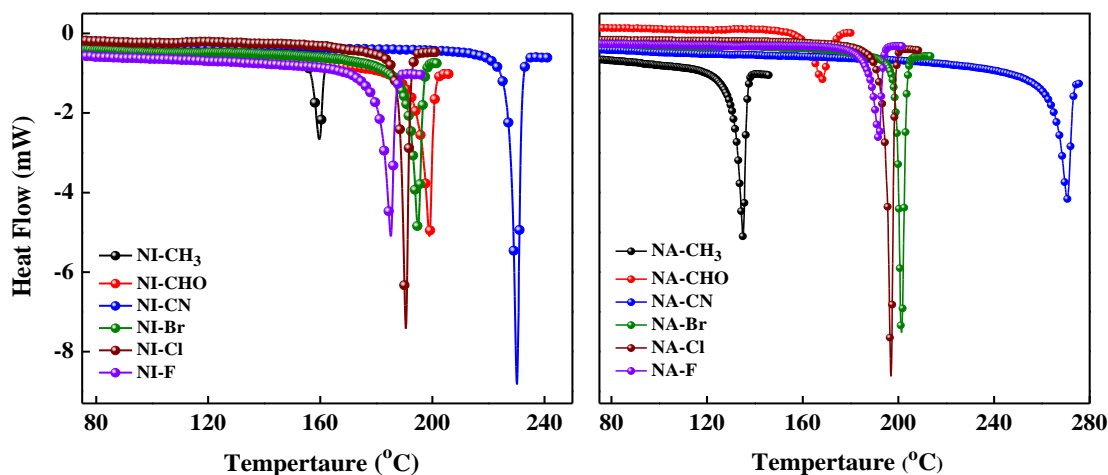


Figure 3.12 DSC thermograms of the naphthalimides under nitrogen atmosphere.

3.5 SURFACE MORPHOLOGY

The formation of uniform amorphous thin films, with low surface roughness value in molecular size range (nm) upon vacuum thermal vapor deposition plays an important role in the performance of the organic electroluminescent devices [Singh et al. 2011]. Hence, the surface morphology of the vacuum-deposited films (50 nm) prepared on n-Si substrates by thermal vapor deposition at a deposition rate of 0.5 \AA/s has been studied by Atomic force microscopy (AFM). The three dimensional AFM images ($10 \times 10 \mu\text{m}$) of the derivatives **NI-Cl** and **NA-Cl** are presented in Figure 3.13. The root-mean-square (rms) roughness values were obtained to be 2.581 nm for **NI-Cl** and 3.574 nm for **NA-Cl**. Our studies indicate that the derivatives are capable of forming quite smooth film and the roughness of deposited films fall in range 2-4 nm, which is of the size of the molecules themselves. Thus, the deposited films have adequate morphology for making good OLED devices.

3.6 ELECTROCHEMICAL PROPERTIES

The electrochemical properties of the naphthalimides have been studied in order to determine HOMO and LUMO energy levels as well as to explore the charge injection capabilities using cyclic voltammetry (CV) measurements. The CV studies were done in acetonitrile solutions (10^{-3} M) using Pt containing Bu_4NPF_6 (0.1 M) as supporting electrolyte, ferrocene/ferrocenium as calibrant and Ag/AgNO_3 electrode as reference [Wang et al. 2010]. The scanning rate for the derivatives was kept as 10 Vs^{-1} . Nitrogen

purging was done for all the solutions prior to the measurements. The onset oxidation, reduction potentials, HOMO-LUMO energy levels, and the band gaps of all the naphthalimide derivatives are outlined in Table 3.6. The derivatives possess free hydroxyl groups, which form hydrogen bonds with the solvent. The cathodic scans of the derivatives exhibited quasi-reversible reduction waves with onset reduction potentials of -1.49 V to -1.37 V versus Ag/AgNO₃ whereas the anodic scans exhibited irreversible waves with onset oxidation potentials of 1.41 to 1.56 V versus Ag/AgNO₃. The energy levels of the derivatives were predicted by comparing the onset potentials of ferrocene (4.8 eV versus vacuum) [Xiao et al. 2009].

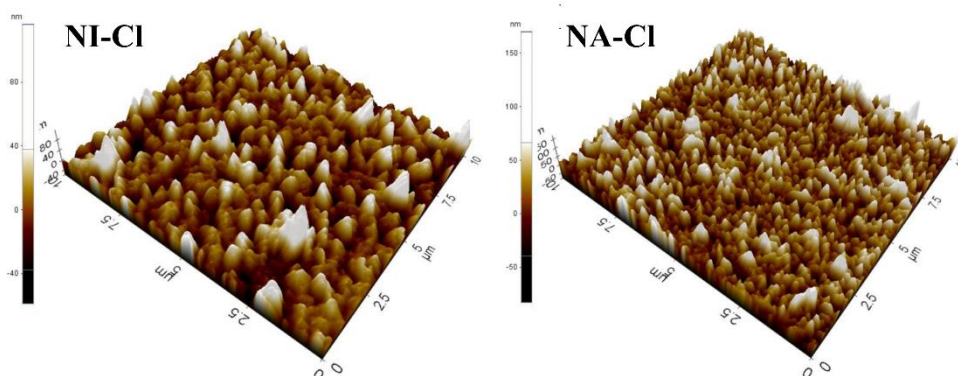


Figure 3.13 AFM images of thermally evaporated NI-Cl and NA-Cl

The HOMO energy levels of the derivatives, estimated from the onset of the oxidation wave ($\text{HOMO} = -4.8 - E_{\text{onset}}^{\text{ox}}$), are in the range -6.36 – -6.21 eV and the LUMO energy levels, estimated from the onset of the reduction wave ($\text{LUMO} = -4.8 - E_{\text{onset}}^{\text{red}}$), are in the range -3.43 – 3.31 eV (below vacuum). Both the HOMO and LUMO energy levels of the derivatives are lower than the reported naphthalimides [Grabchev et al. 2001, Bojinov and Simeonov 2010, Georgiev and Bojinov 2010, Wang et al. 2010]. These low-lying LUMO energy levels reveal that the derivatives have high electron affinities and, hence they are promising blue emitters with electron-transporting nature (n-type) for OLED applications. The HOMO-LUMO energy gaps of the derivatives are in the range 2.84-3.0 eV, which are quite close to the calculated optical band gaps.

Table 3.6 Electrochemical and thermal data of the novel naphthalimide derivatives

Compound	$E_{\text{onset}}^{\text{ox}}$ versus E_{fc} (V) ^a	E_{fc}	$E_{\text{onset}}^{\text{red}}$ versus E_{fc} (V) ^a	HOMO (eV)	LUMO (eV)	E_{g}^{EC} (eV) ^b	T_{d} (°C) ^c	T_{m} (°C) ^d	T_{max} (°C) ^e
NI - CH ₃	1.56	-1.37	-6.36	-3.43	2.93	260 (278)	160	381	
NI - CHO	1.56	-1.41	-6.36	-3.39	2.97	274 (293)	199	335	
NI - CN	1.54	-1.40	-6.34	-3.40	2.94	270 (308)	230	324	
NI - Br	1.41	-1.49	-6.21	-3.31	2.90	277 (294)	195	344	
NI - Cl	1.44	-1.47	-6.24	-3.33	2.91	280 (299)	191	348	
NI - F	1.47	-1.45	-6.27	-3.35	2.92	282 (301)	185	351	
NA - CH ₃	1.51	-1.49	-6.31	-3.31	3.00	268 (287)	135	320	
NA - CHO	1.50	-1.49	-6.30	-3.31	2.99	275 (293)	168	343	
NA - CN	1.55	-1.45	-6.35	-3.35	3.00	264 (294)	271	357	
NA - Br	1.51	-1.48	-6.31	-3.32	2.99	284 (303)	201	343	
NA - Cl	1.47	-1.41	-6.27	-3.39	2.88	278 (295)	197	339	
NA - F	1.44	-1.40	-6.24	-3.40	2.84	274 (292)	192	335	

^a $E_{\text{onset}}^{\text{ox}}$ and $E_{\text{onset}}^{\text{red}}$ are measured versus ferrocene/ferrocenium; ^b $E_{\text{g}}^{\text{ec}} = (E_{\text{onset}}^{\text{ox}} - E_{\text{onset}}^{\text{red}})$; ^c Decomposition temperatures T_5 at 5% and T_{10} at 10% (in parantheses) weight loss; ^d Melting point of the derivatives from DSC; ^e Derivative weight loss.

3.7 CONCLUSIONS

A series of novel naphthalimide derivatives containing electron-donating halogen-phenoxy groups at the C-4 position of 1,8-naphthalimide were studied. These derivatives have high electron affinity with desired wide band gap required for blue light emission. The crystal structure, optical, thermal, morphological and electrochemical studies of the naphthalimides were investigated using single crystal XRD, UV-Vis absorption spectrometry, PL spectrometry, TGA, DSC, AFM and cyclic voltammetry, respectively. Single crystal XRD analysis of **NI-Br** confirmed its molecular structure; **NI-Br** crystallizes in the triclinic space group *P*-1. The UV-Vis absorption spectra of the derivatives in the solid thin film form showed red shifted broad bands as compared with that in the solution form, indicating that the conjugation lengths are slightly increased. The derivatives in the solid state showed blue photoluminescence with excellent chromaticity and high Stokes' shifts. The evaluated thermal properties revealed that the derivatives have high melting points and good thermal stabilities. Electrochemical properties, determined using cyclic voltammetry, show that the derivatives have low-lying HOMO-LUMO levels making them good electron-transporting and hole-blocking materials. These results demonstrate that these derivatives are promising candidates for non-doped blue emitters with electron-transport/hole-blocking properties (n-type) and could play an important role in the development of OLEDs.

CHAPTER 4

NAPHTHALIMIDE DERIVATIVES FOR ORGANIC LIGHT EMITTING DIODES

Overview

Chapter 4 discusses the suitability of naphthalimide derivatives as blue light emitting electron transport materials for organic light emitting diodes. This is realized by fabricating OLEDs with naphthalimides as electroluminescent materials, electron transporting materials and electron transporting emitters using different device configurations. The role of naphthalimides as host material is investigated by fabricating red OLEDs using DCM and Rubrene as dopants. The results suggest that the naphthalimides could be used as emissive as well as ETL and host materials in OLEDs.

4.1 INTRODUCTION

Naphthalimide derivatives are an attractive class of organic materials for OLEDs. They have high electron affinities, wide energy gaps and low reduction potentials, and making them good candidates for use as n-type materials in OLED [Niu et al. 2006 Bojinov et al. 2009 Lee et al. 2013 Wang et al. 2014]. Many naphthalimide derivatives have low luminescence efficiencies at room temperature due to strong intersystem crossing to their triplet states [Cacialli et al. 1998 Islam et al. 2005 Liu et al. 2008 Wang et al. 2014]. Naphthalimides substituted at the 4 position with electron-donating groups can have high fluorescent quantum yields [Wang et al. 2010]. Moreover, naphthalimides have been especially attractive because the synthesis procedures are simpler and they exhibit good spectral response. Naphthalimides have been utilized in OLEDs based on both small molecules and polymers [Xiao and Deng 2012 Wang et al. 2014 Triboni et al. 2015]. The high electron affinities and ionization potentials of 1,8-naphthalimides suggest that they may be useful electron-transport or hole-blocking materials in OLEDs.

Also, for full-colour displays, three basic colours, red, green, and blue (RGB) are needed. One of the most widely used methods to generate red light is guest-host structure. In this structure often a higher energy-emitting host (donor) material is doped with lower energy red emitting guest (acceptor) materials to bring about energy transfer from the host to the guest molecules. Doping techniques have been well developed to achieve various emission colours by choosing appropriate fluorescent dyes as the dopant. A small amount of dopant can dramatically change the emission wavelength

and emission intensity. Further, higher efficiency is obtained compared to undoped devices [Barros et al. 1993 Cacialli et al. 1998 Bojinov and Grabchev 2001 Chatterjee et al. 2007 Banerjee et al. 2013]. The energy transfer mechanism from the host to the dopant has been reported earlier [Tang et al. 1989 Hosokawa et al. 1995]. The mechanism of dopant excitation is explained by the energy transfer from the excited host molecules to the dopant molecules [Tang et al. 1989] or by the direct recombination at the dopant molecules resulting from carrier trapping [Littman and Martic 1992]. Devices doped with additional dopant have been reported [Hamada et al. 1999]. An important aspect of host–guest systems is the choice of host and guest materials for both single and multidoped systems. The energy transfer from host to guest can be either Förster [Lakowicz 2007] type energy transfer or Dexter type [Turro 1991] charge transfer or due to the formation of excimer or exciplexes. The primary condition to enable such energy transfers is a large overlap of the emission spectrum of the host and absorption spectrum of the guest. Therefore, the host material is always one with emission at higher energies, generally a blue-emitting material.

In this chapter, the role of naphthalimide derivatives as blue light emitting electron transport materials is realized by fabricating OLEDs with naphthalimides as electroluminescent materials, electron transporting materials and electron transporting emitters. Further, the role of naphthalimides as host material in red OLEDs is studied using DCM and Rubrene as dopants.

4.2 OLEDs USING NAPHTHALIMIDES AS ACTIVE MATERIALS

The electroluminescent properties of the naphthalimide derivatives were evaluated by fabricating OLEDs using naphthalimide derivatives.

4.2.1 Naphthalimide derivative as emissive materials

The electroluminescent properties of naphthalimide derivatives (**Naph**) as blue emitters were evaluated by fabricating multilayer OLEDs with the device configuration **I**: ITO (120 nm)/ α -NPD (30 nm)/ **Naph** (35 nm)/ BCP (6 nm)/ Alq₃ (35 nm)/ LiF (1 nm)/ Al (150 nm). Here ITO was used as a transparent anode, α -NPD as HTL, BCP as HBL and Alq₃ as ETL; LiF and Al were used as the EIL and cathode, respectively. The related HOMO/LUMO energy levels of the materials used are illustrated in Figure 4.1.

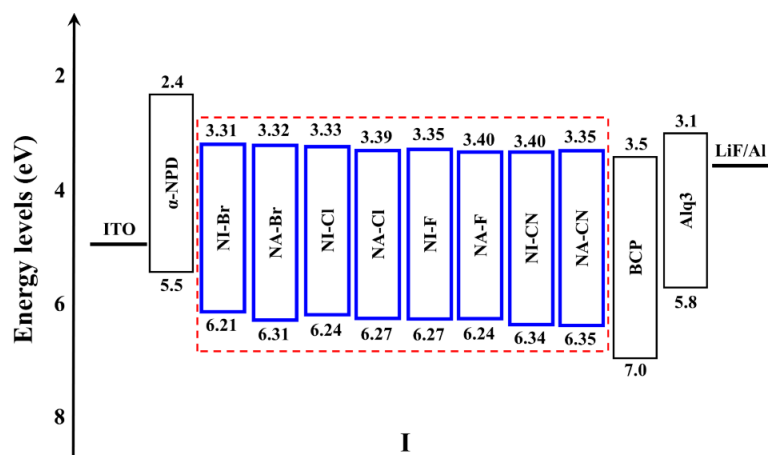


Figure 4.1. Energy-level diagram of the materials used in the devices (**I**) with naphthalimide derivatives as EL materials

The J-V-L characteristics of the fabricated OLEDs are shown in Figure 4.2. The characteristics of the current density as a function of applied voltage reveal ideal diode like behaviour. The performance data of the devices are summarized in Table 4.1. The devices utilizing **Naph** as emitter materials exhibit drive voltages of ~ 6 V corresponding to light output of 1 cd/m^2 with maximum luminance of $\sim 1300 \text{ cd/m}^2$ at 15 V, current efficiency (η_c) of $\sim 1.1 \text{ cd/A}$, power efficiency (η_p) of $\sim 0.3 \text{ lm/W}$ and external quantum efficiency (η_{EQE}) of $\sim 0.5 \%$. The current density-luminance (J-L) characteristics (Figure 4.3) show a linear relationship between current density and luminance.

The variations of EL intensity with different applied voltages are shown in Figure 4.4. The EL spectra of the devices with **Naph** as emissive materials show greenish-blue light emission with peaks centered at $\sim 480 \text{ nm}$ with FWHM of $\sim 70 \text{ nm}$. The narrow FWHM in EL spectra suggests that the derivatives are capable of forming device with good chromaticity. The CIE chromaticity coordinates of the derivatives as EL materials are determined using the EL spectra of the devices at 15 V. The CIE coordinates are summarized in Table 4.1 and chromaticity diagram is shown in Figure 4.5. It can also be observed from Figure 4.4 that the variation of applied voltage has no effect on the shape and the peak of the EL spectra. Compared to the thin film PL spectra ($\lambda_{\text{PL}} \sim 460 \text{ nm}$), bathochromic shifts of $\sim 20 \text{ nm}$ were observed in the EL emission peaks for all the derivatives. This may be ascribed to the intermolecular interactions in the excited states [Zhuang et al. 2014].

Table 4.1 Electroluminescent performance data of naphthalimide derivatives as emissive materials

Device ^a	V_{onset} (V) ^b	L_{max} (cd/m ²) ^c	η_c (cd/A) ^d	η_p (lm/W) ^e	η_{ext} (%) ^f	λ_{em} (FWHM) (nm) ^g	CIE (x,y) ^h
NI-Cl	7.03	889	0.89 (13.5)	0.21 (14.0)	0.41 (13.0)	487 (70)	(0.190, 0.283)
NA-Cl	6.92	1072	0.96 (14.5)	0.23 (13.0)	0.47 (13.5)	485 (71)	(0.181, 0.279)
NI-Br	7.43	866	0.84 (14.0)	0.21 (13.5)	0.44 (14.5)	487 (69)	(0.184, 0.331)
NA-Br	7.31	983	0.92 (14.0)	0.23 (13.5)	0.48 (14.0)	481 (70)	(0.180, 0.281)
NI-CN	6.34	1238	1.13(14.5)	0.32 (14.0)	0.51 (14.5)	473 (73)	(0.173, 0.212)
NA-CN	6.19	1384	1.18 (14.0)	0.37 (13.5)	0.55 (14.5)	468 (71)	(0.170, 0.254)
NI-F	6.91	1094	0.98 (14.0)	0.28 (14.5)	0.46 (13.5)	483 (72)	(0.182, 0.294)
NA-F	6.73	1186	1.03(14.5)	0.31 (14.5)	0.49 (14.0)	479 (74)	(0.176, 0.268)

^a Device Configuration I: ITO (120 nm)/ α -NPD (30 nm)/**Naph** (35 nm)/BCP (6 nm)/Alq₃ (35 nm)/LiF (1 nm)/Al (150 nm).

^b V_{onset} : turn-on voltage at luminance of 1 cd m⁻²

^c L_{max} : Maximum luminance at 15 V

^d η_c : Maximum current efficiency measured at applied voltage (in parentheses)

^e η_p : Maximum power efficiency measured at applied voltage (in parentheses)

^f η_{ext} : Maximum external quantum efficiency measured at applied voltage (in parentheses)

^g λ_{em} : Emission wavelength maximum. FWHM: at 15 V

^h CIE color coordinate

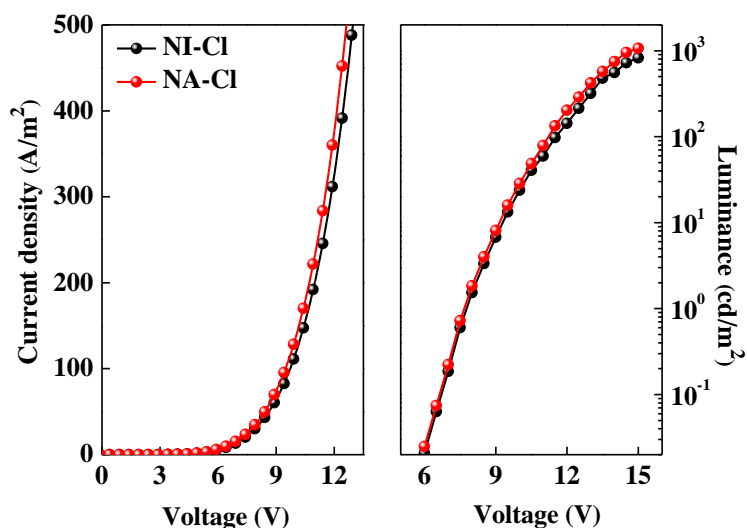


Figure 4.2 J-V-L characteristics for OLEDs with naphthalimides (NI-Cl and NA-Cl) as EL materials

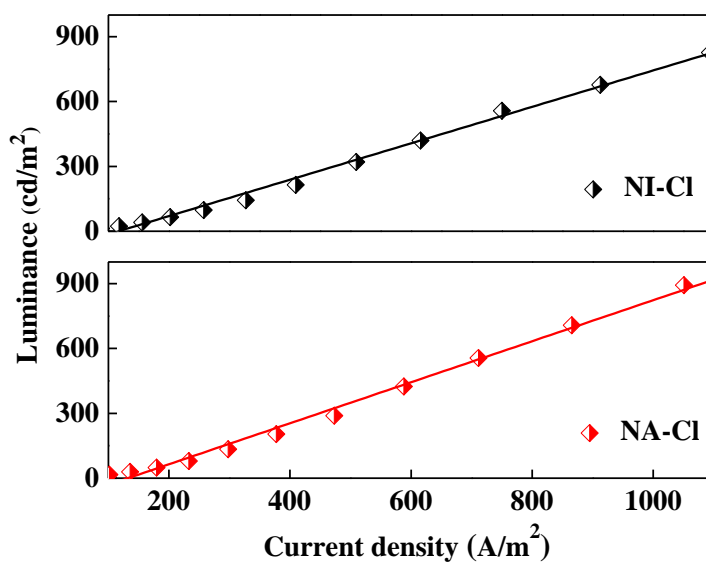


Figure 4.3 J-L characteristics for OLEDs with naphthalimides (NI-Cl and NA-Cl) as EL materials

4.2.2 Naphthalimide as ETL material in phosphorescent OLEDs

The electron transport properties of the derivatives were investigated by fabricating devices with tris[2-phenylpyridinato-C2,N]iridium(III) (Ir(ppy)₃) doped 4,4'-bis(9-carbazolyl)-biphenyl (CBP) as phosphorescent emitter with the following device configurations:

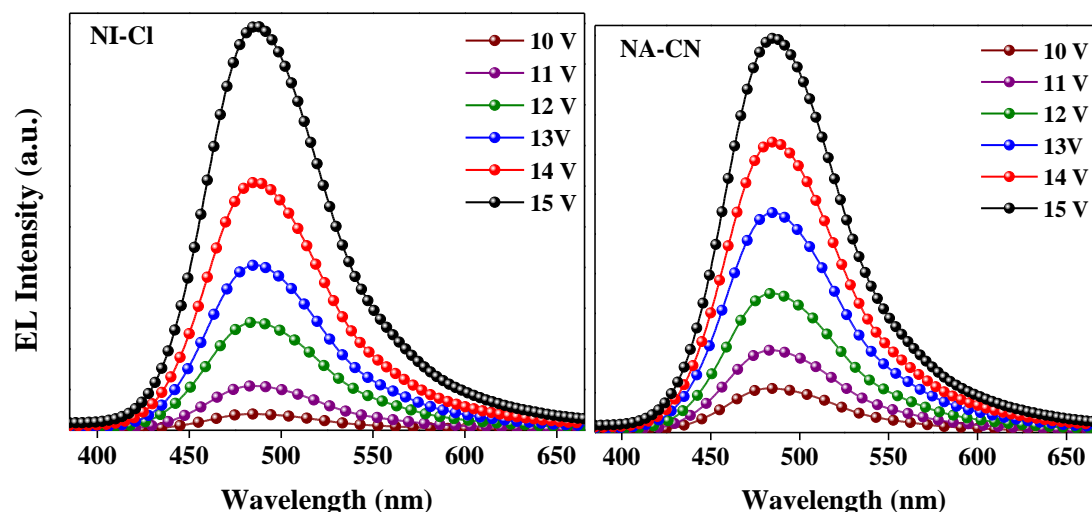


Figure 4.4 EL spectra of the OLEDs with naphthalimides as EL materials at different applied voltages

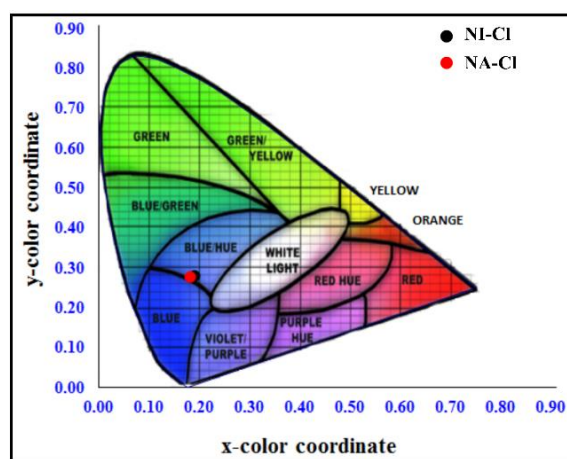


Figure 4.5 Chromaticity diagram of the OLEDs with naphthalimides as EL materials

Device **II**: ITO (120 nm)/ α -NPD (40 nm)/ Ir(ppy)₃ doped CBP (35 nm)/ BCP (6 nm)/ LiF (1 nm)/ Al (150 nm).

Device **III**: ITO (120 nm)/ α -NPD (40 nm)/ Ir(ppy)₃ doped CBP (35 nm)/ BCP (6 nm)/ Alq₃ (30 nm)/ LiF (1 nm)/ Al (150 nm).

Device **IV**: ITO (120 nm)/ α -NPD (40 nm)/ Ir(ppy)₃ doped CBP (35 nm)/ BCP (6 nm)/ Naph (30 nm)/ LiF (1 nm)/ Al (150 nm).

Here only ETL was changed while the rest of the device configuration was kept same. The devices were fabricated without any ETL material (**II**), with **Alq₃** as ETL (**III**) and with **Naph** as ETL (**IV**). The related HOMO/LUMO energy levels of the materials used are illustrated in Figure 4.6.

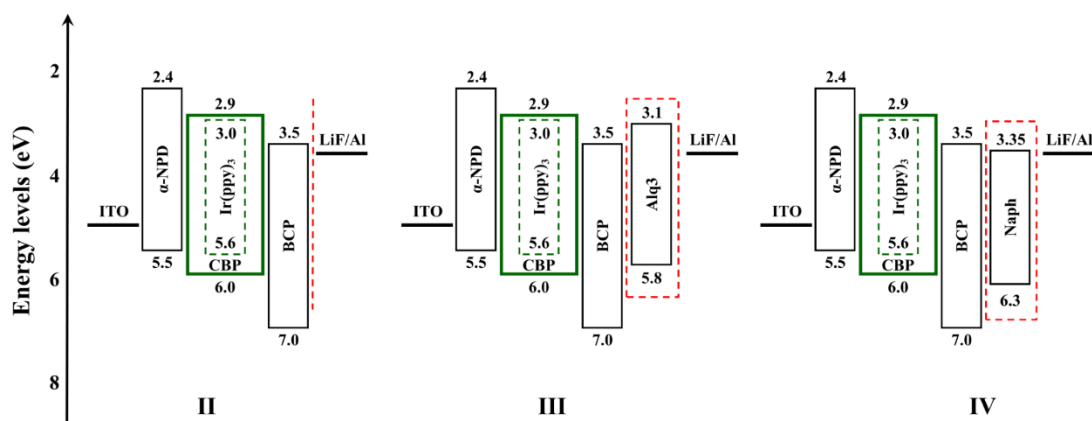


Figure 4.6 Energy-level diagram of the materials used in the phosphorescent OLEDs with triplet emitter Ir(ppy)_3 doped with CBP (**II**) without ETL (**III**) with standard AlQ_3 as ETL and (**IV**) with Naph as ETL

The data for each of these devices are depicted in Table 4.2. The J-V-L and J-L characteristics of the devices are shown in Figure 4.7 and Figure 4.8, respectively. The EL spectrum (Figure 4.9) is observed to be similar for all the devices, with a λ_{max} of 516 nm which is due to Ir(ppy)_3 . It is evident from Figure 4.7 and Table 4.2 that with the inclusion of **Naph** as ETL, there is a drastic increase in the efficiencies: 9.0 cd/A (η_c), 1.98 lm W^{-1} (η_p) and 1.46 % (η_{EQE}) when compared to the device without ETL: 5.39 cd A^{-1} (η_c), 1.23 lm W^{-1} (η_p) and 0.94 % (η_{EQE}). These results reveal that by using **Naph** as ETL, a significant improvement in performance is achieved as compared to the device without any ETL and is comparable to the device with Alq_3 as ETL.

4.2.3 Naphthalimide derivative as EL and ETL material

The role of naphthalimide derivatives as electron transporting and light emitting materials was studied by fabricating OLEDs with the following device configurations:

Device **V**: ITO (120 nm)/ α -NPD (40 nm)/ **Naph** (50 nm)/ LiF (1 nm)/ Al (150 nm)

Table 4.2 Electroluminescent data of OLEDs using of triplet emitter Ir(ppy)₃ doped with CBP

Device ^a	V _{onset} (V) ^b	L _{max} (cd/m ²) ^c	η _c (cd/A) ^d	η _p (lm/W) ^e	η _{ext} (%) ^f	λ _{em} (nm) ^g
Without ETL	12.76	1714	5.39 (19)	1.23 (18)	0.94 (18)	516
Alq₃	9.09	9650	9.79 (20)	2.71 (19)	1.70 (18)	516
NI-Br	9.41	5078	8.81 (20.0)	1.78 (18.0)	1.40 (20.0)	516
NI-Cl	9.23	5341	8.9 (19.5)	1.82 (19)	1.39 (19.5)	516
NA-Cl	9.14	5962	9.04 (20.0)	1.98 (19.0)	1.46 (19.5)	516
NI-F	9.67	4873	8.12 (19.5)	1.67 (19.0)	1.32 (20.0)	516
NA-CN	9.83	4056	7.32 (20.0)	1.53 (19.5)	1.21 (20.0)	516

^a Device Configuration **II-IV**: ITO (120 nm)/α-NPD (40 nm)/ Ir(ppy)₃ doped CBP (35 nm)/ BCP (6 nm)/ **No ETL** or **Alq₃** or **Naph** (30 nm)/ LiF (1 nm)/ Al (150 nm)

^b V_{onset}: turn-on voltage at luminance of 1 cd m⁻²

^c L_{max}: Maximum luminance at 21 V

^d η_c: Maximum current efficiency measured at applied voltage (in parentheses)

^e η_p: Maximum power efficiency measured at applied voltage (in parentheses)

^f η_{ext}: Maximum external quantum efficiency measured at applied voltage (in parentheses)

^g λ_{em}: Emission wavelength maximum at 21 V

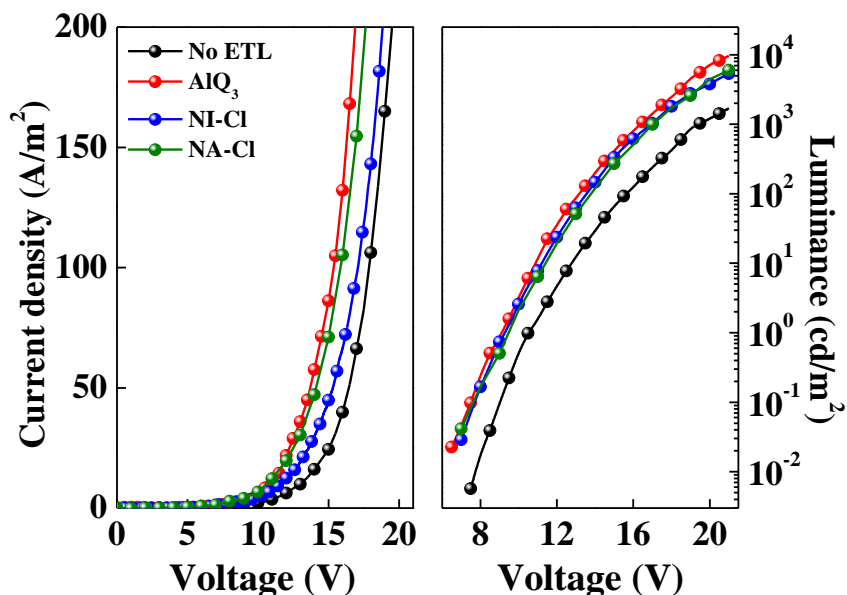


Figure 4.7 J-V-L characteristics of triplet emitter Ir(ppy)₃ doped with CBP without ETL/with Alq₃/Naph as ETL

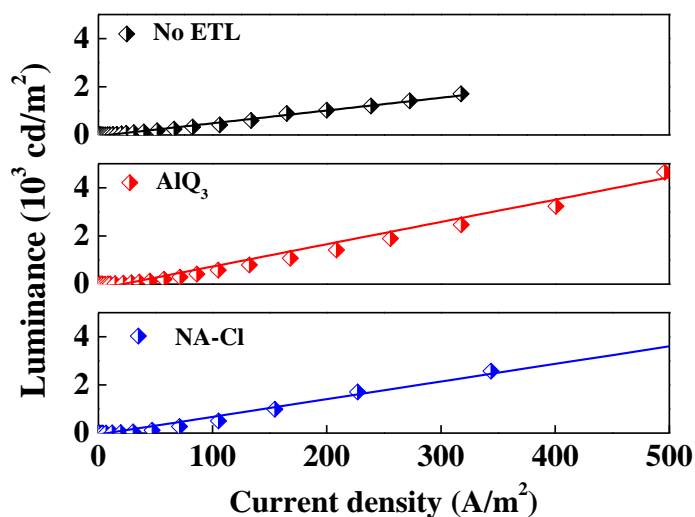


Figure 4.8 J-L characteristics of triplet emitter Ir(ppy)₃ doped with CBP without ETL/with Alq₃/Naph as ETL

Device **VI**: ITO (120 nm)/ F₄TCNQ (4 nm)/ α -NPD (40 nm)/ **Naph** (50 nm)/ LiF (1 nm)/ Al (150 nm)

Device **VII**: ITO (120 nm)/ F₄TCNQ (4 nm)/ α -NPD (40 nm)/ **Naph** (50 nm)/ BCP (6 nm)/ LiF (1 nm)/ Al (150 nm)

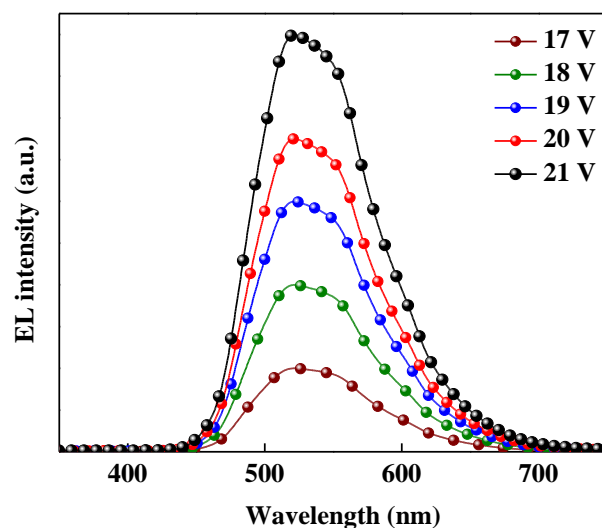


Figure 4.9 EL spectra of the OLEDs with triplet emitter Ir(ppy)₃ doped with CBP at different applied voltages

Here F₄TCNQ acts as HIL for efficient hole injection from ITO anode to hole transport layer α -NPD. The related HOMO/LUMO energy levels of the materials used are illustrated in Figure 4.10. An optimized thickness of F₄TCNQ (4 nm) was used for better hole injection. The device performance data is presented in Table 4.3. It is evident from Table 4.3 that the device **V** using NI-Cl as active material without F₄TCNQ and BCP has low efficiencies of 0.45 cd A⁻¹ (η_c), 0.11 lm W⁻¹ (η_p) and 0.24 % (η_{EQE}). With the inclusion of 4 nm of F₄TCNQ layer (device **VI**) there is a considerable increase in efficiencies; 1.79 cd A⁻¹ (η_c), 0.51 lm W⁻¹ (η_p) and 0.40 % (η_{EQE}). This can be ascribed to the efficient injection of holes from the ITO anode to the hole transport layer. Furthermore, in device **VII**, with the use of BCP as an HBL, a further increase in the efficiencies to 1.87 cd A⁻¹ (η_c), 0.86 lm W⁻¹ (η_p) and 0.69 % (η_{EQE}) was achieved. This increase in efficiencies may be due to the confining of holes in the emitting layer which didn't recombine with the electrons in the emitting zone [Tomova et al. 2010]. The device structure **VII** used for all the other derivatives. It is evident from Table 4.3 that the devices with structure **VII** with naphthalimides as active materials show efficiencies close to 1.99 cd A⁻¹ (η_c), 1.2 lm W⁻¹ (η_p) and 0.83 % (η_{EQE}). Our investigations indicate that the synthesized naphthalimide derivatives could be used as emissive as well as ETL materials in OLEDs.

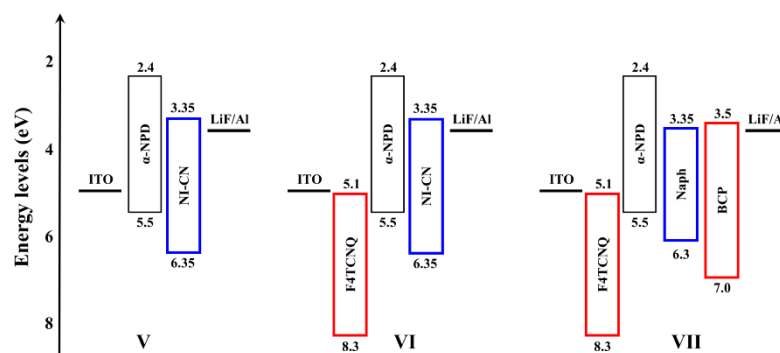


Figure 4.10 Energy-level diagram of the materials with naphthalimides as EL and ETL materials (**V**) without F₄TCNQ and BCP (**VI**) with F₄TCNQ and without BCP, and (**VII**) with F₄TCNQ and BCP

Table 4.3 Electroluminescence data of OLEDs using naphthalimides as both EL and ETL materials

Device	V_{onset} (V) ^d	L_{max} (cd m ⁻²) ^e	η_{c} (cd A ⁻¹) ^f	η_{p} (lm W ⁻¹) ^g	η_{ext} (%) ^h
NI-Cl ^a	9.67	472	0.45 (14.5)	0.11(12.5)	0.24 (14.0)
NI-Cl ^b	6.62	1493	1.79 (14.0)	0.51 (13.5)	0.40 (13.5)
NI-Cl ^c	6.35	1580	1.87 (14.0)	0.86 (14.5)	0.69 (14.0)
NA-Cl ^c	6.18	1681	1.89 (14.05)	0.98 (13.5)	0.71 (13.0)
NI-Br ^c	6.67	1429	1.63 (14.0)	0.82 (14.0)	0.49 (14.5)
NA-Br ^c	6.58	1462	1.70 (13.0)	0.81 (13.0)	0.52 (14.5)
NI-CN ^c	6.13	1854	1.96 (14.0)	1.13 (14.0)	0.78 (14.0)
NA-CN ^c	6.01	1963	1.99 (14.5)	1.20 (14.0)	0.83 (14.0)
NI-F ^c	6.30	1654	1.88 (14.5)	0.91 (14.0)	0.72 (14.5)
NA-F ^c	6.28	1672	1.90 (14.0)	0.94 (13.5)	0.73 (14.0)

^a Device Configuration **V**: ITO (120 nm)/ α -NPD (40 nm)/ **NI-Cl** (50 nm)/ LiF (1 nm)/ Al (150 nm)

^b Device Configuration **VI**: ITO (120 nm)/ F₄TCNQ (4 nm)/ α -NPD (40 nm)/ **NI-Cl** (50 nm)/ LiF (1 nm)/ Al (150 nm)

^c Device Configuration **VII**: ITO (120 nm)/ F₄TCNQ (4 nm)/ α -NPD (40 nm)/ **Naph** (50 nm)/ BCP (6 nm)/ LiF (1 nm)/ Al (150 nm)

^d V_{onset} : turn-on voltage at luminance of 1 cd m⁻²

^e L_{max} : Maximum luminance at 15 V

^f η_{c} : Maximum current efficiency measured at applied voltage (in parentheses)

^g η_{p} : Maximum power efficiency measured at applied voltage (in parentheses)

^h η_{ext} : Maximum external quantum efficiency measured at applied voltage (in parentheses)

4.3 OLEDS USING NAPHTHALIMIDES AS HOST MATERIALS

In this section, the role of naphthalimide derivatives as host materials for red OLEDs is discussed. Red OLEDs were fabricated by doping DCM and Rubrene in NA-CN. Also, a red OLED with standard host material, Alq₃, was fabricated and compared. The energy values of NA-CN, rubrene and DCM are shown in Figure 4.11.

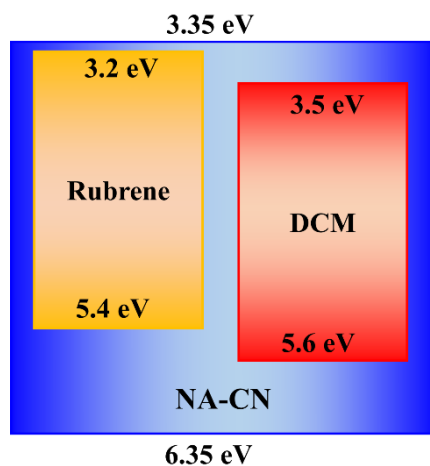


Figure 4.11 HOMO-LUMO levels of NA-CN, Rubrene and DCM

In this study, Rubrene was employed as an assistive dopant in order to enhance energy transfer from host to dopant and thus improve the EL efficiencies. The electron transfer from rubrene to DCM in the device is facilitated by the fact that the LUMO level of DCM is below that of rubrene. The electrons on the LUMO of rubrene transfer into that of DCM readily. For hole transfer, the HOMO level of DCM is just below that of rubrene. The hole transfer from rubrene to DCM is hard to occur [Hongyu Liu et al. 2002]. However, the mobility of holes in α -NPD is approximately two orders of magnitude higher than that of electrons in n-type materials [Chen and Liu 1997, Stolka et al. 1984, Kepler et al. 1995]. The holes injected from the hole transport layer are the majority carriers in the recombination zone. Therefore, the recombination of electrons and holes in DCM may occur more readily.

Figure 4.12 shows the absorption spectra of DCM, and PL spectra of the NA-CN. According to the theory of dipole-dipole energy transfer, the energy transfer rate is proportional to the spectral overlap integral between the donor emission and the acceptor absorption [Galanin et al. 1999]. There is a good overlap between the

absorption spectrum DCM with NA-CN emission spectrum. This overlap guarantees the energy transfer from NA-CN as the host to DCM as the guest.

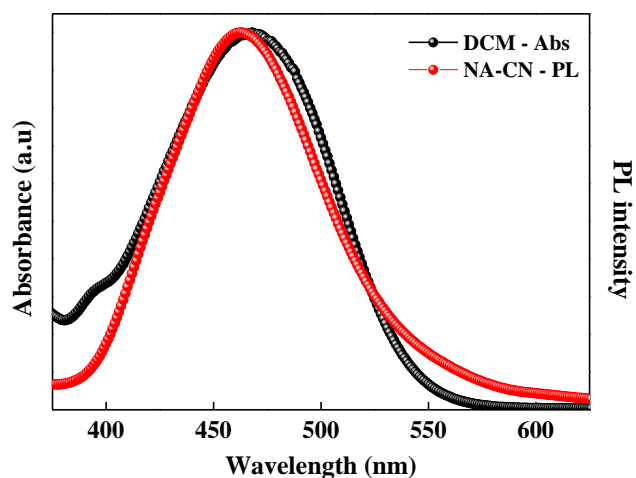


Figure 4.12 PL spectra of NA-CN and absorbance spectra of DCM

Multilayer OLEDs using NA-CN as a new host material was realized by fabrication of red OLEDs using rubrene and DCM as dopants with the following device configurations:

Device **R₁**: ITO/ F₄TCNQ (10 nm)/ α -NPD (40 nm)/ NA-CN (40 nm)/ LiF (1 nm)/ Al (150 nm)

Device **R₂-R₇**: ITO/ F₄TCNQ (10 nm)/ α -NPD (40 nm)/ NA-CN: DCM (2 %):Rubrene (**x** %) (40 nm)/ NACN (5 nm)/ LiF (1 nm)/ Al (150 nm), where **x** = 0 % (**R₂**), 1 % (**R₃**), 2 % (**R₄**), 3 % (**R₅**), 4 % (**R₆**) and 5 % (**R₇**)

Device **R₈**: ITO/ F₄TCNQ (10 nm)/ α -NPD (40 nm)/ NA-CN: DCM (2 %):Rubrene (4 %) (40 nm)/ AlQ₃(5 nm)/ LiF (1 nm)/ Al (150 nm)

Device **R₉**: ITO/ F₄TCNQ (10 nm)/ α -NPD (40 nm)/ NA-CN: DCM (2 %):Rubrene (4 %) (40 nm)/ BCP (6 nm)/ AlQ₃ (5 nm)/ LiF (1 nm)/ Al (150 nm)

Device **R_{STD}**: ITO/ F₄TCNQ (10 nm)/ α -NPD (40 nm)/ AlQ₃: DCM (2 %):Rubrene (4 %) (40 nm)/ BCP (6 nm)/ AlQ₃ (5 nm)/ LiF (1 nm)/ Al (150 nm)

Figure 4.13 shows the chromaticity diagrams for devices **R**₁ – **R**₆ estimated from the EL spectra at 15 V. In the absence of the dopants, the device **R**₁ produced a blue emission with CIE coordinates (x=0.17, y=0.25) that comes from **NA-CN**. Doping **NA-CN** with the red dopant DCM (2 %), the device (**R**₂) produces red emission (x=0.44, y=0.22). The device did not exhibit a pure red emission which may be due to the simultaneous blue emission from the host **NA-CN**. The contribution of blue component from **NA-CN** indicates that the complete energy transfer did not take place from **NA-CN** to DCM. The CIE coordinates of the fabricated devices are tabulated in Table 4.4.

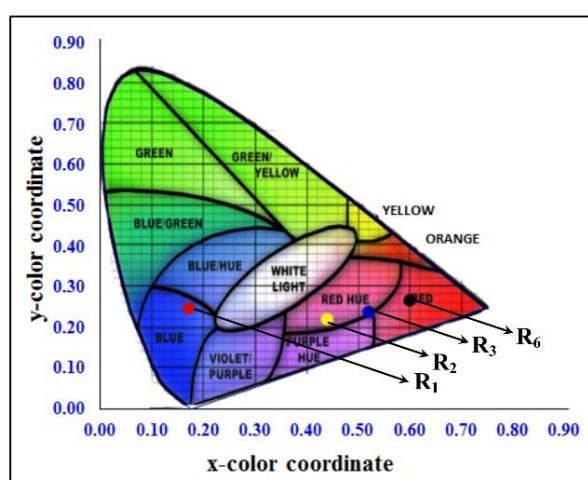


Figure 4.13 Variation in the CIE chromaticity coordinates for devices **R**₁, **R**₂, **R**₃ and **R**₆ with different concentration of Rubrene.

It can be seen from the Figure 4.13 and Table 4.4 that addition of Rubrene to **NA-CN**: DCM (devices **R**₃) resulted in better chromaticity which may be due to the suppression the blue emission from **NA-CN**. The device **R**₆ with 2% DCM and 4 % Rubrene doped into the **NA-CN** shows good red purity with $EL_{max} = 621$ nm (x=0.62, y=0.27) among the devices **R**₂–**R**₆. This may be the result of efficient charge transfer from **NA-CN** to DCM via Rubrene. Hence, electrons and holes recombine on DCM, and DCM molecules emit in red region. Thus, red purity of Rubrene-doped device is improved. It was observed that there was no much change in the shape of EL spectra beyond 4 % doping concentration of Rubrene. However, the EL peak of device **R**₇ with 5 % Rubrene is 617 nm. The red purity of device **R**₇ (x=0.62, y=0.27) is lower than that of device **R**₆ (Table 4.4). This may be due the recombination of part of injected

electrons and holes in the Rubrene molecules. Since Rubrene emit in the yellow region, the red purity of device is reduced. Hence, for the host material **NA-CN**, if concentration of rubrene (4%) is over-high with regard to that of DCM (2%), red purity of the decreases. This indicates complete energy transfer from the **NA-CN** to DCM at 4% Rubrene doping concentration.

Table 4.4 Electroluminescent data of the red OLEDs with different concentration of Rubrene

Device	DCM (%)	Rubrene (%)	CIE _{x,y}
R₁	0	0	(0.17, 0.25)
R₂	2	0	0.44, 0.22
R₃	2	1	(0.52, 0.24)
R₄	2	2	(0.56, 0.25)
R₅	2	3	(0.58, 0.26)
R₆	2	4	(0.60, 0.27)
R₇	2	5	(0.62, 0.27)
R₈	2	4	(0.62, 0.29)
R₉	2	4	(0.62, 0.26)
R_{STD}	2	4	(0.65, 0.33)

Though the HOMO/LUMO levels of **NA-CN** is comparable with that of Alq₃, the electron-transporting ability of **NA-CN** is lower than that of Alq₃ (see Section 4.2.2). Therefore, Alq₃ may be potential candidates to enhance the efficiency in our device configuration. Therefore, more holes and electrons can recombine in the emission layer, and more excitons can form in this layer. Due to the efficient energy transfer from host to dopant, more emission from DCM can be obtained. This may lead to the high efficiency of the red OLED based on the new host material. In the device configuration **R₈**, Alq₃ was used in place of **NA-CN** as the ETL material. It can be seen Table 4.5 that the device **R₈** showed better performance than device **R₆** with maximum luminance of 8839 cd/m² with efficiencies of 4.54 cd/A (η_c), 2.85 lm/W (η_p) and 2.11 % (η_{EXE}). Further increase in luminance (9164 cd/m²) and efficiencies (η_c : 4.65 cd/A, η_p : 2.93 lm/W and η_{EXE} : 2.18 %) was observed in device **R₉**, which has BCP as hole blocking layer. This can be ascribed to the confinement of holes in the emitting layer. Device **R_{STD}** was fabricated using a standard host material Alq₃. In the standard device,

R_{STD}, only host material was changed while the rest of the configuration was same as device **R₉**. Figure 4.14 shows the EL spectra of devices **R₉** and **R_{STD}**. It can be seen from the Figure 4.14 and Table 4.5 that the device **R₉** showed narrow FWHM with EL maximum at 626 nm compared to device **R_{STD}**. It can be from Figure 4.15 that the CIE coordinates device **R₉** are located in the deep red region of the chromaticity diagram.

Table 4.5 Electroluminescent performance data of red OLEDs

Device	V_{onset} (V) ^a	L_{max} (cd/m ²) ^b	η_c (cd/A) ^c	η_p (lm W ⁻¹) ^d	η_{ext} (%) ^e	λ_{em} (FWHM) (nm) ^f
R6	6.75	6042	3.81 (8.5)	2.23 (8.5)	1.42 (9.0)	621 (59)
R8	5.86	8839	4.54 (8.5)	2.85 (8.5)	2.11 (9.0)	622 (54)
R9	5.81	9164	4.65 (9.5)	2.93 (8.5)	2.18 (9.5)	626 (51)
RSTD	6.02	8320	4.38 (9.0)	2.68 (8.0)	1.93 (9.5)	611 (67)

^a V_{onset} : turn-on voltage at luminance of 1 cd m⁻²

^b L_{max} : Maximum luminance at 15 V

^c η_c : Maximum current efficiency measured at applied voltage (in parentheses)

^d η_p : Maximum power efficiency measured at applied voltage (in parentheses)

^e η_{ext} : Maximum external quantum efficiency measured at applied voltage (in parentheses)

^f λ_{em} : Emission wavelength maximum. FWHM: at 15 V

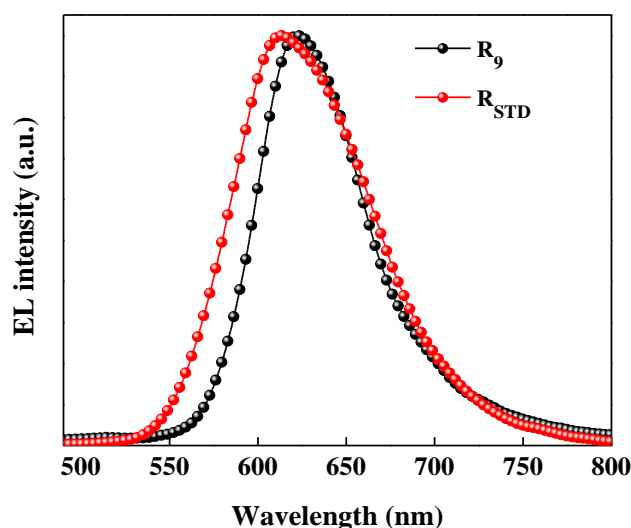


Figure 4.14 EL spectra of the OLEDs with NA-CN (**R₉**) and Alq₃ (**R_{STD}**) as hosts

Figure 4.16 shows the EL spectra of the device **R₉** at different applied bias voltages. In general, EL spectra of many red OLEDs based on the host-dopant systems

will change with an increase in applied voltage. The emission from the host will be observed, and this will lead to the change of the color purity, especially in high bias voltages. Notably, the EL spectra in this work almost remained intact with an increase in voltage from 15 to 20 V, no emission from NA-CN in the device was observed. This shows that the naphthalimides are promising candidates for fabrication of low cost red OLEDs.

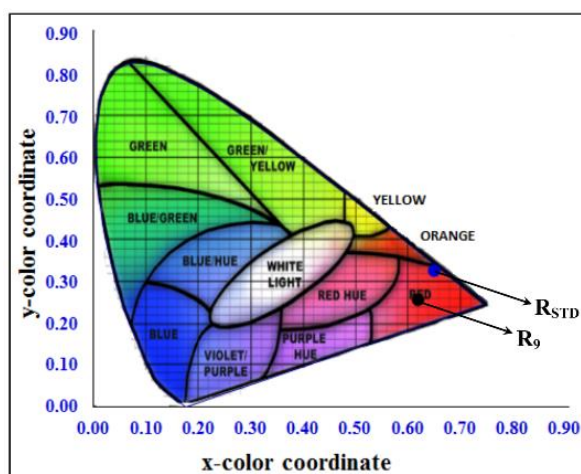


Figure 4.16 Chromaticity diagram of the red OLEDs **R₉** with NA-CN as host material and **R_{STD}** with Alq₃ as host material

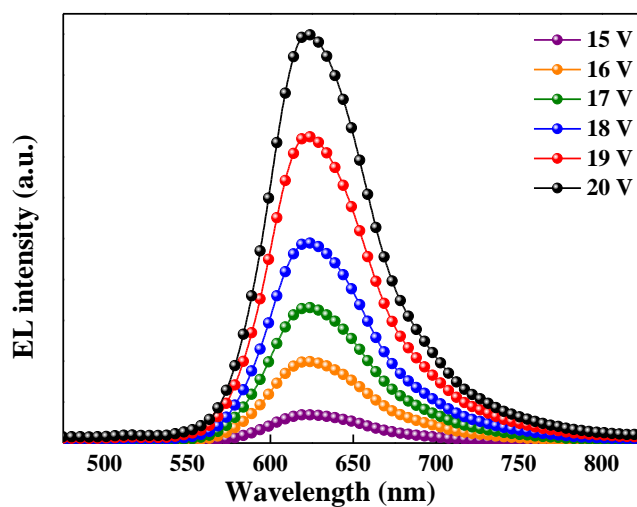


Figure 4.16 EL spectra of the OLEDs with NA-CN as host material (**R₉**) at different applied voltages

4.4 CONCLUSIONS

OLEDs using naphthalimides as emissive materials showed efficiencies of 1.18 cd/A (V), 0.37 lm/W (η_p) and 0.55 % (η_{EQE}). As ETL material, naphthalimide derivatives exhibited much better performance (η_c : 9.04 cd/A, η_p : 1.98 lm/W and η_{EQE} : 1.46 %) than the device without any ETL (η_c : 5.39 cd/A, η_p : 1.23 lm/W and η_{EQE} : 0.94 %) and was comparable with the device using standard ETL material, Alq₃. Furthermore, naphthalimides as both EL and ETL materials showed efficiencies of 1.99 cd/A (η_c), 1.2 lm/W (η_p) and 0.83 % (η_{EQE}) revealing that they can act as electron transporting emitters. These results demonstrate that naphthalimide derivatives are promising candidates as blue emitters with good electron transport property and could play an important role in the development of OLEDs. The devices with naphthalimides as host materials showed better chromaticity devices when compared to the devices with Alq₃ as hosts.

CHAPTER 5

PYRENE DERIVATIVES FOR ORGANIC LIGHT EMITTING DIODES

Overview

Chapter 5 discusses the application of pyrene derivatives (ME, TBUT and OME) in organic light emitting diodes. This is realized by fabricating OLEDs with pyrene derivatives as electroluminescent materials, electron transporting materials and electron transporting emitters using different device configurations. The results suggest that the derivatives could be used as emissive as well as ETL materials in OLEDs. Further, the transport mechanism in TBUT pyrene has been investigated by analysing its temperature dependence (160-320 K) in electron only devices.

5.1 INTRODUCTION

Pyrene and its derivatives have attracted great interest from the scientific community and extensively investigated for many organic electronic device applications, particularly in OLEDs over recent years due to their unique photophysical and electrochemical properties [Tao et al. 2005, Tang et al. 2006, Liu et al. 2011, Figueira-Duarte and Müllen 2011, Krotkus et al. 2012, Thomas et al. 2012]. Additionally, pyrene has proved to be a promising chromophore for actual device fabrications such as intense luminescence efficiency, long fluorescence lifetime, high thermal stability, enhanced charge carrier mobility due to their large π -conjugated systems [Figueira-Duarte and Müllen 2011, Krotkus et al. 2012, Thomas et al. 2012]. It is a well-known building block for blue and green light-emitting materials [Figueira-Duarte and Müllen 2011, Zhao et al. 2011, Thomas et al. 2012]. However, the high tendency towards π - π stacking of the pyrene moieties generally lends the pyrene-containing emitters strong intermolecular interactions in the solid state, which leads to a substantial redshift of their PL emission and a decrease of the PL quantum yields [Figueira-Duarte and Müllen 2011]. Pyrene has been the subject of extensive investigation because its photophysical and electrochemical properties can be readily tuned by incorporating electron donor or electron acceptor and by multiple substitutions of chromophores at different nuclear positions to develop numerous analogues [Kim et al. 2008, Figueira-Duarte and Müllen 2011, Feng et al. 2013, Kawano et al. 2013]. Researchers have modified pyrene in various ways in order to improve device performance [Wu et al. 2008, Wee et al. 2009, Gu et al. 2010, Lai et al. 2011, Thomas et al. 2012, Wang et al. 2012, Kotchapradist et al. 2013]. Various pyrene-based light-

emitting materials have been reported in recent literature including functionalized pyrene-based light-emitting molecules [Thomas et al. 2000, Wu et al. 2008], functionalized pyrene-based light-emitting dendrimers [Bernhardt et al. 2006, Zhao et al. 2008], oligomers and polymers. To date, many kinds of pyrene-based materials have been synthesized and considered for several applications [Figueira-Duarte and Müllen 2011], and some of them were proven to be promising blue emitters for OLEDs. Previously, there have been reports on pyrene compounds, but most of them are blue emitting materials [Lo et al. 2007, Salunke et al. 2014]. Pyrene functionalized triphenylamine based dyes as green-emitting materials in OLEDs have been reported by Zhan et al. [2013]. However, pyrene functionalized green emitters for OLEDs were less explored. On the other hand, an easy fabrication process is expected with fewer layers for large area fabrication point of view. Thus, in order to avoid deposition of both charge-transporting layer and an emitting layer, it is imperative to use organic materials with both light-emission and charge transporting properties. Hence, development of multifunctional materials, which can be used for both carrier transport and light-emission, is thus highly desirable [Figueira-Duarte and Müllen 2011].

With an aim to develop efficient electron transporting green emitters, we have investigated three new pyrene derivatives (**ME**, **TBUT** and **OME**). OLEDs with pyrene derivatives as green emitting materials, as electron transport materials and electron transporting emitters were studied. The role of hole injection or hole-blocking materials in OLEDs with these materials was also investigated. Further, electron only devices based on **TBUT** pyrene were fabricated and the temperature dependent electrical properties were investigated.

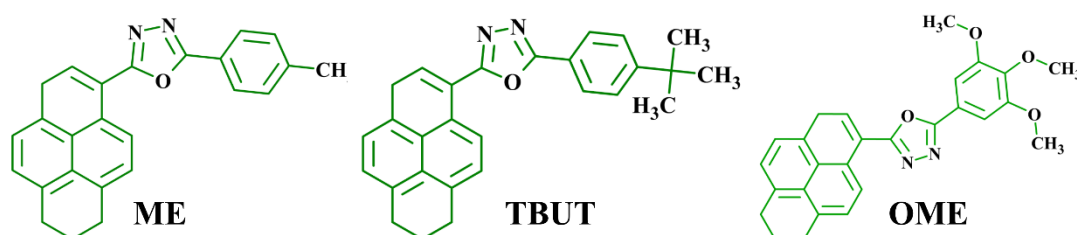


Figure 5.1 Chemical structure of the pyrene derivatives **ME**, **TBUT** and **OME**

Figure 5.1 shows the chemical structures of the pyrene derivatives: 2-(pyren-1-yl)-5-p-tolyl-1,3,4-oxadiazole (**ME**), 2-(4-tert-butylphenyl)-5-(pyren-1-yl)-1,3,4-

oxadiazole (**TBUT**) and 2-(pyren-1-yl)-5-(3,4,5-trimethoxyphenyl)-1,3,4-oxadiazole (**OME**). The photophysical, electrochemical and thermal data of the derivatives are presented in Table 5.1.

Table 5.1 Photophysical, electrochemical and thermal data of the pyrene derivatives.

	λ_{Abs} (nm)		λ_{Em} (nm)		Φ_{PL}	HOMO (eV)	LUMO (eV)	T_{m} (°C)	T_{d} (°C)
	CHCl ₃	Thin film	CHCl ₃	Thin film					
ME	268, 369, 394	292, 381, 403	426, 450	511	0.85	5.72	2.88	182	314
TBUT	288, 364, 394	287, 390, 402	426, 456	517	0.85	5.7	2.9	178	354
OME	283, 372, 396	291, 394, 407	428, 457	531	0.90	5.8	2.92	194	363

All the three derivatives were measured with 10^{-5} M concentration at room temperature.

Φ_{PL} : Fluorescence yields relative to 9,10-diphenyl anthracene ($\Phi = 0.9$ in cyclohexane).

T_{m} : melting point;

T_{d} : decomposition temperature (corresponding to 5% weight loss)

5.2 ELECTROLUMINESCENCE STUDIES

5.2.1 Pyrene derivatives as Emissive materials

The electroluminescent properties of pyrene derivatives as green emitters were evaluated by fabricating OLEDs with the device configuration **I-III**: ITO (120 nm)/ α -NPD (30 nm)/ **Pyrene** (35 nm)/BCP (6 nm)/ Alq₃ (35 nm)/ LiF (1 nm)/ Al (150 nm). Here ITO was used as a transparent anode, α -NPD was used as the HTL, BCP was used as the HBL and Alq₃ was used as the ETL; LiF and Al were used as the EIL and cathode, respectively. The related HOMO/LUMO energy levels of the materials are illustrated in Figure 5.2.

The J-V-L characteristics of the fabricated OLEDs are shown in Figure 5.3. The plots of current density as a function of applied voltage reveal good diode behaviour. The devices utilizing **ME**, **TBUT** and **OME** as emitter materials exhibit drive voltage (corresponding to 1 cd/m²) of 3.28, 3.17, 2.98 V, respectively. The devices showed maximum luminance (L_{max}) of 4390 cd/m² (**ME**), 6627 cd/m² (**TBUT**) and 5034 cd/m² (**OME**) at 10 V. The J-L plots (Figure 5.4) show a linear relationship with **TBUT** showing luminance of 5339 cd/m² compared to 3871 cd/m² and 4533 cd/m² for **ME** and

OME, respectively at 500 A/m^2 . The EL spectra of the devices with ME, TBUT and OME are shown in Figure 5.5. The materials emit green light with peaks centred at 522, 518 and 527 nm, respectively with FWHM of $\sim 60 \text{ nm}$. The narrow FWHM in EL spectra indicate the possibility of making devices with good chromaticity using these materials. The CIE chromaticity coordinates of the derivatives as EL materials are determined using the EL spectra of the devices at 10 V. The chromaticity diagram is shown in Figure 5.5 and the CIE coordinates are tabulated in Table 5.2. The variation of EL intensity with different applied voltages is shown in Figure 5.6. It can be observed from Figure 5.6 that the variation of applied voltage has no effect on the shape and the peak of the EL spectra.

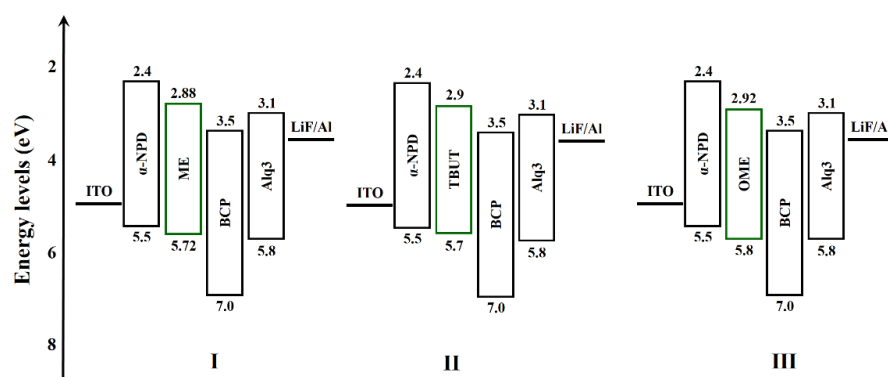


Figure 5.2. Energy-level diagram of the materials used in the devices (I) ME, (II) TBUT and (III) OME Pyrene derivatives as EL materials

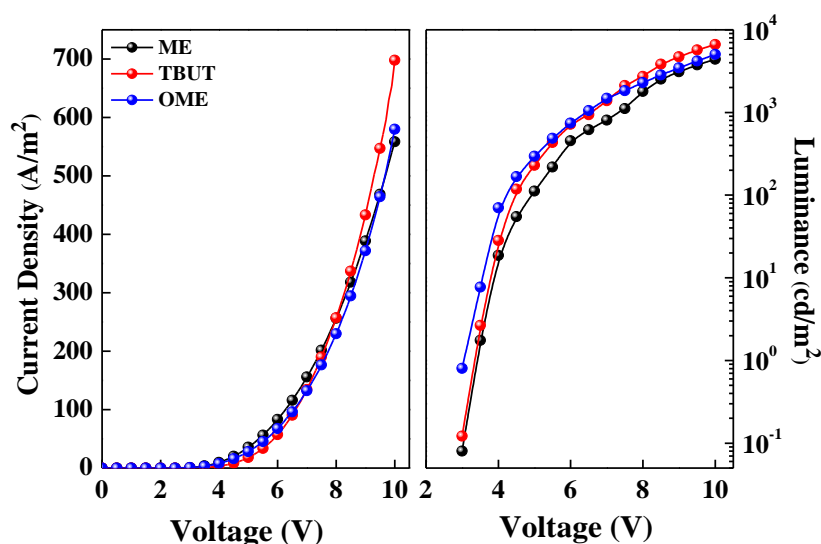


Figure 5.3 J-V-L characteristics for OLEDs with pyrene as EL materials.

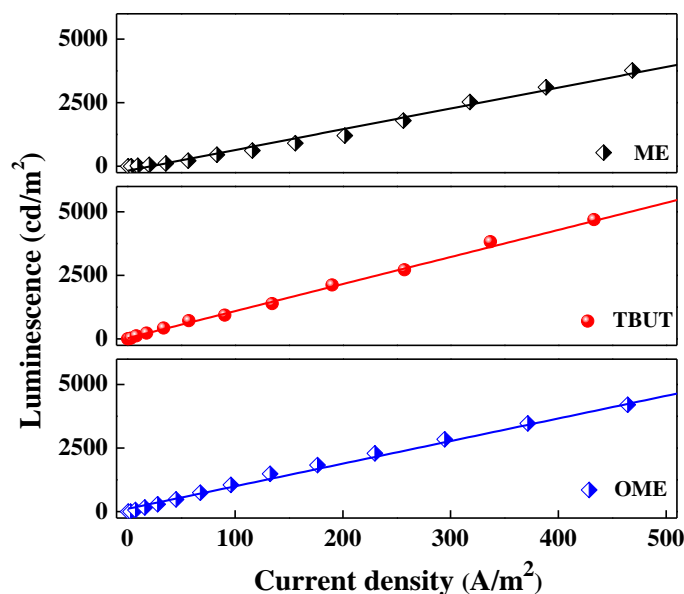


Figure 5.4 J-L characteristics for OLEDs with pyrene as EL materials.

The current, output power and external quantum efficiencies for all the devices along with other parameters of the devices are summarized in Table 5.2. Out of the three derivatives investigated, device fabricated with **TBUT** as emissive material showed best performance with current efficiency (η_c) of 13.27 cd/A, power efficiency (η_p) of 9.73 lm/W and external quantum efficiency (η_{ext}) of 4.99%. Compared to the thin film PL spectra, bathochromic shifts were observed in the EL emission peaks for all the derivatives. This may be ascribed to the intermolecular interactions in the excited states [Zhuang et al. 2014].

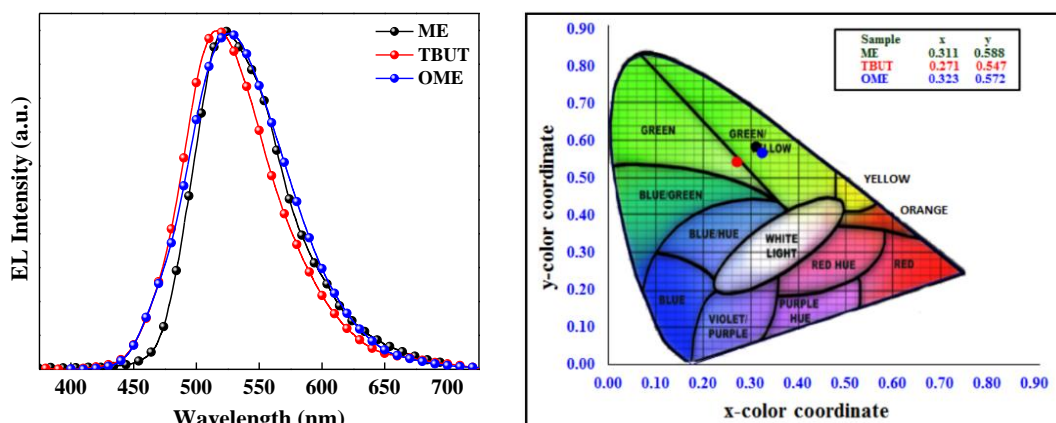


Figure 5.5 EL spectra and chromaticity diagram of the OLEDs with pyrene derivatives as EL materials.

Table 5.2. Electroluminescent data of pyrene derivatives as emissive materials

Device^a	V_{onset} (V)^b	L_{max} (cd/m²)^c	η_c (cd/A)^d	η_p (lm/W)^e	η_{ext} (%)^f	λ_{em} (FWHM) (nm)^g	CIE_(x,y)^h
ME	3.28	4390	10.86 (8V)	6.93 (6.0V)	4.25 (8V)	522 (58)	(0.311, 0.588)
TBUT	3.17	6627	13.27 (8V)	9.73 (5.5V)	4.99 (8V)	518 (56)	(0.271, 0.547)
OME	2.98	5034	11.24 (7V)	7.42 (4.5V)	3.46 (7V)	527 (62)	(0.323, 0.572)

^a Device Configuration **I**: ITO (120 nm)/ α -NPD (30 nm)/ **Pyrene** (35 nm)/BCP (6 nm)/ Alq₃ (35 nm)/ LiF (1 nm)/ Al (150 nm)

^b V_{onset} : turn-on voltage at luminance of 1 cd/m²

^c L_{max} : Maximum luminance at 10 V

^d η_c : Maximum current efficiency measured at applied voltage (in parentheses)

^e η_p : Maximum power efficiency measured at applied voltage (in parentheses)

^f η_{ext} : Maximum external quantum efficiency measured at applied voltage (in parentheses)

^g λ_{em} : Emission wavelength maximum. FWHM: full width half maximum at 10 V

^h CIE colour coordinate

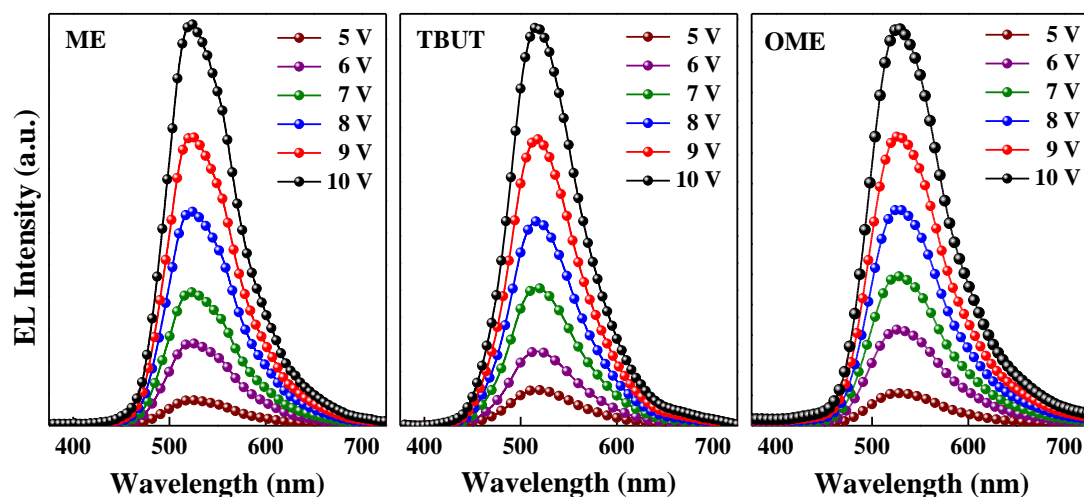


Figure 5.6 EL spectra of the OLEDs with pyrene derivatives as EL materials at different applied voltages.

5.2.2 Pyrene derivatives as ETL material for phosphorescent OLEDs

The electron transporting properties of pyrene derivatives were investigated by fabricating phosphorescent OLED with **TBUT** as ETL material. Also, OLEDs without any ETL material and with Alq₃ as standard ETL material were fabricated for comparison. Here Ir(ppy)₃ doped CBP was used as phosphorescent emitter for all the devices.

Device **IV**: ITO (120 nm)/ α -NPD (40 nm)/ Ir(ppy)₃ doped CBP (35 nm)/ BCP (6 nm)/ LiF (1 nm)/ Al (150 nm).

Device **V**: ITO (120 nm)/ α -NPD (40 nm)/ Ir(ppy)₃ doped CBP (35 nm)/ BCP (6 nm)/ Alq₃ (30 nm)/ LiF (1 nm)/ Al (150 nm).

Device **VI**: ITO (120 nm)/ α -NPD (40 nm)/ Ir(ppy)₃ doped CBP (35 nm)/ BCP (6 nm)/ **TBUT** (30 nm)/ LiF (1 nm)/ Al (150 nm).

Only ETL was changed while the rest of the device configurations were kept same. The first configuration (device **IV**) was without any ETL material, while the second (device **V**) was with Alq₃ as the ETL material and third one was with **TBUT** (device **VI**) as the ETL material. The related HOMO/LUMO energy levels of the materials are illustrated in Figure 5.7. The data from each of these devices are tabulated in Table 5.3. The J-V-L characteristics of the OLEDs with different ETL materials are

shown in Figure 5.8. The J-L characteristics show a linear relationship as shown in Figure 5.9.

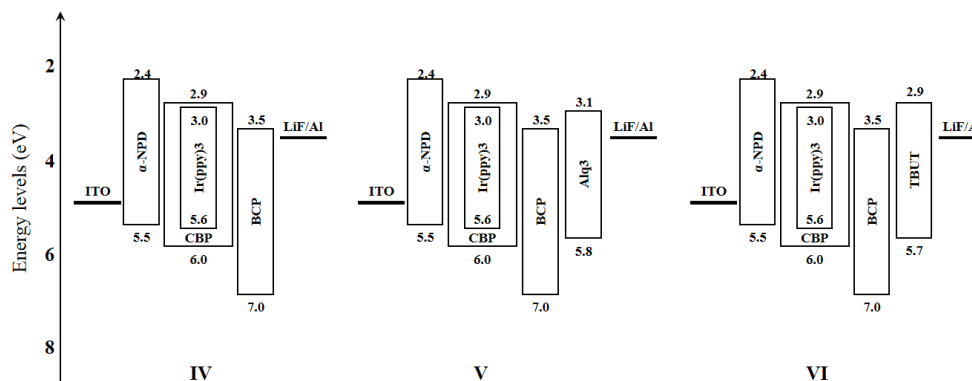


Figure 5.7 Energy-level diagram of the materials used in the phosphorescent OLEDs with triplet emitter Ir(ppy)₃ doped with CBP (**IV**) indicates without ETL (**V**) is with standard AlQ₃ as ETL and (**VI**) is with TBUT as ETL

A similar EL spectrum for Ir(ppy)₃ with λ_{\max} at 516 nm was observed for all the devices prepared either without ETL or with **TBUT** /Alq₃ as ETL materials (Figure 5.10). It can be seen from the Figure 5.8 and Table 5.3 that the OLED with **TBUT** pyrene shows superior performance in comparison to the OLED with Alq₃ as ETL in terms of higher luminous intensities at all voltages and better efficiencies.

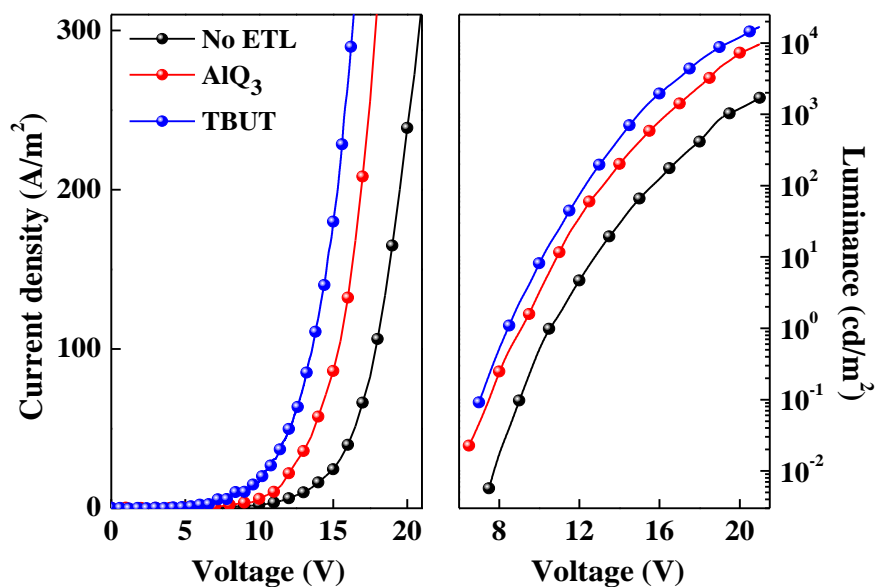


Figure 5.8 J-V-L characteristics of OLEDs with triplet emitter Ir(ppy)₃ doped with CBP without ETL, with Alq₃ and TBUT as ETLs.

The device with **TBUT** as ETL was found to be the most efficient. At the same time, it can be seen from Figure 5.8 and Table 5.3 that a drastic increase in the luminance and efficiencies can be achieved by the inclusion of ETL in the device configuration. Luminous intensities were found to be 9650 cd/m² and 12769 cd/m² at 21 V for OLEDs with Alq₃ and **TBUT** as ETL materials, respectively. The better electron transport in **TBUT** is seen to improve the current density in the device. Hence, we can infer that the performance of the devices with the pyrene derivatives as ETL materials are superior compared to device made using commercially available Alq₃.

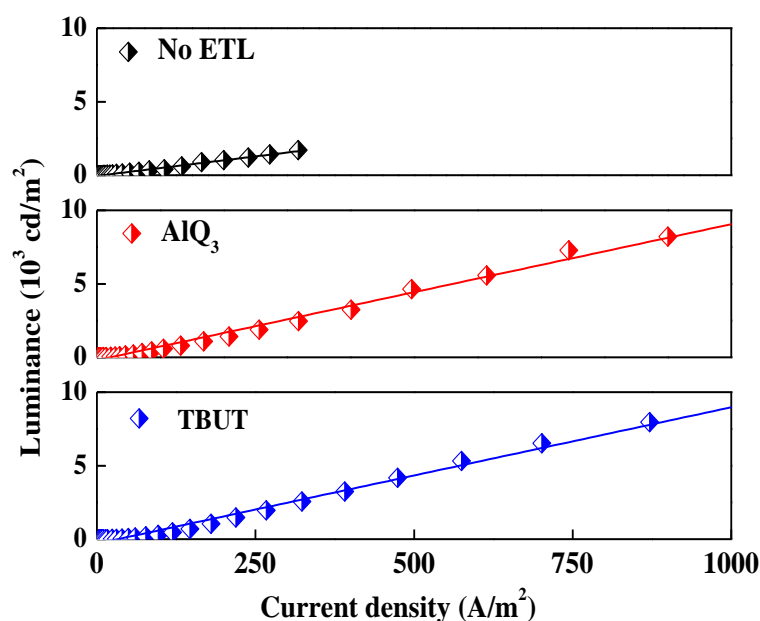


Figure 5.9 J-L characteristics of OLEDs for triplet emitter Ir(ppy)₃ doped with CBP without ETL/with Alq₃/TBUT as ETLs

5.2.3 Pyrene as both EL and ETL materials

The role of pyrene derivatives acting as both electron transporting and emitting materials were studied by fabricating OLEDs with the following device configurations

Device **VII**: ITO (120 nm)/ α -NPD (40 nm)/ Pyrene (50 nm)/ LiF (1 nm)/ Al (150 nm).

Device **VIII**: ITO (120 nm)/ F₄TCNQ (4 nm)/ α -NPD (40 nm)/ **Pyrene** (50 nm)/ LiF (1 nm)/ Al (150 nm).

Device **IX**: ITO (120 nm)/ F₄TCNQ (4 nm)/ α -NPD (40 nm)/ **Pyrene** (50 nm)/ BCP (6 nm)/ LiF (1 nm)/ Al (150 nm).

Table 5.3 Electroluminescent data of OLEDs using of triplet emitter Ir(ppy)₃ doped with CBP

Device ^a	V_{onset} (V) ^b	L_{max} (cd/m ²) ^c	η_c (cd/A) ^d	η_p (lm/W) ^e	η_{ext} (%) ^f	λ_{em} (nm) ^g
Without ETL	12.76	1714	5.39 (19 V)	1.23 (18 V)	0.94 (18 V)	516
Alq₃	9.09	9650	9.79 (20 V)	2.71 (19 V)	1.70 (18 V)	516
TBUT	8.24	12769	10.10 (19 V)	3.04 (18 V)	1.73 (19 V)	516

^a Device Configuration **IV-VI**: ITO (120 nm)/ α -NPD (40 nm)/ Ir(ppy)₃ doped CBP (35 nm)/ BCP (6 nm)/ No ETL or with Alq₃ or TBUT (30 nm)/ LiF (1 nm)/ Al (150 nm)

^b V_{onset} : turn-on voltage at luminance of 1 cd/m²

^c L_{max} : Maximum luminance at 10 V

^d η_c : Maximum current efficiency measured at applied voltage (in parentheses)

^e η_p : Maximum power efficiency measured at applied voltage (in parentheses)

^f η_{ext} : Maximum external quantum efficiency measured at applied voltage (in parentheses)

^g λ_{em} : Emission wavelength maximum. FWHM: full width half maximum at 10 V

^h CIE colour coordinate

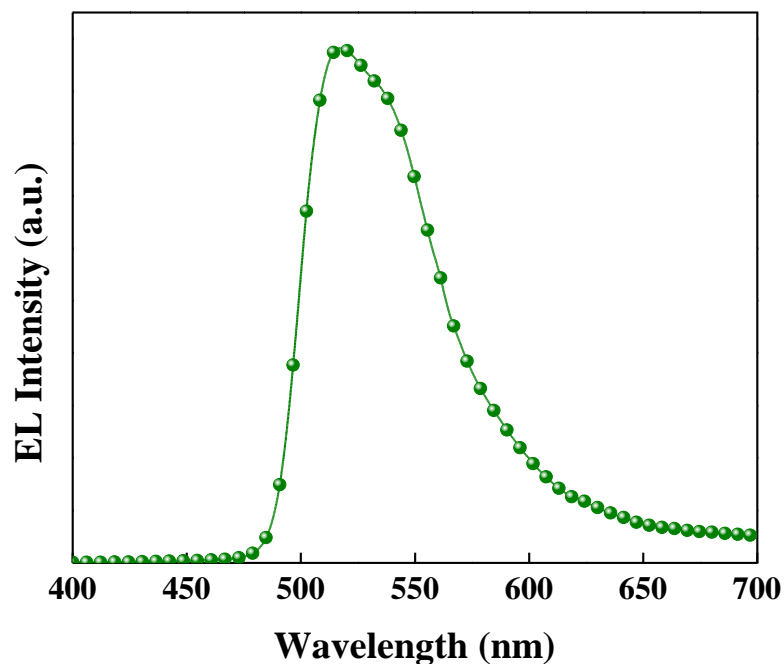


Figure 5.10 EL spectra of the OLEDs triplet emitter Ir(ppy)₃ doped with CBP without ETL/with Alq₃/ with TBUT as ETLs

The related HOMO/LUMO energy levels of the materials are illustrated in Figure 5.11. Here F₄TCNQ acts as HIL for efficient hole injection from the ITO anode to hole transport layer α -NPD. An optimized thickness of F₄TCNQ was used for better hole injection. The device performance data is presented in Table 5.4. Figure 5.12 shows the J-V-L characteristics of the devices **VII-IX**. It is evident from Figure 5.12 and Table 5.4 that the device **VII** without F₄TCNQ and BCP has low efficiencies of 2.67 cd/A (η_c), 1.36 lm/W (η_p) and 0.77 % (η_{ext}). With the inclusion of 4 nm of F₄TCNQ layer (device **VIII**) there is a drastic increase of efficiencies; 13.56 cd/A (η_c), 9.56 lm/W (η_p) and 5.34 % (η_{ext}). This can be ascribed to the efficient injection of holes from the ITO anode to the hole transport layer α -NPD. Furthermore, in device **IX**, with the use of BCP as a HBL, there is further increase in the efficiencies. This increase in efficiencies may be due to the confining of redundant holes in the emitting layer which didn't recombine with the electrons in the emitting zone [Tomova et al. 2010]. The device structure **IX** was used for the other two derivatives (**4** and **6**). It is evident from Table 5.4 that the devices show very high efficiencies close to 15 cd/A (η_c), 11 lm/W (η_p) and 6 % (η_{ext}).

Table 5.4 Electroluminescent data of OLEDs using pyrene as both EL and ETL material

Device	V_{onset} (V) ^d	L_{max} (cd/m ²) ^e	η_c (cd/A) ^f	η_p (lm/W) ^g	η_{ext} (%) ^h
TBUT ^a	6.78	809	2.67 (9.0)	1.36 (8.5)	0.77 (9.5)
TBUT ^b	3.23	7605	13.56 (7.0)	9.56 (6.5)	5.34 (7.0)
TBUT ^c	2.76	8524	15.13 (7.5)	10.95 (6.5)	5.96 (7.5)
ME ^c	2.93	6387	13.06 (8.5)	8.34 (5.5)	5.14 (8.5)
OME ^c	2.61	7050	14.30 (7.5)	9.46 (5.0)	5.49 (7.5)

^a Device Configuration **VII**: ITO (120 nm)/ α -NPD (40 nm)/ **5** (50 nm)/ LiF (1 nm)/ Al (150 nm)

^b Device Configuration **VIII**: ITO (120 nm)/ F₄TCNQ (4 nm)/ α -NPD (40 nm)/ **5** (50 nm)/ LiF (1 nm)/ Al (150 nm)

^c Device Configuration **IX**: ITO (120 nm)/ F₄TCNQ (4 nm)/ α -NPD (40 nm)/ **Pyrene** (50 nm)/ BCP (6 nm)/ LiF (1 nm)/ Al (150 nm)

^d V_{onset} : turn-on voltage at luminance of 1 cd/m²

^e L_{max} : Maximum luminance at 10 V

^f η_c : Maximum current efficiency measured at applied voltage (in parentheses)

^g η_p : Maximum power efficiency measured at applied voltage (in parentheses)

^h η_{ext} : Maximum external quantum efficiency measured at applied voltage (in parentheses)

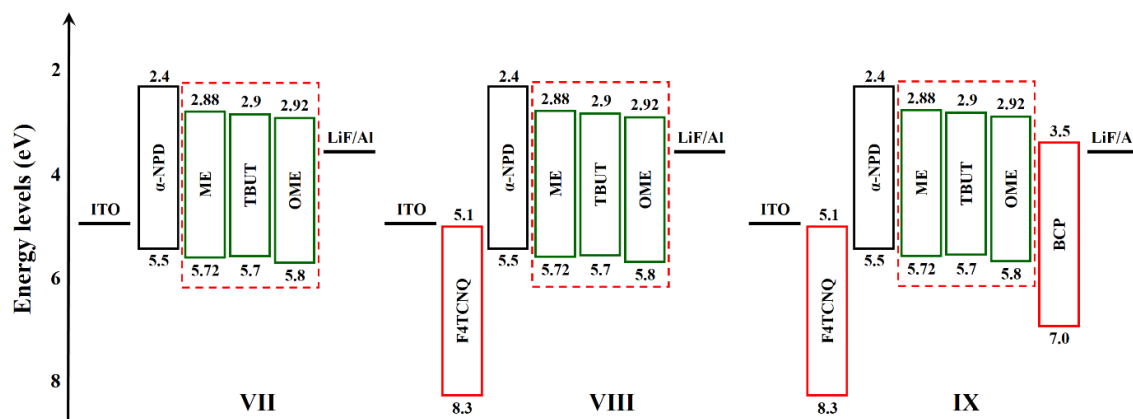


Figure 5.11 Energy-level diagram of the materials with Pyrene derivatives as EL and ETL materials (**VII**) without F₄TCNQ and BCP (**VIII**) with F₄TCNQ and without BCP and (**IX**) with F₄TCNQ and BCP

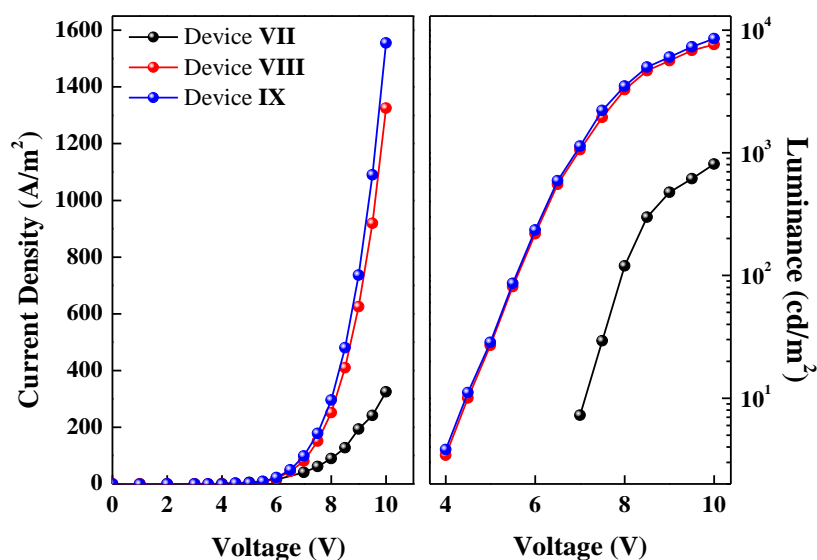


Figure 5.12 J-V-L characteristics of OLEDs with TBUT pyrene as EL and ETL material showing the role of F₄TCNQ and BCP. Here **VII** is without F₄TCNQ and BCP; **VIII** is with F₄TCNQ and without BCP; and **IX** is with both F₄TCNQ and BCP

5.3 ELECTRON TRANSPORT STUDIES ON TBUT PYRENE

(*The studies in this section were done at Prof. Ghosh's laboratory, JNU Delhi)

In order to understand the behaviour of electronic devices, an in-depth understanding of charge carrier transport in the material is required. Equally important is to know how the charge carrier transport is affected by external parameters such as the applied voltage, temperature and thickness. In organic semiconductors, electric

current is mainly due to the two mechanisms depending on the concentration of charge carrier traps. When the concentration of traps is relatively low, trap free space charge limited conduction (SCLC) dominates the conduction processes but as the concentration of traps become relatively high trap charge limited conduction (TCLC) starts dominating over the SCLC [Lampert and Mark 1970]. In organic thin films, traps are introduced in the form of impurities and structural disorders created by the lattice deformation and other irregularities in first few layers. It has been shown [Lampert and Mark 1970, Blom et al. 2005] that structural disorder in organic solids is the main cause for creation of charge carriers traps. The trap states distribution lies between HOMO and LUMO, it immobilizes most of the injected charge carriers in the OMS. Whenever these trap states are completely filled, the charge transport becomes SCLC. The underlying mechanism of conduction processes as to whether it is ohmic, SCLC or TCLC, can be investigated from the nature of the J-V characteristics of two terminal devices. Measuring the J-V characteristics at different temperatures and different thicknesses is an effective way to study the charge carrier transport mechanism operating in of organic semiconductor devices.

With the intention of studying electron transport in Pyrene derivatives, electron only devices with a structure of Al (150 nm)/**TBUT** /Al (150 nm) were fabricated with various thickness of **TBUT** layer. Work function of Al is about 3.7 eV [Krishna et al. 2009]. The EA and IP values of **TBUT** pyrene are 2.9 eV and 5.7 eV, respectively. The potential barrier for electron injection is very low (0.8 eV) when compared to that for hole injection (2.0 eV). Therefore, hole injection in our devices is very inefficient in comparison to electron injection. Since the current in the device will be due to electron only, these devices may be considered as electron only devices. Figure 5.13 (a) shows the schematic device structure used in this study. Figure 5.13 (b) shows the energy level diagram for electron only devices. It is indicated in the figure that current is constituted by electrons only, in these devices.

The J-V characteristics are measured at ambient conditions. Figure 5.14 shows the J-V characteristics in a log-log scale for the electron only devices fabricated using 100 nm thicknesses of **TBUT** measured at 300 K. At low applied bias voltages ($V < 1$ V), the device shows ohmic conduction. This may be attributed to the background

doping by the thermally generated free carriers. The injected electrons remain confined near the Al contact and the carrier density is constant everywhere. Hence, space charge is created and it is expected that Ohm's law will be obeyed [Jain et al. 2001]. The current density is given by [Lampert and Mark 1970]

$$J = n_0 q \mu \frac{V}{d} \quad (5.1)$$

where, n_0 is the concentration of free carriers, q charge of electron, μ is the charge carrier mobility, V applied bias voltage and d is the thickness of the organic layer.

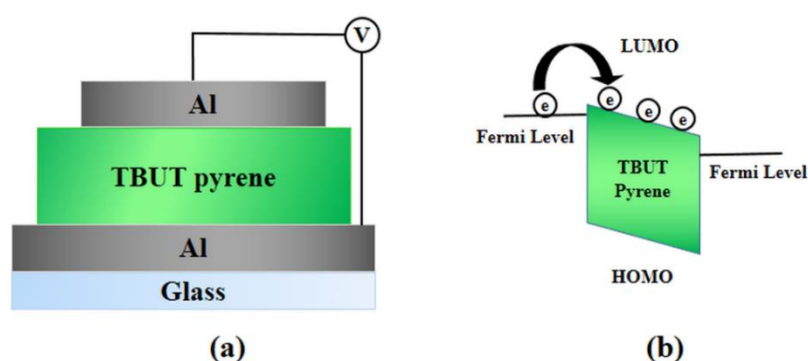


Figure 5.13 (a) Schematic device structure of the electron only devices, (b) energy level diagram for the electron only devices.

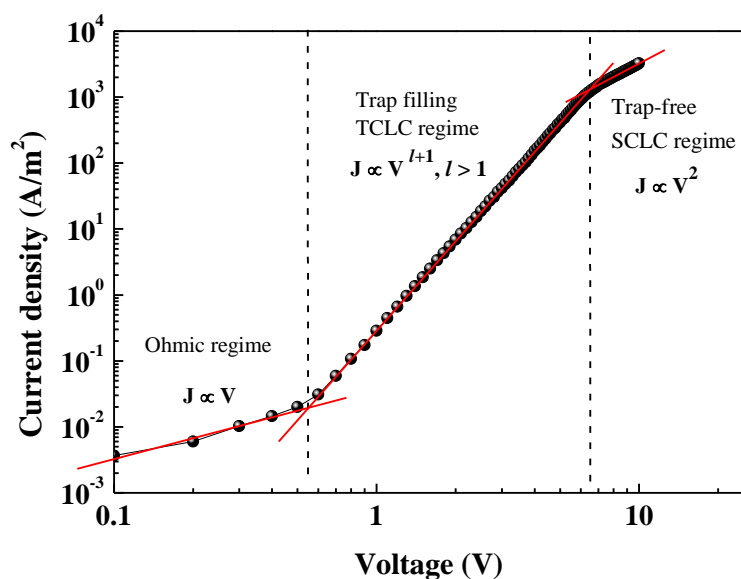


Figure 5.14 J–V characteristics in log-log scale of the electron only device with TBUT having 100 nm thickness showing typical behaviour of SCLC in materials with deep traps (Ohmic regime → trap filling transition → SCLC regime)

When the bias voltage is further increased, the injected carriers spread into regions farther away from the Al contact and the injected carrier density exceeds the intrinsic free carrier density in almost the entire OMS layer, which results in the nonlinear increase of current with voltage. The conduction mechanism at such voltages is expected to be dominated by SCLC regime due to low carrier mobility in organic materials. In the SCLC regime the current density varies according to the well-known V^2 law if there are no traps and the mobility is independent of the electric field. The current density in this regime is given by [Jain et al. 2001]

$$J = \frac{9}{8} \varepsilon \varepsilon_0 \mu \left(\frac{V^2}{d^3} \right) \quad (5.2)$$

Here ε is the dielectric constant of OMS and ε_0 is the permittivity of the free space. However, in our devices, SCLC regime is not observed in the low bias region, which may be due to the presence of relatively high density of traps. If either trapping or effect of field on mobility is important, the J-V characteristics obey $J \propto V^{l+1}$ ($l > 1$) power law behaviour. This indicates that TCLC mechanism dominates in our devices, wherein the current density is given by [Kao and Hwang 1981 Brütting et al. 2001 Kumar et al. 2010]

$$J = \frac{\mu N_v}{q^{l-1}} \left(\frac{2l+1}{l+1} \right)^{l+1} \left(\frac{l}{l+1} \frac{\varepsilon \varepsilon_0}{H_b} \right)^l \frac{V^{l+1}}{d^{2l+1}} \quad (5.3)$$

where N_v is the atomic density, $l = T_c/T$ and H_b is the trap density. Here T_c is the characteristic temperature of trap distribution given by trap energy $E_t = k T_c$.

As the bias voltage is further increased, traps start getting filled up and the current starts to follow trap free SCLC rather than TCLC mechanism. Finally when all the traps are filled, conduction will be due to SCLC and the current density obeys Equation 5.2 [Lampert and Mark 1970]. This transition from higher power dependence to quadratic power dependence is due to the filling of traps [Lampert and Mark 1970]. The voltage at which traps start to fill, is known as trap filling voltage (V_{TFL}), which is the cross over voltage between the trap-dominated regime at low fields and trap free

SCLC regime at high fields. At this limit ($V=V_{\text{TFL}}$), the trap density (H_b) can be obtained using the Equation 5.4 [Jain et al. 2001, Blom et al. 2005, Kumar et al. 2010] which suggests that the trap filling voltage, V_{TFL} , for TCLC increases with the increase of the device thickness.

$$V_{\text{TFL}} = \frac{qd^2}{\varepsilon} \left[\frac{9 H_b^l}{8 N_v} \left(\frac{l+1}{l} \right)^l \left(\frac{l+1}{2l+1} \right)^{l+1} \right]^{1/l-1} \quad (5.4)$$

We have performed the J–V measurements of the devices at different temperatures, in order, to get further insight into the conduction mechanism. Figure 5.15 shows the J–V characteristics for **TBUT** electron only device at temperatures 160, 180, 200, 220, 240, 260, 280, 300 and 320 K. It is seen that the current density is temperature dependent and decreases with the decrease in temperature. This indicates a decrease in conductivity with temperature which is a typical semiconductor characteristic. For confirmation of the conduction mechanism, thickness dependent J–V measurements were also carried out in detail. Electron only devices were fabricated having 60, 80, 100 and 120 nm thicknesses of **TBUT**. Figure 5.16 shows the thickness scaling of current density with voltage of electron only devices with different thicknesses of **TBUT**.

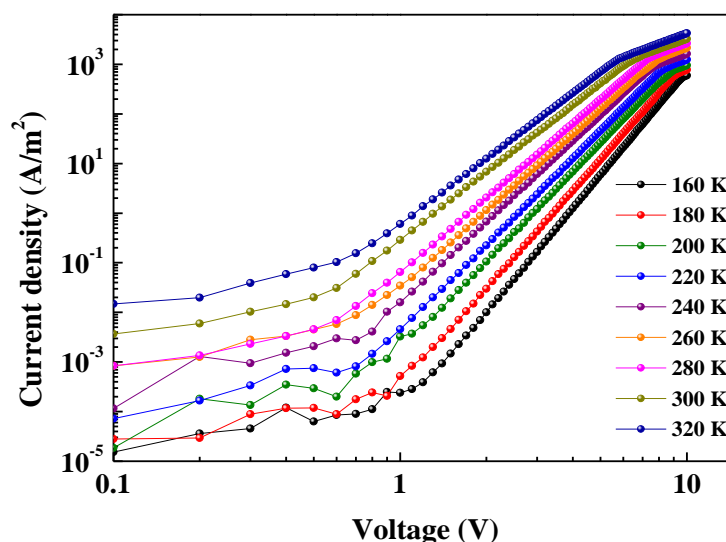


Figure 5.15 J–V characteristics for electron only devices with 100 nm thickness of TBUT at different temperatures.

In TCLC mechanism, the value of exponent l is given by T_c/T . Hence, increase in the value of l is expected with decrease in the temperature. The value of l was obtained from the respective J–V characteristics of **TBUT** at each temperature and plotted as a function of $1000/T$ for the devices of different thicknesses as shown in Figure 5.17. From the slope of these plots, the value of trap energy has been calculated. The value of trap energy were found to be 63, 74, 85 and 104 meV for the devices with 60, 80, 100 and 120 nm thicknesses of **TBUT**, respectively. The thickness dependent trap energy data indicate that the trap energy is strongly dependent on thickness of the **TBUT** layer. Trap energy depth has been found to increase with the increase in layer thickness.

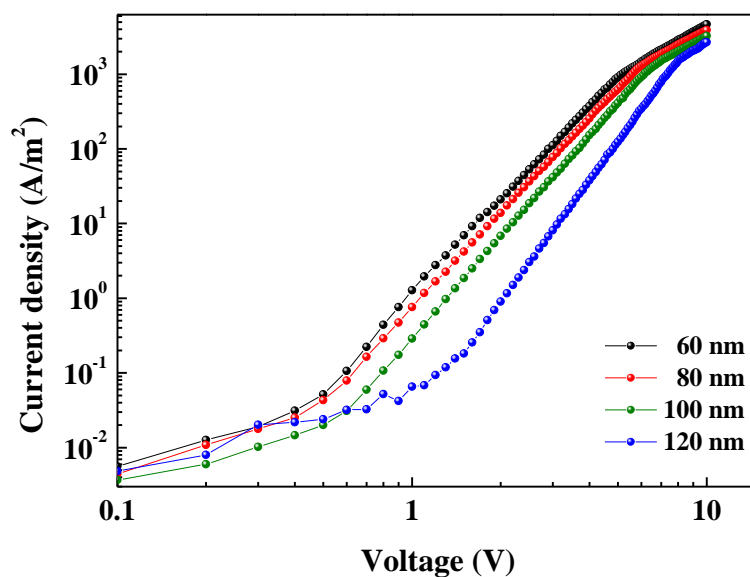


Figure 5.16 J–V characteristics of electron only devices of TBUT having 60, 80, 100 and 120 nm thicknesses.

The devices show low trap energies implying that the trap levels are close to the transport levels. Therefore, the trap levels can be filled in these molecules by increasing the operating electric field and the electron only devices may show a trap filled SCLC regime. In this regime, current density is proportional to the square of the bias voltage. It can be seen from Figure 5.14 that beyond $V=6$ V, the slope of J–V characteristics of **TBUT** device has changed and is found to be very close to 2. Therefore, this suggests that the **TBUT** electron only devices have three different conduction regimes in their J–V characteristics. Further, for quantifying the thickness dependence of trap energy,

change in trap energy per unit increase in thickness of the active layer was calculated. The value was found to be 0.67 meV/nm for the **TBUT** electron only devices. This suggests that the thickness dependence of current density should also vary for the devices. It is worth noting that the trap energy decreases with decreasing thickness.

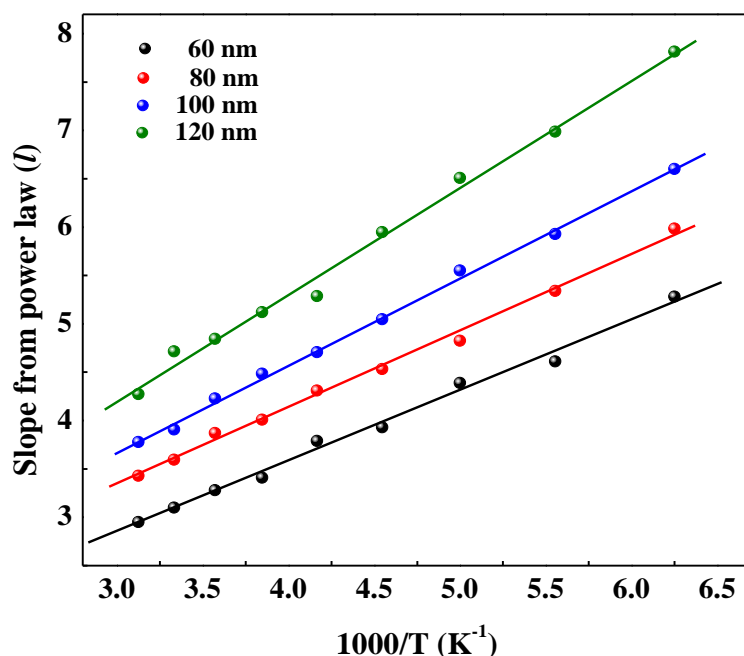


Figure 5.17 Slope of power law dependent current density (l) as a function of $1000/T$ of electron only devices with 60, 80, 100 and 120 nm thicknesses of TBUT.

As already mentioned, the devices were found to possess trap filled SCLC regime for bias voltages greater than V_{TFL} . The trap filling voltage was plotted with the square of the thickness for the devices at 260, 280, 300 and 320 K temperatures as shown in Figure 5.18. It can be observed from the graphs that the trap filling voltage drops from ~ 10 V to ~ 6 V when the device thickness is reduced from 120 nm to 60 nm, which is in accordance with Equation 5.4. This shows that density of trap states are highly thickness dependent. Thus, from thickness and temperature dependence of current, it can be concluded that the electron current is predominantly space charge limited and trapping in distributed trap states becomes important at low voltages and the effect of traps increases with thickness. Therefore, further analysis of trap states and trap density can be carried out based on TCLC model of J–V characteristics. The value of trap density is required in addition to the trap energy for a complete analysis of trap

states. Equation 5.4 was utilized to calculate the values of trap density for **TBUT** at all temperatures. Figure 5.19 shows the plot of trap energy and trap density as a function of thicknesses for **TBUT** devices. The trap energy has been found to increase with the increase in sample thickness. It can be seen from the figure that the trap density has increased with the decrease in trap energy. This behaviour is in complete agreement with the model wherein the traps have an exponential type of distribution given by [Jain et al. 2007, Kumar et al. 2010]

$$H_t(E) = \left(\frac{H_b}{E_t}\right) \exp\left(-\frac{E - E_t}{E_t}\right) \quad (5.5)$$

For lower thickness of organic film, the exponential distribution of trap states in energy is close to LUMO. As a result, more electrons can be transported between trap states and the LUMO of pyrene for thinner films. Therefore, the electron transport for the thinner **TBUT** films will be better. Generally, the thickness of electron transport layer in OLEDs is 30-50 nm. This favours **TBUT** to be used as an electron transport material in OLEDs. The variation of trap density with the thickness is high in the case of **TBUT**. The trap density value was 8.5×10^{16} per cm^3 for 60 nm and decreased to 7.7×10^{15} per cm^3 for 120 nm. The data of trap energy and trap density show that they are highly dependent on thickness for **TBUT**. Presence of trap states affects the charge carrier mobility in SCLC regime. Therefore, charge carrier mobility has been calculated to have a deeper understanding of the charge carrier transport mechanism. In the case of low trap density, further increase in bias leads to field dependent carrier mobility. Therefore, we have included a field dependent mobility of the Poole–Frenkel type exponential form given by Equation 5.6 with parameters zero field charge carrier mobility (μ_o) and field dependent factor (β) to be determined for each temperature [Brütting et al. 2001].

$$\mu(F, T) = \mu_o \exp(\beta(t)\sqrt{F}) \quad (5.6)$$

The experimental data of J–V characteristics were fitted using Equation 5.3 with a field dependent mobility by varying the values of μ_o and β . The material parameters were taken to be $N_v = 10^{21}$ per cm^3 [Attar and Monkman 2006], $\epsilon = 3$. We have

calculated the charge carrier mobilities for **TBUT** using the zero field mobility and field dependent factor at different field values.

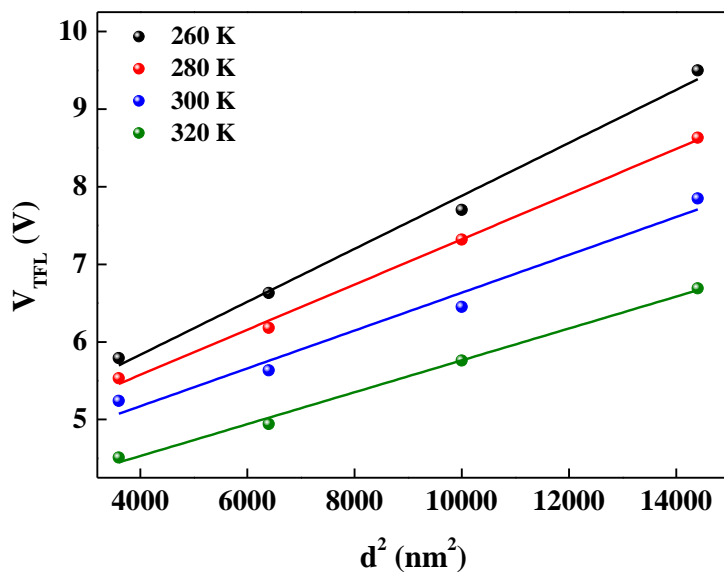


Figure 5.18 Trap filling voltage with the square of thickness at temperatures 260, 280, 300 and 320 K for TBUT electron only devices

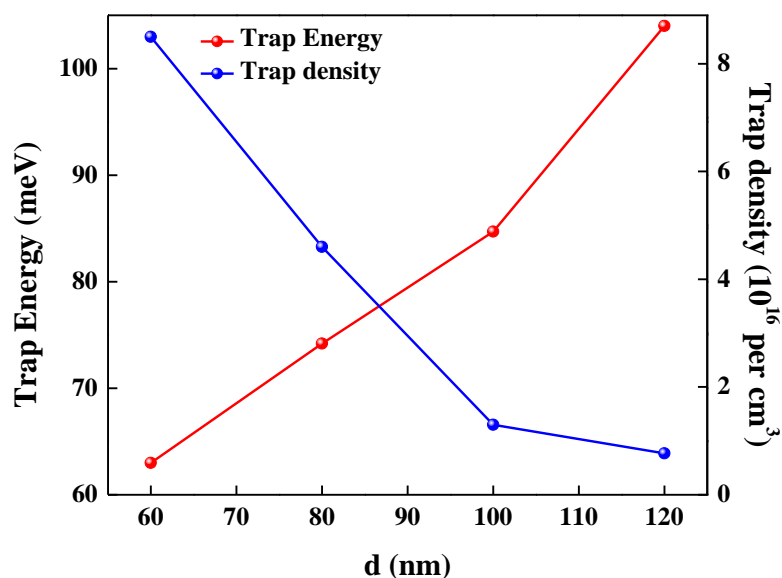


Figure 5.19 Trap energy and trap density as a function of thickness for TBUT

Figure 5.20 shows the charge carrier mobilities for **TBUT** at different electric field values for a 100 nm thick active layer. It can be seen from Figure 5.20 that the charge carrier mobility of **TBUT** can reach a value as high as $10^{-3} \text{ cm}^2\text{V}^{-1}\text{s}^{-1}$ for electric field values of interest for OLEDs ($\sim 1 \times 10^6 \text{ Vcm}^{-1}$).

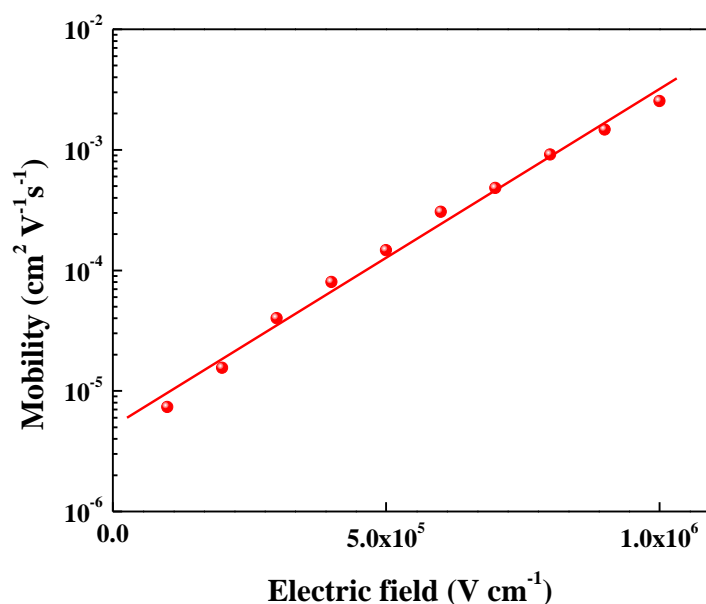


Figure 5.20 Mobility values for TBUT for the electron only devices with 100 nm thicknesses of active layer at different electric field values.

5.4 CONCLUSIONS

Pyrene based OLEDs were fabricated and characterized to demonstrate the emitter, electron transport and emissive/electron transport properties of pyrene derivatives (**TBUT**, **ME** and **OME**). All the derivatives emitted green light with the **TBUT** device showing best performance with η_c , η_p and η_{ext} of 13.27 cd/A, 9.73 lm/W and 4.99%, respectively. Among the fabricated phosphorescent OLEDs, the device with **TBUT** as ETL showed better performance than the device with standard ETL material **Alq₃**. Bi-layer devices showed both the emissive and electron transporting properties of pyrene derivatives. The electron transport studies on **TBUT** pyrene were carried out. Electron transport in **TBUT** has been found to be thickness dependent and current densities are seen to follow TCLC model. TCLC model with field dependent mobility has been used to explain the J–V characteristics for electron only devices. Thickness dependent trap states were observed for **TBUT**. Calculated values of trap energy were found to be increasing with increasing thickness. Electron mobility was found to increase with the decrease in thickness, which favours their use for organic electronic devices. **TBUT** was found to have better electron transport in comparison to the well-established electron transport material **Alq₃**.

CHAPTER 6

SUMMARY AND CONCLUSIONS

Overview

Chapter 6 outlines the summary of the work presented in the thesis along with the important conclusions drawn from the study. Scope for further research has also been included here.

6.1 SUMMARY

A series of novel naphthalimide derivatives containing electron-donating phenoxy groups at the C-4 position of 1, 8-naphthalimide were investigated for applications in OLEDs. These derivatives have high electron affinity with desired wide band gap required for blue light emission. The crystal structure, optical, thermal, morphological and electrochemical features of the naphthalimides were investigated using single crystal XRD, UV-Vis absorption spectrometry, PL spectrometry, TGA, DSC, AFM and cyclic voltammetry, respectively. Single crystal XRD analysis of **NI-Br** confirmed its molecular structure; **NI-Br** crystallizes in the triclinic space group *P*-1. The UV-Vis absorption spectra of the derivatives in the thin solid-state form showed broad bands with red shifts in contrast to the spectra from the samples in solution form indicating that the conjugation lengths are slightly increased. The derivatives in the solid state showed blue photoluminescence with excellent chromaticity and large Stokes' shifts. The evaluated thermal properties revealed that the derivatives have high melting point and good thermal stability. Electrochemical properties determined using cyclic voltammetry show that the derivatives have low-lying HOMO-LUMO levels making them possess good electron-transporting and hole-blocking properties.

OLEDs using naphthalimides as emissive materials showed efficiencies of 1.18 cd/A (η_v), 0.37 lm/W (η_p) and 0.55 % (η_{EQE}). As ETL materials, naphthalimide derivatives exhibited good performance (η_c : 9.04 cd/A, η_p : 1.98 lm/W and η_{EQE} : 1.46 %) than the device without any ETL (η_c : 5.39 cd/A, η_p : 1.23 lm/W and η_{EQE} : 0.94 %) and was also comparable with the device using standard ETL material, Alq₃. Furthermore, naphthalimides as both EL and ETL materials showed efficiencies of 1.99 cd/A (η_c), 1.2 lm/W (η_p) and 0.83 % (η_{EQE}) revealing that they can act as emitters with good electron transporting capability. These results demonstrate that the naphthalimide derivatives are promising candidates as undoped blue emitters with electron transport

and could play an important role in the development of OLEDs. The devices with naphthalimides as host materials showed better chromaticity as compared to the devices with Alq₃ as hosts.

Pyrene based OLEDs were fabricated and characterized to demonstrate the emitter, electron transport and emissive/electron transport properties of pyrene derivatives (**TBUT**, **ME** and **OME**). All the derivatives emitted in green region. The device made using **TBUT** showed best performance with η_c , η_p and η_{ext} of 13.27 cd/A, 9.73 lm/W and 4.99%, respectively. Among the fabricated phosphorescent OLEDs, the device with **TBUT** as ETL showed better performance than the device with standard ETL material **Alq₃**. Bi-layer devices showed the combined emissive and electron transporting properties of pyrene derivatives.

Electron transport studies on **TBUT** pyrene indicated that electron transport is thickness dependent and the current densities to follow TCLC model of space charge limited current. TCLC model with field dependent mobility has been used to explain the J–V characteristics for electron only devices. Thickness dependent trap states were observed for **TBUT**. Calculated values of trap energy were found to be increasing with increasing thickness. Electron mobility was found to increase with the decrease in thickness of **TBUT**, which favors their use for organic electronic devices. **TBUT** was found to have better electron transport in comparison to the well-established electron transport material Alq₃.

6.2 CONCLUSIONS

The major overall conclusions drawn from the present research work are listed below:

1. The naphthalimide derivatives showed blue photoluminescence with excellent chromaticity and large Stokes' shifts. They have good thermal stability and are capable of forming quite smooth films. They have low-lying HOMO-LUMO levels making them possess good electron-transporting and hole-blocking properties.
2. OLEDs based on naphthalimide derivatives demonstrate that they are promising candidates as undoped blue emitters with good electron transporting properties.

3. Red OLEDs using naphthalimide as host material showed better performance compared to the devices with standard Alq₃ as host in terms of efficiency and chromaticity.
4. The OLEDs based on pyrene derivatives demonstrate that they are promising candidates as undoped green emitters with good electron transporting properties. The pyrene derivative TBUT as electron transport material showed better performance than the standard electron transport material Alq₃.
5. The charge transport studies show that TBUT pyrene has better electron transport in comparison to the well-established electron transport material Alq₃.

6.3 SCOPE FOR FUTURE WORK

1. The structure related electroluminescent and charge carrier properties of naphthalimide derivatives need to be studied
2. The role of naphthalimides as host in phosphorescent OLEDs need to be studied.
3. The structure related charge transport properties of pyrene derivatives need to be studied, which will help in further improving the efficiency of pyrene OLEDs.
4. The devices need to be optimized in order to get better efficiencies. Hence, the electrical studies on the organic/organic and organic/metal interfaces need to be done.
5. The thermally activated delayed fluorescence (TADF) phenomenon facilitates the harvesting of triplets in to singlets resulting in enhanced fluorescence leading to higher efficiencies. Hence, the TADF materials based on pyrene derivatives need to be studied.

REFERENCES

Abkowitz, M.A., Mizes, H.A. and Facci, J.S. (1995). "Emission limited injection by thermally assisted tunneling into a trap-free transport polymer." *Appl. Phys. Lett.*, 66 (10), 1288–1290.

Adamovich, V.I., Cordero, S.R., Djurovich, P.I., Tamayo, A., Thompson, M.E., D'Andrade, B.W. and Forrest, S.R. (2003). "New charge-carrier blocking materials for high efficiency OLEDs." *Org. Electron.*, 4 (2–3), 77–87.

Alexiou, M.S., Tychopoulos, V., Ghorbanian, S., Tyman, J.H.P., Brown, R.G. and Brittain, P.I. (1990). "The UV-visible absorption and fluorescence of some substituted 1,8-naphthalimides and naphthalic anhydrides." *J. Chem. Soc. Perkin Trans. 2*, (5), 837.

Arkhipov, V.I., Wolf, U. and Bäessler, H. (1999). "Current injection from a metal to a disordered hopping system. II. Comparison between analytic theory and simulation." *Phys. Rev. B*, 59 (11), 7514–7520.

Arunchai, R., Sudyoadsuk, T., Prachumrak, N., Namuangruk, S., Promarak, V., Sukwattanasinitt, M. and Rashatasakhon, P. (2015). "Synthesis and characterization of new triphenylamino-1,8-naphthalimides for organic light-emitting diode applications." *New J. Chem.*, 39 (4), 2807–2814.

Ashcroft, N.W. and Mermin, N.D. (1976). "Solid State Physics (Holt, Rinehart and Winston).

Atkins, P.W. and Friedman, R.S. (2010). "Molecular Quantum Mechanics (OUP Oxford).

Attar, H.A. Al and Monkman, A.P. (2006). "Dopant Effect on the Charge Injection, Transport, and Device Efficiency of an Electrophosphorescent Polymeric Light-Emitting Device." *Adv. Funct. Mater.*, 16 (17), 2231–2242.

Balaganesan, B., Shen, W.-J. and Chen, C.H. (2003). "Synthesis of t-butylated diphenylanthracene derivatives as blue host materials for OLED applications." *Tetrahedron Lett.*, 44 (30), 5747–5750.

References

- Baldo, M.A., Thompson, M.E. and Forrest, S.R. (2000). "High-efficiency fluorescent organic light-emitting devices using a phosphorescent sensitizer." *Nature*, *403* (6771), 750–753.
- Banerjee, S., Kitchen, J.A., Gunnlaugsson, T. and Kelly, J.M. (2012). "Synthesis and photophysical evaluation of a pyridinium 4-amino-1,8-naphthalimide derivative that upon intercalation displays preference for AT-rich double-stranded DNA." *Org. Biomol. Chem.*, *10* (15), 3033–3043.
- Banerjee, S., Kitchen, J.A., Gunnlaugsson, T. and Kelly, J.M. (2013a). "The effect of the 4-amino functionality on the photophysical and DNA binding properties of alkylpyridinium derived 1,8-naphthalimides." *Org. Biomol. Chem.*, *11* (34), 5642–5655.
- Banerjee, S., Veale, E.B., Phelan, C.M., Murphy, S.A., Tocci, G.M., Gillespie, L.J., Frimannsson, D.O., Kelly, J.M. and Gunnlaugsson, T. (2013b). "Recent advances in the development of 1,8-naphthalimide based DNA targeting binders, anticancer and fluorescent cellular imaging agents." *Chem. Soc. Rev.*, *42* (4), 1601–1618.
- Barros, T.C., Filho, P.B., Toscano, V.G. and Politi, M.J. (1995). "Intramolecular excimer formation from 1,8-N-alkyldinaphthalimides." *J. Photochem. Photobiol. Chem.*, *89* (2), 141–146.
- Barros, T.C., Molinari, G.R., Berci Filho, P., Toscano, V.G. and Politi, M.J. (1993). "Photophysical properties of N-alkylnaphthalimides and analogs." *J. Photochem. Photobiol. Chem.*, *76* (1–2), 55–60.
- Barth, S. and Bässler, H. (1997). "Intrinsic Photoconduction in PPV-Type Conjugated Polymers." *Phys. Rev. Lett.*, *79* (22), 4445–4448.
- Bässler, H. (1993). "Charge Transport in Disordered Organic Photoconductors a Monte Carlo Simulation Study." *Phys. Status Solidi B*, *175* (1), 15–56.
- Bernhardt, S., Kastler, M., Enkelmann, V., Baumgarten, M. and Müllen, K. (2006). "Pyrene as Chromophore and Electrophore: Encapsulation in a Rigid Polyphenylene Shell." *Chem. – Eur. J.*, *12* (23), 6117–6128.

- Bharathan, J. and Yang, Y. (1998). "Polymer electroluminescent devices processed by inkjet printing: I. Polymer light-emitting logo." *Appl. Phys. Lett.*, 72 (21), 2660–2662.
- Blom, P.W.M., Tanase, C., Leeuw, D.M. de and Coehoorn, R. (2005). "Thickness scaling of the space-charge-limited current in poly(p-phenylene vinylene)." *Appl. Phys. Lett.*, 86 (9), 092105.
- Bojinov, V.B. (2004). "Novel adducts of a hindered amine and a blue-emitting fluorophore for 'one-step' fluorescent brightening and stabilisation of polymer materials." *J. Photochem. Photobiol. Chem.*, 162 (1), 207–212.
- Bojinov, V.B., Georgiev, N.I. and Nikolov, P.S. (2008). "Design and synthesis of core and peripherally functionalized with 1,8-naphthalimide units fluorescent PAMAM dendron as light harvesting antenna." *J. Photochem. Photobiol. Chem.*, 197 (2–3), 281–289.
- Bojinov, V.B. and Simeonov, D.B. (2010). "Synthesis of highly photostable blue-emitting 1,8-naphthalimides and their acrylonitrile copolymers." *Polym. Degrad. Stab.*, 95 (1), 43–52.
- Bojinov, V.B., Venkova, A.I. and Georgiev, N.I. (2009). "Synthesis and energy-transfer properties of fluorescence sensing bichromophoric system based on Rhodamine 6G and 1,8-naphthalimide." *Sens. Actuators B Chem.*, 143 (1), 42–49.
- Bojinov, V. and Grabchev, I. (2001). "A new method for synthesis of 4-allyloxy-1,8-naphthalimide derivatives for use as fluorescent brighteners." *Dyes Pigments*, 51 (1), 57–61.
- Bojinov, V., Ivanova, G., Chovelon, J.-M. and Grabchev, I. (2003). "Photophysical and photochemical properties of some 3-bromo-4-alkylamino-N-alkyl-1,8-naphthalimides." *Dyes Pigments*, 58 (1), 65–71.
- Brütting, W. (2005). Introduction to the Physics of Organic Semiconductors. In *Physics of Organic Semiconductors*, W. Brütting, ed. (Wiley-VCH Verlag GmbH & Co. KGaA), pp 1–14.

References

- Brütting, W., Burroughes, J.H., Bradley, D.D.C., Brown, A.R., Marks, R.N., Mackay, K., Friend, R.H., Burns, P.L. and Holmes, A.B. (2001). "Device physics of organic light-emitting diodes based on molecular materials." *Org. Electron.*, 2 (1), 1–36.
- Burroughes, J.H., Bradley, D.D.C., Brown, A.R., Marks, R.N., Mackay, K., Friend, R.H., Burns, P.L. and Holmes, A.B. (1990). "Light-emitting diodes based on conjugated polymers." *Nature*, 347 (6293), 539–541.
- Cacialli, F., Friend, R.H., Bouché, C.-M., Barny, P.L., Facchetti, H., Soyer, F. and Robin, P. (1998). "Naphthalimide side-chain polymers for organic light-emitting diodes: Band-offset engineering and role of polymer thickness." *J. Appl. Phys.*, 83 (4), 2343–2356.
- Cao, H., Diaz, D.I., DiCesare, N., Lakowicz, J.R. and Heagy, M.D. (2002). "Monoboronic Acid Sensor That Displays Anomalous Fluorescence Sensitivity to Glucose." *Org. Lett.*, 4 (9), 1503–1505.
- Chatterjee, S., Pramanik, S., Hossain, S.U., Bhattacharya, S. and Bhattacharya, S.C. (2007). "Synthesis and photoinduced intramolecular charge transfer of N-substituted 1,8-naphthalimide derivatives in homogeneous solvents and in presence of reduced glutathione." *J. Photochem. Photobiol. Chem.*, 187 (1), 64–71.
- Chen, S.-F. and Wang, C.-W. (2004). "Influence of the hole injection layer on the luminescent performance of organic light-emitting diodes." *Appl. Phys. Lett.*, 85 (5), 765–767.
- Conwell, E.M. and Wu, M.W. (1997). "Contact injection into polymer light-emitting diodes." *Appl. Phys. Lett.*, 70 (14), 1867–1869.
- Cosnard, F. and Wintgens, V. (1998). "A new fluoroionophore derived from 4-amino-N-methyl-1,8-naphthalimide." *Tetrahedron Lett.*, 39 (18), 2751–2754.
- Dawson, W.R. and Windsor, M.W. (1968). "Fluorescence yields of aromatic compounds." *J. Phys. Chem.*, 72 (9), 3251–3260.

- Degheili, J.A., Moustafa, R.M., Patra, D. and Kaafarani, B.R. (2009). "Effect of Chain Length on the Photophysical Properties of Pyrene-Based Molecules Substituted with Extended Chains." *J. Phys. Chem. A*, *113* (7), 1244–1249.
- Demeter, A., Biczok, L., Berces, T., Wintgens, V., Valat, P. and Kossanyi, J. (1993). "Laser photolysis studies of transient processes in the photoreduction of naphthalimides by aliphatic amines." *J. Phys. Chem.*, *97* (13), 3217–3224.
- Dimitrakopoulos, C. d. and Malenfant, P. r. l. (2002). "Organic Thin Film Transistors for Large Area Electronics." *Adv. Mater.*, *14* (2), 99–117.
- Ding, G., Xu, Z., Zhong, G., Jing, S., Li, F. and Zhu, W. (2008). "Synthesis, photophysical and electroluminescent properties of novel naphthalimide derivatives containing an electron-transporting unit." *Res. Chem. Intermed.*, *34* (2-3), 299–308.
- Distanov, V.B., Berdanova, V.F., Stepanenko, A.A. and Prezhdo, V.V. (1997). "Influence of triphenylphosphine complexes on condensation of acetylenes with aryl halides." *Dyes Pigments*, *35* (2), 183–189.
- Duke, R.M., Veale, E.B., Pfeffer, F.M., Kruger, P.E. and Gunnlaugsson, T. (2010). "Colorimetric and fluorescent anion sensors: an overview of recent developments in the use of 1,8-naphthalimide-based chemosensors." *Chem. Soc. Rev.*, *39* (10), 3936–3953.
- Edward, J.T. (1970). "Molecular volumes and the Stokes-Einstein equation." *J. Chem. Educ.*, *47* (4), 261.
- Emtage, P.R. and O'Dwyer, J.J. (1966). "Richardson-Schottky Effect in Insulators." *Phys. Rev. Lett.*, *16* (9), 356–358.
- Feng, X., Hu, J.-Y., Tomiyasu, H., Seto, N., Redshaw, C., Elsegood, M.R.J. and Yamato, T. (2013). "Synthesis and photophysical properties of novel butterfly-shaped blue emitters based on pyrene." *Org. Biomol. Chem.*, *11* (48), 8366–8374.
- Figueira-Duarte, T.M. and Müllen, K. (2011). "Pyrene-Based Materials for Organic Electronics." *Chem. Rev.*, *111* (11), 7260–7314.

References

Forrest, S.R., Burrows, P.E., Shen, Z., Gu, G., Bulovic, V. and Thompson, M.E. (1997). "The stacked OLED (SOLED): a new type of organic device for achieving high-resolution full-color displays." *Synth. Met.*, *91* (1–3), 9–13.

Fowler, R.H. and Nordheim, L. (1928). "Electron Emission in Intense Electric Fields." *Proc. R. Soc. Lond. Math. Phys. Eng. Sci.*, *119* (781), 173–181.

Fujii, T., Kodaira, K., Kawauchi, O., Tanaka, N., Yamashita, H. and Anpo, M. (1997). "Photochromic behavior in the fluorescence spectra of 9-anthrol encapsulated in Si-Al glasses prepared by the sol-gel method." *J. Phys. Chem. B*, *101* (50), 10631–10637.

Gaśiowski, P., Danel, K.S., Matusiewicz, M., Uchacz, T., Kuźnik, W., Piątek, Ł. and Kityk, A.V. (2012). "DFT/TDDFT study on the electronic structure and spectral properties in annulated analogue of phenyl heteroazulene derivative." *Mater. Chem. Phys.*, *132* (2–3), 330–338.

Gan, J.-A., Song, Q.L., Hou, X.Y., Chen, K. and Tian, H. (2004). "1,8-Naphthalimides for non-doping OLEDs: the tunable emission color from blue, green to red." *J. Photochem. Photobiol. Chem.*, *162* (2–3), 399–406.

Gao, W. and Kahn, A. (2001). "Controlled p-doping of zinc phthalocyanine by coevaporation with tetrafluorotetracyanoquinodimethane: A direct and inverse photoemission study." *Appl. Phys. Lett.*, *79* (24), 4040–4042.

Gao, Z., Huang, R., Lin, Y., Zheng, Y., Liu, Y. and Wei, B. (2015). "Reduced turn-on voltage and improved efficiency with free interfacial energy barrier in organic light-emitting diodes." *Synth. Met.*, *207* 26–30.

Georgiev, N.I. and Bojinov, V.B. (2010). "Design, Synthesis and Photostability of Novel 1,8-naphthalimide PAMAM Light-harvesting Dendrons." *J. Fluoresc.*, *21* (1), 51–63.

Gordon, P.F. and Gregory, P. (1987). "Organic Chemistry in Colour (Berlin, Heidelberg: Springer Berlin Heidelberg).

- Grabchev, I., Bojinov, V. and Petkov, C. (2001). "Synthesis and photophysical properties of polymerizable 1,8-naphthalimide dyes and their copolymers with styrene." *Dyes Pigments*, 51 (1), 1–8.
- Grabchev, I., Meallier, P., Konstantinova, T. and Popova, M. (1995). "Synthesis of some unsaturated 1,8-naphthalimide dyes." *Dyes Pigments*, 28 (1), 41–46.
- Grabchev, I., Qian, X., Bojinov, V., Xiao, Y. and Zhang, W. (2002). "Synthesis and photophysical properties of 1,8-naphthalimide-labelled PAMAM as PET sensors of protons and of transition metal ions." *Polymer*, 43 (21), 5731–5736.
- Grayshan, P.H., Kadhim, A.M. and Perters, A.T. (1974). "Heterocyclic derivatives of naphthalene-1,8-dicarboxylic anhydride. Part III. Benzo[k,l] thioxanthene-3,4-dicarboximides." *J. Heterocycl. Chem.*, 11 (1), 33–38.
- Gu, J.-F., Xie, G.-H., Zhang, L., Chen, S.-F., Lin, Z.-Q., Zhang, Z.-S., Zhao, J.-F., Xie, L.-H., Tang, C., Zhao, Y., Liu, S.-Y. and Huang, W. (2010). "Dumbbell-Shaped Spirocyclic Aromatic Hydrocarbon to Control Intermolecular π - π Stacking Interaction for High-Performance Nondoped Deep-Blue Organic Light-Emitting Devices." *J. Phys. Chem. Lett.*, 1 (19), 2849–2853.
- Gupta, B.K., Thanikaivelan, P., Narayanan, T.N., Song, L., Gao, W., Hayashi, T., Leela Mohana Reddy, A., Saha, A., Shanker, V., Endo, M., Martí, A.A. and Ajayan, P.M. (2011). "Optical Bifunctionality of Europium-Complexed Luminescent Graphene Nanosheets." *Nano Lett.*, 11 (12), 5227–5233.
- Hamai, S. and Hirayama, F. (1983). "Actinometric determination of absolute fluorescence quantum yields." *J. Phys. Chem.*, 87 (1), 83–89.
- Hammond, H.K. and Mason, H.L. (1971). "Radiometry and Photometry (U.S. Government Printing Office).
- Hebner, T.R., Wu, C.C., Marcy, D., Lu, M.H. and Sturm, J.C. (1998). "Ink-jet printing of doped polymers for organic light emitting devices." *Appl. Phys. Lett.*, 72 (5), 519–521.

References

- Helander, M.G., Morse, G.E., Qiu, J., Castrucci, J.S., Bender, T.P. and Lu, Z.-H. (2010). "Pentafluorophenoxy Boron Subphthalocyanine As a Fluorescent Dopant Emitter in Organic Light Emitting Diodes." *ACS Appl. Mater. Interfaces*, 2 (11), 3147–3152.
- Helfrich, W. and Schneider, W.G. (1965). "Recombination Radiation in Anthracene Crystals." *Phys. Rev. Lett.*, 14 (7), 229–231.
- Horowitz, G. (2004). "Organic thin film transistors: from theory to real devices. J. Mater. Res. 19, 1946-1962." *J. Mater. Res. - J MATER RES*, 19 (7), 1946–1962.
- Hosokawa, C., Higashi, H., Nakamura, H. and Kusumoto, T. (1995). "Highly efficient blue electroluminescence from a distyrylarylene emitting layer with a new dopant." *Appl. Phys. Lett.*, 67 3853–3855.
- Hossain, S.U., Sengupta, S. and Bhattacharya, S. (2005). "Synthesis and evaluation of antioxidative properties of a series of organoselenium compounds." *Bioorg. Med. Chem.*, 13 (20), 5750–5758.
- Huh, J.W., Kim, Y.M., Park, Y.W., Choi, J.H., Lee, J.W., Lee, J.W., Yang, J.W., Ju, S.H., Paek, K.K. and Ju, B.K. (2008). "Characteristics of organic light-emitting diodes with conducting polymer anodes on plastic substrates." *J. Appl. Phys.*, 103 (4), 044502.
- Hu, J.-Y., Feng, X., Seto, N., Iwanaga, F., Era, M., Matsumoto, T., Tanaka, J. and Yamato, T. (2013). "Synthesis, crystal structure and photophysical properties of 5-mono- and 5,9-bis-(arylethynyl)-functionalized pyrenes." *J. Lumin.*, 141 111–120.
- Hwang, J., Amy, F. and Kahn, A. (2006). "Spectroscopic study on sputtered PEDOT · PSS: Role of surface PSS layer." *Org. Electron.*, 7 (5), 387–396.
- Idzik, K.R., Ledwon, P., Licha, T., Kuznik, W., Lapkowski, M. and Frydel, J. (2014). "Furyl derivatives of pyrene: Efficient synthesis and relevant optical properties." *Dyes Pigments*, 103 55–61.
- Inzelt, G. (2012). "Conducting Polymers (Berlin, Heidelberg: Springer Berlin Heidelberg).

- Ishii, H., Sugiyama, K., Ito, E. and Seki, K. (1999). "Energy Level Alignment and Interfacial Electronic Structures at Organic/Metal and Organic/Organic Interfaces." *Adv. Mater.*, *11* (8), 605–625.
- Islam, A., Cheng, C.-C., Chi, S.-H., Lee, S.J., Hela, P.G., Chen, I.-C. and Cheng, C.-H. (2005). "Aminonaphthalic anhydrides as red-emitting materials: electroluminescence, crystal structure, and photophysical properties." *J. Phys. Chem. B*, *109* (12), 5509–5517.
- Jain, A., Kumar, P., Jain, S.C., Kumar, V., Kaur, R. and Mehra, R.M. (2007a). "Trap filled limit voltage (VTFL) and V² law in space charge limited currents." *J. Appl. Phys.*, *102* (9), 094505.
- Jain, S.C., Geens, W., Mehra, A., Kumar, V., Aernouts, T., Poortmans, J., Mertens, R. and Willander, M. (2001). "Injection- and space charge limited-currents in doped conducting organic materials." *J. Appl. Phys.*, *89* (7), 3804–3810.
- Jain, S.C., Willander, M. and Kumar, V. (2007b). Conducting Organic Materials and Devices. In Semiconductors and Semimetals, M.W. and V.K. S.C. Jain, ed. (Elsevier), pp i–188.
- Jiang, X.-Y., Zhang, Z.-L., Zheng, X.-Y., Wu, Y.-Z. and Xu, S.-H. (2001). "A blue organic emitting diode from anthracene derivative." *Thin Solid Films*, *401* (1–2), 251–254.
- Jin, R. and Ahmad, I. (2015). "Theoretical study on photophysical properties of multifunctional star-shaped molecules with 1,8-naphthalimide core for organic light-emitting diode and organic solar cell application." *Theor. Chem. Acc.*, *134* (7), 1–13.
- Jin, R. and Tang, S. (2013). "Theoretical study on optical and electronic properties of bipolar molecules with 1,8-naphthalimide and triphenylamine moieties as organic light-emitting materials." *J. Mol. Graph. Model.*, *42* 120–128.
- Justin Thomas, K.R., Lin, J.T., Tao, Y.-T. and Ko, C.-W. (2001). "Light-Emitting Carbazole Derivatives: Potential Electroluminescent Materials." *J. Am. Chem. Soc.*, *123* (38), 9404–9411.

References

- Kahn, A., Koch, N. and Gao, W. (2003). "Electronic structure and electrical properties of interfaces between metals and π -conjugated molecular films." *J. Polym. Sci. Part B Polym. Phys.*, *41* (21), 2529–2548.
- Kao, K.-C. and Hwang, W. (1981). "Electrical transport in solids: with particular reference to organic semiconductors (Pergamon Press).
- Karamancheva, I., Tadjer, A., Philipova, T., Madjarova, G., Ivanova, C. and Grozeva, T. (1998). "Calculated and experimental spectra of some 1,8-naphthalimide derivatives." *Dyes Pigments*, *36* (3), 273–285.
- Kawano, S., Baumgarten, M., Chercka, D., Enkelmann, V. and Müllen, K. (2013). "Electron donors and acceptors based on 2,7-functionalized pyrene-4,5,9,10-tetraone." *Chem. Commun.*, *49* (44), 5058–5060.
- Kepler, R.G., Beeson, P.M., Jacobs, S.J., Anderson, R.A., Sinclair, M.B., Valencia, V.S. and Cahill, P.A. (1995). "Electron and hole mobility in tris(8-hydroxyquinolinolato-N1,O8) aluminum." *Appl. Phys. Lett.*, *66* (26), 3618–3620.
- Kim, H.M., Lee, Y.O., Lim, C.S., Kim, J.S. and Cho, B.R. (2008). "Two-Photon Absorption Properties of Alkynyl-Conjugated Pyrene Derivatives." *J. Org. Chem.*, *73* (13), 5127–5130.
- Kityk, A.V. (2012). "Absorption and Fluorescence Spectra of Heterocyclic Isomers from Long-Range-Corrected Density Functional Theory in Polarizable Continuum Approach." *J. Phys. Chem. A*, *116* (11), 3048–3055.
- Klauk, H. (2006). "Organic Electronics: Materials, Manufacturing, and Applications (John Wiley & Sons).
- Kotchapradist, P., Prachumrak, N., Tarsang, R., Jungsuttiwong, S., Keawin, T., Sudyoadsuk, T. and Promarak, V. (2013). "Pyrene-functionalized carbazole derivatives as non-doped blue emitters for highly efficient blue organic light-emitting diodes." *J. Mater. Chem. C*, *1* (32), 4916–4924.

- Krishna, J.B.M., Saha, A., Okram, G.S., Purakayastha, S. and Ghosh, B. (2009). "Influence of traps on charge transport in metal ion doped polyaniline." *J. Phys. Appl. Phys.*, *42* (11), 115102.
- Krotkus, S., Kazlauskas, K., Miasojedovas, A., Gruodis, A., Tomkeviciene, A., Grazulevicius, J.V. and Jursenas, S. (2012). "Pyrenyl-Functionalized Fluorene and Carbazole Derivatives as Blue Light Emitters." *J. Phys. Chem. C*, *116* (13), 7561–7572.
- Kulkarni, A.P., Tonzola, C.J., Babel, A. and Jenekhe, S.A. (2004). "Electron Transport Materials for Organic Light-Emitting Diodes." *Chem. Mater.*, *16* (23), 4556–4573.
- Kumar, A., Srivastava, R., Kumar, A., Nishal, V., Kadyan, P.S., Kamalasanan, M.N. and Singh, I. (2013). "Ternary zinc complexes as electron transport and electroluminescent materials." *J. Organomet. Chem.*, *740* 116–122.
- Kumar, A., Srivastava, R., Tyagi, P., Mehta, D.S., Kamalasanan, M.N., Reddy, M.A. and Bhanuprakash, K. (2010). "Field, temperature and thickness dependent electron transport in 5,5'-(2,6-di-tert-butylanthracene-9,10-diyl)bis(2-p-tolyl-1,3,4-oxadiazole)." *Synth. Met.*, *160* (7–8), 774–778.
- Kumar, D. and Thomas, K.R.J. (2011). "Optical properties of pyrene and anthracene containing imidazoles: Experimental and theoretical investigations." *J. Photochem. Photobiol. Chem.*, *218* (1), 162–173.
- Lai, S.L., Tong, Q.X., Chan, M.Y., Ng, T.W., Lo, M.F., Ko, C.C., Lee, S.T. and Lee, C.S. (2011). "Carbazole–pyrene derivatives for undoped organic light-emitting devices." *Org. Electron.*, *12* (3), 541–546.
- Lakowicz, J.R. (2007). "Principles of Fluorescence Spectroscopy (Springer Science & Business Media).
- Lampert, M.A. and Mark, P. (1970). "Current injection in solids (Academic Press).
- Ledwon, P., Lapkowski, M., Licha, T., Frydel, J. and Idzik, K.R. (2014). "The role of furyl substituents of pyrene on monomer and polymer properties." *Synth. Met.*, *191* 74–82.

References

Lee, H., Kang, C.-M., Park, M., Kwak, J. and Lee, C. (2013). "Improved Efficiency of Inverted Organic Light-Emitting Diodes Using Tin Dioxide Nanoparticles as an Electron Injection Layer." *ACS Appl. Mater. Interfaces*, 5 (6), 1977–1981.

Liang, Z.-Q., Chu, Z.-Z., Yang, J.-X., Yuan, C.-X., Tao, X.-T. and Zou, D.-C. (2011). "X-shaped tetra-substituted pyrenes: Synthesis, photophysics, and electroluminescence." *Synth. Met.*, 161 (15–16), 1691–1698.

Liao, Y.-L., Lin, C.-Y., Wong, K.-T., Hou, T.-H. and Hung, W.-Y. (2007). "A Novel Ambipolar Spirobifluorene Derivative that Behaves as an Efficient Blue-Light Emitter in Organic Light-Emitting Diodes." *Org. Lett.*, 9 (22), 4511–4514.

Lippert, E. (1957). "Spektroskopische Bestimmung des Dipolmomentes aromatischer Verbindungen im ersten angeregten Singulettzustand." *Z. Für Elektrochem. Berichte Bunsenges. Für Phys. Chem.*, 61 (8), 962–975.

Liu, F., Tang, C., Chen, Q.-Q., Shi, F.-F., Wu, H.-B., Xie, L.-H., Peng, B., Wei, W., Cao, Y. and Huang, W. (2009). "Supramolecular π - π Stacking Pyrene-Functioned Fluorenes: Toward Efficient Solution-Processable Small Molecule Blue and White Organic Light Emitting Diodes." *J. Phys. Chem. C*, 113 (11), 4641–4647.

Liu, J., Cao, J., Shao, S., Xie, Z., Cheng, Y., Geng, Y., Wang, L., Jing, X. and Wang, F. (2008). "Blue electroluminescent polymers with dopant–host systems and molecular dispersion features: polyfluorene as the deep blue host and 1,8-naphthalimide derivative units as the light blue dopants." *J. Mater. Chem.*, 18 (14), 1659.

Liu, J., Li, Y., Wang, Y., Sun, H., Lu, Z., Wu, H., Peng, J. and Huang, Y. (2012). "Synthesis and luminescent properties of blue sextuple-hydrogen-bond self-assembly molecular duplexes bearing 4-phenoxy-1,8-naphthalimide moieties." *Opt. Mater.*, 34 (9), 1535–1542.

Liu, J., Min, C., Zhou, Q., Cheng, Y., Wang, L., Ma, D., Jing, X. and Wang, F. (2006). "Blue light-emitting polymer with polyfluorene as the host and highly fluorescent 4-dimethylamino-1,8-naphthalimide as the dopant in the sidechain." *Appl. Phys. Lett.*, 88 (8), 083505.

- Liu, S.-W., Yuan, C.-H., Yeh, S.-J., Wu, M.-F., Chen, C.-T. and Lee, C.-C. (2011). "Efficiency enhancement of solution-processed single-layer blue-phosphorescence organic light-emitting devices having co-host materials of polymer (PVK) and small-molecule (SimCP2)." *J. Soc. Inf. Disp.*, 19 (4), 346–352.
- Li, Z.R. (2015). "Organic Light-Emitting Materials and Devices, Second Edition (CRC Press).
- Lo, M.Y., Zhen, C., Lauters, M., Jabbour, G.E. and Sellinger, A. (2007). "Organic–Inorganic Hybrids Based on Pyrene Functionalized Octavinylsilsesquioxane Cores for Application in OLEDs." *J. Am. Chem. Soc.*, 129 (18), 5808–5809.
- Luo, S., Lin, J., Zhou, J., Wang, Y., Liu, X., Huang, Y., Lu, Z. and Hu, C. (2015). "Novel 1,8-naphthalimide derivatives for standard-red organic light-emitting device applications." *J. Mater. Chem. C*, 3 (20), 5259–5267.
- Magalhães, J.L., Pereira, R.V., Triboni, E.R., Berci Filho, P., Gehlen, M.H. and Nart, F.C. (2006). "Solvent effect on the photophysical properties of 4-phenoxy-N-methyl-1,8-naphthalimide." *J. Photochem. Photobiol. Chem.*, 183 (1–2), 165–170.
- Mahajan, A., Aulakh, R.K., Bedi, R.K., Kumar, S., Kumar, S. and Aswal, D.K. (2012). "Synthesis and characterization of excited state intramolecular proton transfer based 2-hydroxylaryl imidazole fluorescent materials." *Synth. Met.*, 162 (1–2), 58–63.
- Marinova, N.V., Georgiev, N.I. and Bojinov, V.B. (2013). "Facile synthesis, sensor activity and logic behaviour of 4-aryloxy substituted 1, 8-naphthalimide." *J. Photochem. Photobiol. Chem.*, 254 54–61.
- Mark, P. and Helfrich, W. (1962). "Space-Charge-Limited Currents in Organic Crystals." *J. Appl. Phys.*, 33 (1), 205–215.
- Martín, E., Coronado, J.L.G., Camacho, J.J. and Pardo, A. (2005). "Experimental and theoretical study of the intramolecular charge transfer on the derivatives 4-methoxy and 4-acetamide 1,8-naphthalimide N-substituted." *J. Photochem. Photobiol. Chem.*, 175 (1), 1–7.

References

- Martin, E., Weigand, R. and Pardo, A. (1996). "Solvent dependence of the inhibition of intramolecular charge-transfer in N-substituted 1,8-naphthalimide derivatives as dye lasers." *J. Lumin.*, 68 (2-4), 157–164.
- Martin, R.E. and Diederich, F. (1999). "Linear Monodisperse π -Conjugated Oligomers: Model Compounds for Polymers and More." *Angew. Chem. Int. Ed.*, 38 (10), 1350–1377.
- Mataga, N., Kaifu, Y. and Koizumi, M. (1956). "Solvent Effects upon Fluorescence Spectra and the Dipolemoments of Excited Molecules." *Bull. Chem. Soc. Jpn.*, 29 (4), 465–470.
- May, B., Poteau, X., Yuan, D. and Brown, R.G. (1999). "A study of a highly efficient resonance energy transfer between 7-N,N-diethylamino-4-methylcoumarin and 9-butyl-4-butylamino-1,8-naphthalimide." *Dyes Pigments*, 42 (1), 79–84.
- Mikroyannidis, J.A., Ye, S. and Liu, Y. (2009). "Electroluminescent divinylene- and trivinylene-molecules with terminal naphthalimide or phthalimide segments." *Synth. Met.*, 159 (5–6), 492–500.
- Miller, A. and Abrahams, E. (1960). "Impurity Conduction at Low Concentrations." *Phys. Rev.*, 120 (3), 745–755.
- Mishra, A., Nayak, P.K., Ray, D., Patankar, M.P., Narasimhan, K.L. and Periasamy, N. (2006). "Synthesis and characterization of spin-coatable tert-amine molecules for hole-transport in organic light-emitting diodes." *Tetrahedron Lett.*, 47 (27), 4715–4719.
- Moorthy, J.N., Natarajan, P., Venkatakrishnan, P., Huang, D.-F. and Chow, T.J. (2007). "Steric Inhibition of π -Stacking: 1,3,6,8-Tetraarylpyrenes as Efficient Blue Emitters in Organic Light Emitting Diodes (OLEDs)." *Org. Lett.*, 9 (25), 5215–5218.
- Murakami, S., Herren, M., Rau, D. and Morita, M. (2000). "Photoluminescence and decay profiles of undoped and Fe³⁺, Eu³⁺-doped PLZT ceramics at low temperatures down to 10 K." *Inorganica Chim. Acta*, 300–302 1014–1021.

- Murphy, S., Bright, S.A., Poynton, F.E., McCabe, T., Kitchen, J.A., Veale, E.B., Williams, D.C. and Gunnlaugsson, T. (2014). "Synthesis, photophysical and cytotoxicity evaluations of DNA targeting agents based on 3-amino-1,8-naphthalimide derived Tröger's bases." *Org. Biomol. Chem.*, 12 (34), 6610–6623.
- Naka, S., Okada, H., Onnagawa, H., Yamaguchi, Y. and Tsutsui, T. (2000). "Carrier transport properties of organic materials for EL device operation." *Synth. Met.*, 111–112 331–333.
- Niu, X., Ma, L., Yao, B., Ding, J., Tu, G., Xie, Z. and Wang, L. (2006). "White polymeric light-emitting diodes with high color rendering index." *Appl. Phys. Lett.*, 89 (21), 213508.
- Oelgemöller, M. and Kramer, W.H. (2010). "Synthetic photochemistry of naphthalimides and related compounds." *J. Photochem. Photobiol. C Photochem. Rev.*, 11 (4), 210–244.
- Oh, H.-Y., Lee, C. and Lee, S. (2009). "Efficient blue organic light-emitting diodes using newly-developed pyrene-based electron transport materials." *Org. Electron.*, 10 (1), 163–169.
- Okamoto, Y. and Brenner, W. (1964). "Organic semiconductors (New York: Reinhold Pub.).
- Patra, D. and Barakat, C. (2011). "Synchronous fluorescence spectroscopic study of solvatochromic curcumin dye." *Spectrochim. Acta. A. Mol. Biomol. Spectrosc.*, 79 (5), 1034–1041.
- Peng, J., Ye, K., Zhang, G., Zhan, Y., Jia, J., Xue, P. and Lu, R. (2014). "Synthesis, photophysical and electroluminescent properties of phenanthroimidazole derivatives with terminal carbazole or pyrene." *Synth. Met.*, 193 94–101.
- Pope, M., Kallmann, H.P. and Magnante, P. (1963). "Electroluminescence in Organic Crystals." *J. Chem. Phys.*, 38 (8), 2042–2043.

References

- P. S. Vincett, W.A.B. (1982). "Electrical conduction and low voltage blue electroluminescence in vacuum-deposited organic films." *Thin Solid Films*, 94 (2), 171–183.
- Rakurthi, A. (2010). Improvement of Efficiencies and Lifetimes of White Light-Emitting Organic Diodes Using a Novel Co-evaporated 'Hole-Confining' Structure. University of Cincinnati.
- Reichardt, C. (1994). "Solvatochromic Dyes as Solvent Polarity Indicators." *Chem. Rev.*, 94 (8), 2319–2358.
- Roichman, Y., Preezant, Y. and Tessler, N. (2004). "Analysis and modeling of organic devices." *Phys. Status Solidi A*, 201 (6), 1246–1262.
- Ruden, A.L. Von, Cosimbescu, L., Polikarpov, E., Koech, P.K., Swensen, J.S., Wang, L., Darsell, J.T. and Padmaperuma, A.B. (2010). "Phosphine Oxide Based Electron Transporting and Hole Blocking Materials for Blue Electrophosphorescent Organic Light Emitting Devices." *Chem. Mater.*, 22 (20), 5678–5686.
- Salunke, J.K., Sonar, P., Wong, F.L., Roy, V. a. L., Lee, C.S. and Wadgaonkar, P.P. (2014). "Pyrene based conjugated materials: synthesis, characterization and electroluminescent properties." *Phys. Chem. Chem. Phys.*, 16 (42), 23320–23328.
- Schmechel, R. and Seggern, H. von (2005). Electronic Traps in Organic Transport Layers. In *Physics of Organic Semiconductors*, W. Brütting, ed. (Wiley-VCH Verlag GmbH & Co. KGaA), pp 271–303.
- Scott, J.C. and Malliaras, G.G. (1999). "Charge injection and recombination at the metal–organic interface." *Chem. Phys. Lett.*, 299 (2), 115–119.
- Seo, J.H., Seo, J.H., Park, J.H., Kim, Y.K., Kim, J.H., Hyung, G.W., Lee, K.H. and Yoon, S.S. (2007). "Highly efficient white organic light-emitting diodes using two emitting materials for three primary colors (red, green, and blue)." *Appl. Phys. Lett.*, 90 (20), 203507.

- Shirakawa, H., Louis, E.J., MacDiarmid, A.G., Chiang, C.K. and Heeger, A.J. (1977). "Synthesis of electrically conducting organic polymers: halogen derivatives of polyacetylene, (CH)_x." *J. Chem. Soc. Chem. Commun.*, (16), 578–580.
- Simmons, J.G. (1965). "Richardson-Schottky Effect in Solids." *Phys. Rev. Lett.*, 15 (25), 967–968.
- Singh, K., Kumar, A., Srivastava, R., Kadyan, P.S., Kamalasanan, M.N. and Singh, I. (2011). "Synthesis and characterization of 5, 7-dimethyl-8-hydroxyquinoline and 2-(2-pyridyl) benzimidazole complexes of zinc (II) for optoelectronic application." *Opt. Mater.*,
- Singh, P., Negi, J.S., Singh, K., Pant, G.J., Rawat, M.S.M. and Joshi, G.C. (2012). "Synthesis and structure dependent photophysical properties of novel 2-pyrazolines." *Synth. Met.*, 162 (21–22), 1977–1980.
- Slyke, S.A.V., Chen, C.H. and Tang, C.W. (1996). "Organic electroluminescent devices with improved stability." *Appl. Phys. Lett.*, 69 (15), 2160–2162.
- S.M.Sze (2008). "SEMICONDUCTOR DEVICES: PHYSICS AND TECHNOLOGY, 2ND ED (John Wiley & Sons).
- So, F. (2010). "Organic electronics: materials, processing, devices and applications (Boca Raton, FL: CRC Press).
- Sonar, P., Soh, M.S., Cheng, Y.H., Henssler, J.T. and Sellinger, A. (2010). "1,3,6,8-Tetrasubstituted Pyrenes: Solution-Processable Materials for Application in Organic Electronics." *Org. Lett.*, 12 (15), 3292–3295.
- Srikun, D., Miller, E.W., Domaille, D.W. and Chang, C.J. (2008). "An ICT-Based Approach to Ratiometric Fluorescence Imaging of Hydrogen Peroxide Produced in Living Cells." *J. Am. Chem. Soc.*, 130 (14), 4596–4597.
- Suppan, P. and Ghoneim, N. (1997). "Solvatochromism (Royal Society of Chemistry).

References

- Tang, C., Liu, F., Xia, Y.-J., Lin, J., Xie, L.-H., Zhong, G.-Y., Fan, Q.-L. and Huang, W. (2006). "Fluorene-substituted pyrenes—Novel pyrene derivatives as emitters in nondoped blue OLEDs." *Org. Electron.*, 7 (3), 155–162.
- Tang, C.W. and VanSlyke, S.A. (1987). "Organic electroluminescent diodes." *Appl. Phys. Lett.*, 51 (12), 913–915.
- Tang, C.W., VanSlyke, S.A. and Chen, C.H. (1989a). "Electroluminescence of doped organic thin films." *J. Appl. Phys.*, 65 (9), 3610–3616.
- Tao, S.L., Peng, Z.K., Zhang, X.H., Wang, P.F., Lee, C.-S. and Lee, S.-T. (2005). "Highly Efficient Non-Doped Blue Organic Light-Emitting Diodes Based on Fluorene Derivatives with High Thermal Stability." *Adv. Funct. Mater.*, 15 (10), 1716–1721.
- Tao, S., Zhou, Y., Lee, C.-S., Zhang, X. and Lee, S.-T. (2010). "High-Efficiency Nondoped Deep-Blue-Emitting Organic Electroluminescent Device." *Chem. Mater.*, 22 (6), 2138–2141.
- Thomas, K.R.J., Kapoor, N., Bolisetty, M.N.K.P., Jou, J.-H., Chen, Y.-L. and Jou, Y.-C. (2012). "Pyrene-Fluorene Hybrids Containing Acetylene Linkage as Color-Tunable Emitting Materials for Organic Light-Emitting Diodes." *J. Org. Chem.*, 77 (8), 3921–3932.
- Thomas, K.R.J., Lin, J.T., Tao, Y.-T. and Ko, C.-W. (2000). "Novel Green Light-Emitting Carbazole Derivatives: Potential Electroluminescent Materials." *Adv. Mater.*, 12 (24), 1949–1951.
- Thomas, K.R.J. and Tyagi, P. (2010). "Synthesis, spectra, and theoretical investigations of the triarylaminines based on 6H-indolo[2,3-b]quinoxaline." *J. Org. Chem.*, 75 (23), 8100–8111.
- Tian, H., Su, J., Chen, K., Wong, T.C., Gao, Z.Q., Lee, C.S. and Lee, S.T. (2000). "Electroluminescent property and charge separation state of bis-naphthalimides." *Opt. Mater.*, 14 (1), 91–94.

- Tomova, R., Petrova, P. and Stoycheva-Topalova, R. (2010). "Role of bathocuproine as hole-blocking and electron-transporting layer in organic light emitting devices." *Phys. Status Solidi C*, 7 (3-4), 992–995.
- Tonzola, C.J., Alam, M.M., Kaminsky, W. and Jenekhe, S.A. (2003). "New n-Type Organic Semiconductors: Synthesis, Single Crystal Structures, Cyclic Voltammetry, Photophysics, Electron Transport, and Electroluminescence of a Series of Diphenylanthrazolines." *J. Am. Chem. Soc.*, 125 (44), 13548–13558.
- Tour, J.M. (1996). "Conjugated Macromolecules of Precise Length and Constitution. Organic Synthesis for the Construction of Nanoarchitectures." *Chem. Rev.*, 96 (1), 537–554.
- Triboni, E.R., Fernandes, M.R., Garcia, J.R., Carreira, M.C., Berlinck, R.G.S., Filho, P.B., Roman, L.S., Hümmelgen, I.A., Reyes, R. and Cremona, M. (2015). "Naphthalimide-derivative with blue electroluminescence for OLED applications." *J. Taibah Univ. Sci.*, 9 (4), 579–585.
- Tung, Y.-L., Lee, S.-W., Chi, Y., Chen, L.-S., Shu, C.-F., Wu, F.-I., Carty, A.J., Chou, P.-T., Peng, S.-M. and Lee, G.-H. (2005). "Organic Light-Emitting Diodes based on Charge-Neutral RuII Phosphorescent Emitters." *Adv. Mater.*, 17 (8), 1059–1064.
- Walker, A.B., Kambili, A. and Martin, S.J. (2002). "Electrical transport modelling in organic electroluminescent devices." *J. Phys. Condens. Matter*, 14 (42), 9825–9876.
- Wang, S., Zeng, P.J., Liu, Y.Q., Yu, G., Sun, X.B., Niu, H.B. and Zhu, D.B. (2005). "Luminescent properties of a novel naphthalimide-fluorene molecule." *Synth. Met.*, 150 (1), 33–38.
- Wang, W., Peng, H., Wang, S. and Chen, S. (2015). "Top-emitting organic light-emitting diodes integrated with thermally evaporated scattering film for reducing angular dependence of emission spectra." *Org. Electron.*, 24 195–199.
- Wang, Y., Zhang, X., Han, B., Peng, J., Hou, S., Huang, Y., Sun, H., Xie, M. and Lu, Z. (2010). "The synthesis and photoluminescence characteristics of novel blue light-emitting naphthalimide derivatives." *Dyes Pigments*, 86 (2), 190–196.

References

Wang, Y., Zhou, J., Wang, X., Zheng, X., Lu, Z., Zhang, W., Chen, Y., Huang, Y., Pu, X. and Yu, J. (2014). "An efficient guest/host fluorescent energy transfer pair based on the naphthalimide skeleton, and its application in heavily-doped red organic light-emitting diodes." *Dyes Pigments*, 100 87–96.

Wang, Z., Xu, C., Wang, W., Dong, X., Zhao, B. and Ji, B. (2012). "Novel pyrene derivatives: Synthesis, properties and highly efficient non-doped deep-blue electroluminescent device." *Dyes Pigments*, 92 (1), 732–736.

Wee, K.-R., Ahn, H.-C., Son, H.-J., Han, W.-S., Kim, J.-E., Cho, D.W. and Kang, S.O. (2009). "Emission Color Tuning and Deep Blue Dopant Materials Based on 1,6-Bis(N-phenyl-p-(R)-phenylamino)pyrene." *J. Org. Chem.*, 74 (21), 8472–8475.

Wintgens, V., Valat, P., Kossanyi, J., Demeter, A., Biczok, L. and Berces, T. (1996). "Spectroscopic properties of aromatic dicarboximides. Part 4. On the modification of the fluorescence and intersystem crossing processes of molecules by electron-donating methoxy groups at different positions. The case of 1, 8-naphthalimides." *New J. Chem.*, 20 (11), 1149–1158.

Wolf, U., Arkhipov, V.I. and Bäessler, H. (1999). "Current injection from a metal to a disordered hopping system. I. Monte Carlo simulation." *Phys. Rev. B*, 59 (11), 7507–7513.

Wu, K.-C., Ku, P.-J., Lin, C.-S., Shih, H.-T., Wu, F.-I., Huang, M.-J., Lin, J.-J., Chen, I.-C. and Cheng, C.-H. (2008). "The Photophysical Properties of Dipyranylbenzenes and Their Application as Exceedingly Efficient Blue Emitters for Electroluminescent Devices." *Adv. Funct. Mater.*, 18 (1), 67–75.

Xiao, J. and Deng, Z. (2012). "Synthesis and electroluminescent characterization of a symmetric starburst orange-red light material." *J. Lumin.*, 132 (11), 2863–2867.

Xiao, L., Su, S.-J., Agata, Y., Lan, H. and Kido, J. (2009). "Nearly 100% Internal Quantum Efficiency in an Organic Blue-Light Electrophosphorescent Device Using a Weak Electron Transporting Material with a Wide Energy Gap." *Adv. Mater.*, 21 (12), 1271–1274.

- Xing, Y., Xu, X., Zhang, P., Tian, W., Yu, G., Lu, P., Liu, Y. and Zhu, D. (2005). "Carbazole–pyrene-based organic emitters for electroluminescent device." *Chem. Phys. Lett.*, *408* (1–3), 169–173.
- Xu, L.-H. with Yang, J.-X. and Wang, X.-L., Tusong (2005). "Studies on the synthesis and spectral properties of novel 4-benzofuranyl-1,8-naphthalimide derivatives." *Dyes Pigments*, *67* (1), 27–33.
- Yang, C.-H., Guo, T.-F. and Sun, I.-W. (2007). "Highly efficient greenish blue-emitting organic diodes based on pyrene derivatives." *J. Lumin.*, *124* (1), 93–98.
- Yang, J.X. and Wang, X.H. (2012). "The Synthesis and Electroluminescence Properties of 4-Benzofuranyl-1,8-Naphthalimide Derivatives." *Adv. Mater. Res.*, *557-559* 1031–1036.
- Yang, J.-X., Wang, X.-L., Wang, X.-M. and Xu, L.-H. (2005). "The synthesis and spectral properties of novel 4-phenylacetylene-1,8-naphthalimide derivatives." *Dyes Pigments*, *66* (1), 83–87.
- Zhang, Y., Lai, S.-L., Tong, Q.-X., Lo, M.-F., Ng, T.-W., Chan, M.-Y., Wen, Z.-C., He, J., Jeff, K.-S., Tang, X.-L., Liu, W.-M., Ko, C.-C., Wang, P.-F. and Lee, C.-S. (2012). "High Efficiency Nondoped Deep-Blue Organic Light Emitting Devices Based on Imidazole- π -triphenylamine Derivatives." *Chem. Mater.*, *24* (1), 61–70.
- Zhao, Z., Chen, S., Deng, C., Lam, J.W.Y., Chan, C.Y.K., Lu, P., Wang, Z., Hu, B., Chen, X., Lu, P., Kwok, H.S., Ma, Y., Qiu, H. and Tang, B.Z. (2011). "Construction of efficient solid emitters with conventional and AIE luminogens for blue organic light-emitting diodes." *J. Mater. Chem.*, *21* (29), 10949–10956.
- Zhao, Z., Li, J.-H., Chen, X., Lu, P. and Yang, Y. (2008). "Fluorescent Conjugated Dendrimers with Fluorinated Terminal Groups: Nanofiber Formation and Electroluminescence Properties." *Org. Lett.*, *10* (14), 3041–3044.
- Zhi-Feng, Z., Zhen-Bo, D., Chun-Jun, L., Meng-Xin, Z. and Deng-Hui, X. (2003). "Organic light-emitting diodes with a nanostructured TiO₂ layer at the interface between ITO and NPB layers." *Displays*, *24* (4–5), 231–234.

References

Zhuang, S., Shangguan, R., Huang, H., Tu, G., Wang, L. and Zhu, X. (2014). "Synthesis, characterization, physical properties, and blue electroluminescent device applications of phenanthroimidazole derivatives containing anthracene or pyrene moiety." *Dyes Pigments*, 101 93–102.

PUBLICATIONS

Papers Published in International Journals

1. Chidirala Swetha, **Hidayath Ulla**, V. Anusha, M. Raveendra Kiran, M. N. Satyanarayan, G. Umesh, Maneesha Esther Mohanty, Kotamarthi Bhanuprakash, Vaidya Jayathirtha Rao, "Pyrene-Oxadiazole Derivatives as Electron Transporting Green Emitters for non-doped Organic Light Emitting Devices" **Journal of Organic Chemistry** 81 (2) (2016) 603–614.
2. **Hidayath Ulla**, M. Raveendra Kiran, B. Garudachari, M.N. Satyanarayan, G. Umesh and A.M. Isloor, "Blue Emitting Halogen-Phenoxy Substituted 1,8-Naphthalimides for Potential Organic Light Emitting Diode Applications" **Optical Materials** 37 (2014) 311–321.
3. **Hidayath Ulla**, B. Garudachari, M.N. Satyanarayan, G. Umesh and A.M. Isloor, "Blue Organic Light Emitting Materials: Synthesis and Characterization of Novel 1,8-Naphthalimide Derivatives", **Optical Materials** 36 (2014) 704-711.
4. **Hidayath Ulla**, B. Garudachari, M.N. Satyanarayan, G. Umesh and A.M. Isloor, "Blue Light Emitting Naphthalimides for Organic Light Emitting Diodes", **AIP Conference Proceedings** 1512, 1300 (2013).
5. **Hidayath Ulla**, B. Garudachari, M.N. Satyanarayan, G. Umesh and A.M. Isloor, "Blue Light Emitting Materials for Organic Light Emitting Diodes: Experimental and Simulation Study", **IEEE Conference Publications** (2012).

Papers Presented in International Conferences

1. **Hidayath Ulla**, M. Raveendra Kiran, B. Garudachari, M. N. Satyanarayan, G. Umesh, "1,8-Naphthalimide Based Blue Emitters: Efficient Electron Transporting and Hole-Blocking Molecules for OLEDs", International Winter School on Organic Electronic Materials & Devices (OEMD 2013) at NITK Surathkal, India, 19-21 Dec 2013.
2. **Hidayath Ulla**, B. Garudachari, M.R. Kiran, K.M. Nimith, M.N. Satyanarayan, G. Umesh and A.M. Isloor, "New Blue Emitting Materials Based On Naphthalimides For Organic Light Emitting Diodes", National Conference on Condensed Matter Physics and Applications (CMPA 2012), Department of Physics, Manipal Institute of Technology, Manipal, India, December 27-28, 2012.
3. **Hidayath Ulla**, B. Garudachari, K.M. Nimith, M.R. Kiran, M.N. Satyanarayan, G. Umesh and A.M. Isloor, "Optical and Electrochemical Properties of Novel Materials for Organic Electronics: Experimental and Theoretical Study", National Conference on Condensed

Matter Physics and Applications (CMPA 2012), Department of Physics, Manipal Institute of Technology, Manipal, December 27-28, 2012.

4. **Hidayath Ulla**, B. Garudachari, M.N. Satyanarayan, G. Umesh and A.M. Isloor, “*Blue Light Emitting Naphthalimides for Organic Light Emitting Diodes*” DAE - Solid State Symposium (DAE-SSPS 2012), IIT Bombay, Mumbai, India, December 3-7, 2012.
5. **Hidayath Ulla**, B. Garudachari, M.N. Satyanarayan, G. Umesh and A.M. Isloor, “*Blue Light Emitting Materials for Organic Light Emitting Diodes: Experimental and Simulation Study*”, IEEE International Conference on Optical Engineering (ICOE 2012), VTU Belgaum, Karnataka, India, July 26 – 28, 2012.
6. **Hidayath Ulla**, B. Garudachari, M.N. Satyanarayan, G. Umesh and A.M. Isloor, “*Molecular Designing, Synthesis and Characterization of New Materials Based on 1,8-Naphthalimide for Blue Organic Light Emitting Diodes*”, International Conference on Materials Science and Technology (ICMST 2012), St. Thomas College, Pala, Kerala, India, June 10-14, 2012.
7. **Hidayath Ulla**, B. Garudachari, M.N. Satyanarayan, G. Umesh and A.M. Isloor, “*Potential Blue Emitting Materials For Organic Light Emitting Diodes*”, National Seminar on Current Trends in Materials Science (NSCTMS 2012), NSS Hindu College, Changanacherry, Kerala, India, March 7-8, 2012.
8. **Hidayath Ulla**, B. Garudachari, Jean Maria Fernandes, M.N. Satyanarayan, G. Umesh and A.M. Isloor, “*Synthesis and Characterization of Novel Naphthalimide Derivatives for Blue Organic Light Emitting Diodes*”, International Conference on Recent Trends in Advanced Materials (ICRAM 2012), VIT University, Vellore, India. February 20-22, 2012

BIO-DATA

Hidayath Ulla

Optoelectronics Laboratory, Department of Physics,
National Institute of Technology Karnataka,
Surathkal, Mangalore, India - 575 025
Tel. no.: +91-9986511266
ulla.hid@gmail.com

Education

- Jan 2010 – May 2016 **National Institute of Technology Karnataka, Surathkal, India.**
Ph.D., Physics
Investigations of Naphthalimide and Pyrene Derivatives Based Organic Light Emitting Diodes.
- April 2008 **Mangalore University, Mangalore, Karnataka, India.**
M.Sc., Materials Science
- May 2006 **Mangalore University, Mangalore, Karnataka, India.**
B.Sc. (Physics, Chemistry, Mathematics)

Research Experience

- 01/2010 – 05/2016 **National Institute of Technology Karnataka, Surathkal, India.**
Doctoral Student
Supervisors: Dr. M.N. Satyanarayan and Prof. G. Umesh
- 04/2014 – 09/2014 **National Institute of Technology Karnataka, Surathkal, India.**
Senior Research Fellow
National Program on Micro and Smart Systems, India sponsored project.
Title: Establishment of New National MEMS Design Centers.
Project Leader: Prof. M. Shankaranarayana Bhat
- 03/2010 – 03/2013 **National Institute of Technology Karnataka, Surathkal, India.**
Other Participation
Department of Information Technology, India sponsored project.
Title: Fabrication and Characterization of Blue Organic Light Emitting Diodes
Project Leader: Dr. M.N. Satyanarayan

Academic Experience

- 07/2008 – 12/2009 **Canara First Grade College, Mangalore, India.**
Lecturer, Physics; *Courses taught:* Solid State Physics, Fundamentals of Physics
- 09/2008 – 04/2009 **Canara First Grade College, Mangalore, India.**
Lecturer, Mathematics; *Courses taught:* Calculus
- 07/2009 – 12/2009 **Govt. First Grade College, Mangalore, India.**
Mentor, Physics
Courses taught: Solid State Physics, Fundamentals of Physics

Awards and Achievements

- The research article, “*Blue emitting halogen-phenoxy substituted 1,8-naphthalimides for potential organic light emitting diode applications*” was in top 16th (July to Sept 2014) among the Top 25 Hottest Articles in Optical Materials (Elsevier).
- The research article “*Blue Organic Light Emitting Materials: Synthesis and Characterization of Novel 1,8-Naphthalimide Derivatives*” was in top 7th (Jan to March 2014), top 22nd (July to Sept 2014) and top 11th (Jan to Dec 2014 - full year) among the Top 25 Hottest Articles in Optical Materials (Elsevier).
- **Best Paper Award** (Oral) at National Seminar on Current Trends in Materials Science (NSCTMS 2012), NSS Hindu College, Changanacherry, Kerala, India, March 7-8, 2012.
- **Best Paper Award** (Poster) at National Conference on Condensed Matter Physics and Applications (CMPA 2012), Department of Physics, Manipal Institute of Technology, Manipal, India, December 27-28, 2012.

Publications

Journal papers (Peer Reviewed)

1. Chidirala Swetha, **Hidayath Ulla**, V. Anusha, M. Raveendra Kiran, M. N. Satyanarayan, G. Umesh, Maneesha Esther Mohanty, Kotamarthi Bhanuprakash, Vaidya Jayathirtha Rao, "Pyrene-Oxadiazole Derivatives as Electron Transporting Green Emitters for non-doped Organic Light Emitting Devices" **Journal of Organic Chemistry** 81 (2) (2016) 603–614.
2. **Hidayath Ulla**, M. Raveendra Kiran, B. Garudachari, M.N. Satyanarayan, G. Umesh and A.M. Isloor, “*Blue Emitting Halogen-Phenoxy Substituted 1,8-Naphthalimides for Potential Organic Light Emitting Diode Applications*”, **Optical Materials** 37 (2014) 311–321.
3. **Hidayath Ulla**, B. Garudachari, M.N. Satyanarayan, G. Umesh and A.M. Isloor, “*Blue Organic Light Emitting Materials: Synthesis and Characterization of Novel 1,8-Naphthalimide Derivatives*”, **Optical Materials** 36 (2014) 704-711.
4. **Hidayath Ulla**, B. Garudachari, M.N. Satyanarayan, G. Umesh and A.M. Isloor, “ *Blue Light Emitting Naphthalimides for Organic Light Emitting Diodes*”, **AIP Conference Proceedings** 1512, 1300 (2013).
5. **Hidayath Ulla**, B. Garudachari, M.N. Satyanarayan, G. Umesh and A.M. Isloor, “*Blue Light Emitting Materials for Organic Light Emitting Diodes: Experimental and Simulation Study*”, **IEEE Conference Publications** (2012).
6. M. Raveendra Kiran, **Hidayath Ulla**, Krishnamanohara, M.N. Satyanarayan and G. Umesh, “*Investigation of charge transport in Vanadyl-phthalocyanine with Molybdenum trioxide as a buffer layer: Impedance spectroscopic analysis*”, **Synthetic Metals** 210 (2015) 208–213.

7. M. Raveendra Kiran, **Hidayath Ulla**, Jean M Fernandes, M. N. Satyanarayan and G. Umesh, “*Electrical characterization of hybrid hetero interface using n-ZnO/p-CuPc*”, **Materials Today: Proceedings** 2 (2015) 1230-1233.
8. Jean Maria Fernandes, M. Raveendra Kiran, **Hidayath Ulla**, M.N. Satyanarayan and G. Umesh, “*Investigation of hole-injection in α -NPD using capacitance and impedance spectroscopy techniques with F4TCNQ as hole-injection layer: Initial Studies*”, **Superlattices and Microstructures** 76 (2014) 385-393.
9. Jean Maria Fernandes, M. Raveendra Kiran, **Hidayath Ulla**, M.N. Satyanarayan and G. Umesh, “*Investigation of hole transport in α -NPD using impedance spectroscopy with F₄TCNQ as hole-injection layer*”, **Superlattices and Microstructures** 83 (2015) 766-775.

Academic Conference Presentations

1. Manepalli R Kiran, **Hidayath Ulla**, M. N. Satyanarayan and G. Umesh, “Electrical characterization of Metal-phthalocyanines using Impedance spectroscopy”, International Photovoltaic Solar Energy Conference (Solar Asia- 2015), 30th July-1st August, Savitribai Phule Pune University, Pune.
2. M Raveendra Kiran, **Hidayath Ulla**, J. M. Fernandes, M.N. Satyanarayan and G Umesh, “*Investigation of impedance spectroscopy of inorganic/orgnic hybrid p-n junction based on ZnO and CuPc*”, CMPA2015, March 27-28, Manipal Institute of Technology, Manipal.
3. M. Raveendra Kiran, **Hidayath Ulla**, Jean M Fernandes, M. N. Satyanarayan and G. Umesh, “Electrical characterization of hybrid hetero interface using n-ZnO/p-CuPc”, 4th ICMPC, March 14-15, 2015, GRIET Hyberabad.
4. Jean Maria Fernandes, M. Raveendra Kiran, **Hidayath Ulla**, M.N. Satyanarayan and G. Umesh, “*Studies on Hole Injection Properties of F4-TCNQ in Organic Light Emitting Diodes*”, Emerging Materials: Characterization & Application (EMCA-2014), December 4-6, 2014, Kolkata.
5. Ch.Swetha, P. Nagaraju, G. Malleshm, V. Anusha, **Hidayath Ulla**, M. N. Satyanarayan, K. Bhanuprakash, V. Jayathirtha Rao, “*Pyrene-Oxadiazole Derivatives as Electron Transport Green Emitters for Non-doped Organic Light Emitting Devices: Synthesis, Characterization and DFT Study*”, DAE-BRNS Conference on Organic Devices: The Future Ahead (ODeFA-2014), 3-6 March 2014, Bhabha Atomic Research Centre, Mumbai.
6. **Hidayath Ulla**, M. Raveendra Kiran, B. Garudachari, M. N. Satyanarayan, G. Umesh, “*1,8-Naphthalimide Based Blue Emitters: Efficient Electron Transporting and Hole-Blocking Molecules for OLEDs*”, International Winter School on Organic Electronic Materials & Devices (OEMD 2013), 19-21 Dec 2013, NITK Surathkal.
7. Ch.Swetha, P. Nagaraju, G. Malleshm, **Hidayath Ulla**, M. N. Satyanarayan, K. Bhanuprakash, V. Jayathirtha Rao, "Pyrene-Oxadiazole Derivatives as Electron Transporting Green Emitters for Organic Light Emitting Devices: Synthesis, Characterization and Fabrication", International Winter School on Organic Electronic Materials & Devices (OEMD 2013), 19-21 Dec 2013, NITK Surathkal.

8. Jean Maria Fernandes, B. Garudachari, **Hidayath Ulla**, M.N. Satyanarayan, G. Umesh and A.M. Isloor, “*Novel Naphthalimide Derivatives as Blue Emitting Components in Potential Organic Light Emitting Diode Applications*”, International Conference on Recent Advances in Materials Science and Technology (ICRAMST-13), Jan 17-19 2013, NITK Surathkal.
9. **Hidayath Ulla**, B. Garudachari, M.R. Kiran, K.M. Nimith, M.N. Satyanarayan, G. Umesh and A.M. Isloor, “*New Blue Emitting Materials Based On Naphthalimides For Organic Light Emitting Diodes*”, National Conference on Condensed Matter Physics and Applications (CMPA 2012), December 27-28, 2012, Manipal Institute of Technology, Manipal.
10. **Hidayath Ulla**, B. Garudachari, M.N. Satyanarayan, G. Umesh and A.M. Isloor, “*Blue Light Emitting Naphthalimides for Organic Light Emitting Diodes*” DAE - Solid State Symposium (DAE-SSPS 2012), December 3-7, 2012, IIT Bombay.
11. **Hidayath Ulla**, B. Garudachari, M.N. Satyanarayan, G. Umesh and A.M. Isloor, “*Blue Light Emitting Materials for Organic Light Emitting Diodes: Experimental and Simulation Study*”, IEEE International Conference on Optical Engineering (ICOE 2012), July 26 – 28, 2012, VTU Belgaum.
12. **Hidayath Ulla**, B. Garudachari, M.N. Satyanarayan, G. Umesh and A.M. Isloor, “*Molecular Designing, Synthesis and Characterization of New Materials Based on 1,8-Naphthalimide for Blue Organic Light Emitting Diodes*”, International Conference on Materials Science and Technology (ICMST 2012), June 10-14, 2012, St. Thomas College, Pala.
13. **Hidayath Ulla**, B. Garudachari, M.N. Satyanarayan, G. Umesh and A.M. Isloor, “*Potential Blue Emitting Materials For Organic Light Emitting Diodes*”, National Seminar on Current Trends in Materials Science (NSCTMS 2012), March 7-8, 2012, NSS Hindu College, Changanacherry.
14. **Hidayath Ulla**, B. Garudachari, Jean Maria Fernandes, M.N. Satyanarayan, G. Umesh and A.M. Isloor, “*Synthesis and Characterization of Novel Naphthalimide Derivatives for Blue Organic Light Emitting Diodes*”, International Conference on Recent Trends in Advanced Materials (ICRAM 2012), February 20-22, 2012, VIT University, Vellore.